BRNO UNIVERSITY OF TECHNOLOGY
VYSOKÉ UČENÍ TECHNICKÉ V BRNĚ

FACULTY OF CHEMISTRY
FAKULTA CHEMICKÁ

INSTITUTE OF PHYSICAL AND APPLIED CHEMISTRY
ÚSTAV FYZIKÁLNÍ A SPOTŘEBNÍ CHEMIE

PRINTED BIOSENSOR BASED ON ORGANIC ELECTROCHEMICAL TRANSISTOR
PRINTED BIOSENSOR BASED ON ORGANIC ELECTROCHEMICAL TRANSISTOR

DOCTORAL THESIS
DIZERTAČNÍ PRÁCE

AUTHOR — Ing. Lukáš Omasta
AUTOR PRÁCE

SUPERVISOR — doc. Ing. Ota Salyk, CSc.
ŠKOLITEL

BRNO 2019

VYSOKÉ UČENÍ TECHNICKÉ V BRNĚ
FAKULTA CHEMICKÁ

Zadání dizertační práce

Ústav:	Ústav fyzikální a spotřební chemie
Student:	**Ing. Lukáš Omasta**
Studijní program:	Fyzikální chemie
Studijní obor:	Fyzikální chemie
Vedoucí práce:	**doc. Ing. Ota Salyk, CSc.**
Akademický rok:	2018/19

Název dizertační práce:

Printed Biosensor Based on Organic Electrochemical Transistor

Zadání dizertační práce:

Cílem práce je na základě přehledu současných bioelektronických senzorů navrhnout, vyrobit a otestovat zařízení pro pěstování elektrogenních buněk s možností snímání a vyhodnocování elektrických projevů kardiomyocytů. K tomuto účelu je zadáno použití především materiálového tisku a biokompatibilních materiálů pro aktivní elektronické prvky na bázi vodivých polymerů a ostatních materiálů v kontaktu s materiálem biologickým.

Termín odevzdání dizertační práce: 15.3.2019

Ing. Lukáš Omasta student(ka)	doc. Ing. Ota Salyk, CSc. vedoucí práce	prof. Ing. Miloslav Pekař, CSc. vedoucí ústavu

prof. Ing. Martin Weiter, Ph.D.
děkan

V Brně dne 1.9.2018

ABSTRACT

Organic electronic devices arise as a suitable solution for bioelectronics sensor development, due to the good biocompatibility of organic semiconductors. So-called biosensors can convert electrochemical processes into an electronic signal. A matrix of such biosensors can simultaneously scan a number of biological samples or tissues of the living systems. The active part of the device is an Organic Electrochemical Transistor (OECT). In this work, the theoretical background on such device and its characterization, application in cell-based biosensors, methods of fabrication together with the current state of the art in the field of organic electronics are discussed.

The experimental part contains specific manufacturing procedures of OECT devices development employed. The main emphasis is given on the ability of produced devices to detect response and monitor the stimulation of electrogenic cells. To this end, microplate patterns with a multielectrode array of OECTs based on the semiconductive polymer PEDOT:PSS was developed and fabricated using conventional printing methods (inkjet printing and screen printing). Standard lithographic procedures were also employed. The latest devices with the highest achieved signal amplification of g = 2.5 mS and the time constant of t = 0.15 s were produced. These are comparable or even better than some state of the art fully lithographically prepared ones.

ABSTRAKT

Organické elektronické zariadenia sú vyvíjané ako vhodné riešenia senzorov pre bioelektroniku, a to najmä kvôli dobrej biokompatibilite organických polovodičov v nich použitých. Takzvané biosenzory dokážu premeniť elektrochemické procesy na elektronický signál. Matrica takýchto biosenzorov môže simultánne skenovať množstvo biologických vzoriek, alebo rôznych tkanív v živých systémoch. Aktívnou súčasťou zariadenia je organický elektrochemický tranzistor (OECT). V tejto práci je diskutovaný teoretický rámec fungovania takéhoto zariadenia, jeho elektrická charakterizácia, aplikácia v biosenzoroch na báze buniek, spôsoby výroby a aktuálnym stavom techniky v oblasti organickej elektroniky.

Experimentálna časť obsahuje konkrétne výrobné postupy vývoja OECT zariadení, ktoré boli použité v našom laboratóriu. Hlavný dôraz sa kladie na schopnosť vyrobených zariadení detekovať reakciu a monitorovať stimuláciu elektrogenných buniek. Za týmto účelom boli vyvinuté matice mikroelektródových OECT zariadení založených na polovodivom polyméri PEDOT:PSS. Tieto boli vyrobené s využitím bežnými tlačiarenských techník (atramentová tlač a sieťotlač) spolu so štandardnými litografickými postupmi. Najnovšie nami vyvinuté zariadenia dosahujú najväčšieho zosílením signálu, g = 2,5 mS a časovú konštantu t = 0,15 s. Tieto zariadenia sú porovnateľné, často dokonca lepšie ako niektoré iné najmodernejšie a plne litograficky pripravené senzory.

KEYWORDS

Organic electrochemical transistor, Printed electronics, Inkjet printing, Screen printing, Biosensor, PEDOT:PSS, Photolithography, SU-8 photoresist

KĽÚČOVÉ SLOVÁ

Organický elektrochemický tranzistor, Tlačená elektronika, Atramentová tlač, Sieťotlač, Biosenzor, PEDOT:PSS, Fotolitografia, SU-8 fotorezist

OMASTA, L. *Printed biosensor based on organic electrochemical transistor*. Brno: Vysoké učení technické v Brně, Fakulta chemická, 2019. 103 s. Vedúci dizertačnej práce doc. Ing. Ota Salyk, CSc.

PREHLÁSENIE

Prehlasujem, že som dizertačnú prácu vypracoval samostatne, a že všetky použité literárne zdroje som citoval správne a úplne. Dizertačná práca je z hľadiska obsahu majetkom Fakulty chemickej VUT v BrnĚ a môže byť využitá ku komerčným účelom iba so súhlasom vedúceho dizertačnej práce a dekana FCH VUT.

DECLARATION

I declare that the dissertation thesis has been worked out by myself and that all the quotations from the used literary sources are accurate and complete. The content of the dissertation thesis is the property of the Faculty of Chemistry of Brno University of Technology and all commercial uses are allowed only if approved by both the supervisor and the dean of the Faculty of Chemistry, BUT.

……

Ing. Lukáš Omasta

POĎAKOVANIE

Rád by som poďakoval vedúcemu dizertačnej práce doc. Ing. Otovi Salykovi CSc. za podnetné námety, čas a ochotu pri riešení problémov spojených s jej vypracovaním.

CONTENT

1 AIM AND MOTIVATION

The aim of this dissertation thesis is a comprehensive overview of organic electrochemical transistors and their use as a bioelectronic sensor. Human cell cultures provide a potentially powerful means for pharmacological and toxicological research. Electrogenic cell cultures are advantageously studied by the means of OECTs. They are promising transducers for bio-interfacing. This is due to their biocompatibility, high transconductance, and the possibility of manufacturing in all manner of structures and designs.

Most OECTs reported to date, however, are produced using lithographic techniques with the need for clean room facilities. These standard manufacturing processes are costly, lengthy and the production rate is rather slow. We aimed to alleviate the aforementioned production drawbacks by introducing standard printing techniques, such as inkjet printing and screen printing. Such an envisioned platform is produced cheaply and in large quantities, without the need for cleanroom facilities. It is accessible and easy to implement during routine cell culture measurements.

2 INTRODUCTION

The field of organic electronics has grown significantly in the past twenty years. It has been so mainly because of the many desirable properties of organic semiconductors. Among the most notable are the low cost, ease of processing and their ability to be tuned through synthetic chemistry [1]. Organic electronics can link the fields of electronics and biology, as organics have the ability to conduct both electronic and ionic charges with significant mobility at room temperature. This important property is leveraged in a variety of devices that utilize mixed electronic/ionic conduction [2]. For example, the dimensional changes caused by ion injection can be used to build mechanical actuators, also known as artificial muscles. Ion redistribution within a layer conveys electronic charge injection from metal electrodes. This effect can be utilized to achieve efficient electroluminescence in light-emitting electrochemical cells [3]. In electrochromic displays, ions injected from an electrolyte change the color of a polymer film [4]. Furthermore, ion diffusion across an interface is used to control the energetics of the heterojunction, thus forming diodes [5]. Mixed electronic/ionic conductivity is of particular importance for devices that interface electronics with biology, a subject that is currently attracting a great deal of attention [6]. The intention of organic bioelectronics is to address the current and future diagnostic and therapeutic needs of the biomedical community [7], [8]. These needs include for instance improving compatibility with the biological environment. Also important is the detection of low concentrations of biological analytes, and pathogens, as well as detection of low amplitude brain activity. Electrical methods for biological sensing are considered favorable, in particular, due to the fact that they are label-free. They also do not require expensive and time-consuming techniques which involve fluorophores or chromophores.

Present diagnostic approaches using electrical sensors involve large-scale integrated systems, passive metal electrodes, and electrochemical biosensors. Operating principle of these systems is based on changes in the impedance, local potential or redox reactions. However, for electrochemical sensors, the biological signals are often difficult to record and demand further amplification to become detectable. That is why a push toward more active, sensitive, and biocompatible devices is necessary [9], [10].

As lab-on-chip arrays for biomedical applications become more and more sophisticated by increasing the number of fluidic, electronic, and mechanical components, space and design restrictions become more important [11]. Organic thin film transistors (OTFT) provide unique opportunities when integrated into these systems as transducers that can be easily patterned, individually functionalized, and directly interfaced with biomolecules and living cells. Organic electrochemical transistors (OECTs) as a subset of OTFT have distinguished themselves in recent years due to their simple fabrication and low voltage operation [12]. The ability to operate in aqueous environments and the integration with microfluidics make OECTs excellent candidates for a variety of applications, especially in the area of sensing and biosensing.

3 THEORETICAL PART

The theoretical part of the thesis introduces historical facts concerning conducting polymers, doping of conductive polymers, as well as a number of devices that have been built using these materials. Next, a brief overview of cardiac muscle cells and the formation of cardiac action and field potential are given. The following chapters deal in detail with the organic electrochemical transistor, its physics, circuit model and geometry. The role of PEDOT:PSS as the most commonly used material is discussed together with the current state of the art and potential use of OECTs in bioelectronics. Finally, a short introduction to a few common patterning methods of conjugated polymers is mentioned.

3.1 CONDUCTIVE POLYMERS

Conductive polymers (CPs) were discovered in 1976 by Alan MacDiarmid, Alan Heeger, and Hideki Shirakawa, they collectively won the Nobel Prize for chemistry in 2000. CPs application in organic electronics is invaluable since they possess a broad spectrum of desired characteristics [13]. Mixed (ionic and electronic) conductivity of CPs is the main reason why they are precious in the research of organic electronics and biomedicine as well. The advantage of CPs is their chemical adjustability. They can be designed according to the needs of each application. For example, the CPs used in electrochemical biosensors enhances their stability and sensitivity.

There have been numerous investigations which proved that CPs are biocompatible, have mechanical flexibility similar to the organic tissues, and can be transparent in the visible part of electromagnetic spectra. They were initially investigated as replacements for metals, and their application range has multiplied. Nowadays, conductive polymers are part of several research fields such as electrocatalysis, energy storage, sensing, and tissue engineering and are primarily derivatives of polypyrrole, polythiophene (such as poly(3-hexylthiophene-2,5-diyl) – P3HT) polyaniline and poly(3,4-ethylenedioxythiophene) shown in (Figure 1) [14].

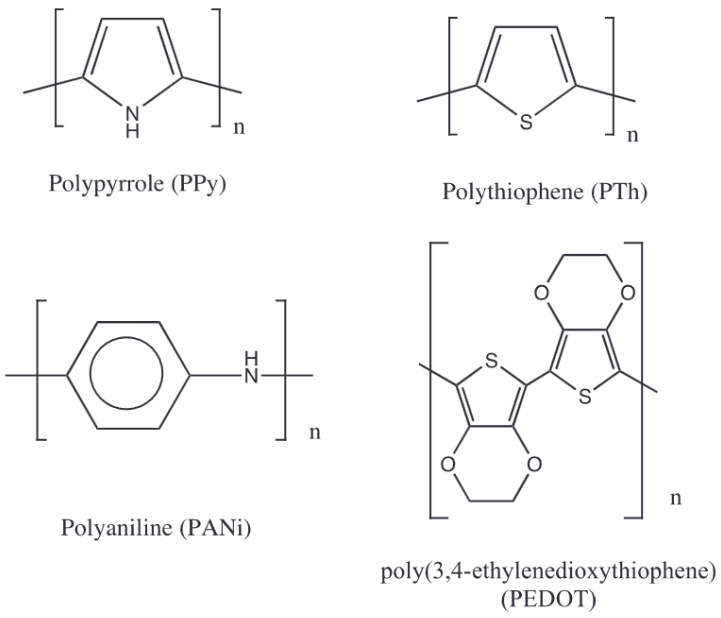

Figure 1 The most common conductive polymers in the undoped form: polypyrrole (PPy), polythiophene (PTh), polyaniline (PANi), and poly(3,4-ethylenedioxythiophene) (PEDOT)

3.1.1 Doping of conductive polymers

Conjugated polymers can be chemically or electrochemically doped. The process of doping in the case of conjugated polymers refers to various redox reactions. The chemical doping is done through the exposition of the polymer to an oxidizing agent (iodine, bromine) or a reducing agent. The oxidation of the polymer is equivalent to p-doping and reduction can be regarded as n-doping. P-doped conjugated polymers are generally more used in comparison to n-doped polymers due to the tendency of the n-doped ones to spontaneously re-oxidize in atmospheres rich in oxygen.

The cause of adding or removing electrons from the conjugated polymer is a formation of new energy states called polaronic states. These arise in the bandgap between the bonding (π) and the antibonding (π^*) bands. A polaron is a quasi-particle which can be understood merely as a charge accompanied by a lattice distortion. When an electron is embedded to or withdrawn from the polymer, the region near this chain segment is geometrically distorted. The polymer relaxes in the response to the new charge configuration by adjusting the bond lengths in the affected chain segment. Charge carrying species in conjugated polymers are represented as polarons and not electrons and holes. The strong electron-lattice coupling also supports usage of the polaron to interpret the charge carrying species in these materials.

The levels of doping in conjugated polymers in comparison to the ones in inorganic semiconductors are much higher. Usually, the amount of doping in the conjugated polymers is within the range of 20–40 %, while in the inorganic semiconductors is this number around 1 % [12].

3.1.2 Materials for OECTs

One of the well-studied and widely used CP is the p-type organic semiconductor Poly(3,4-ethylenedioxythiophene) doped with poly(styrene sulfonate). In the PEDOT:PSS the negative charge of PSS is balanced by a hole in the PEDOT matrix. PEDOT:PSS is highly stable in a broad *pH* range, it has high electronic conductivity, PEDOT:PSS with values around 1000 $S \cdot cm^{-1}$ is readily available. Another advantage of PEDOT:PSS is its low cost and possibility of lithographic processing. The ionic mobility (μ_i) of small ions moving through the PEDOT:PSS may achieve mobility typically found in dilute electrolytes [15]. High ionic and electronic mobility are the main reasons why OECTs are utilizing PEDOT:PSS in them. This CP has been engaged in a variety of technological applications such as chemical and biological sensing, monitoring of cell adhesion and viability.

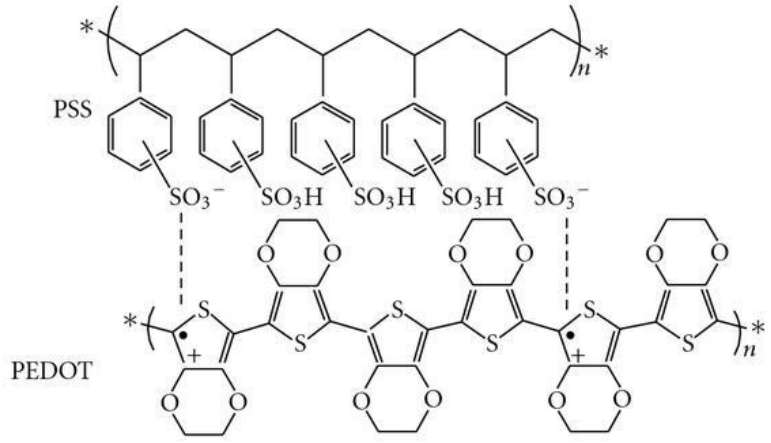

Figure 2 Chemical structure of PEDOT:PSS. The "dot" and "plus" represent the unpaired electron and positive charge on the PEDOT chain, respectively

The dispersible polyelectrolyte complex consisting of positively charged PEDOT and negatively charged polyanion can be formed in the presence of a surplus of free sulfonic acid groups. When EDOT is polymerized with persulfate in the presence of poly(styrene sulfonic acid) (PSS), a polyelectrolyte complex that forms a stable dispersion in water is created [16]. Dispersion is composed of PEDOT:PSS gel particles dispersed in water. Depending on type and concentration it can be stable for months up to years. It can be used in many deposition techniques such as spin-coating, doctor blading, screen printing, dip coating, slot-die coating, curtain coating, ink jet printing and many others [17].

The gel particles of the PEDOT:PSS have usually size in between 20–500 nm [18] and typically have 1–5 % of solid content. It is possible to prepare very smooth films with a surface roughness of around 1 nm or less since the gel particles collapse upon drying. Viscosities of PEDOT:PSS dispersions are typically in the range of 10–500 mPa s and have a low pH value, predominantly in the range of 1–2, due to the excess of the PSS. The PEDOT:PSS can be neutralized, however, if the neutralization proceeds above *pH* 7 the positively charged PEDOT is not stable. As a consequence of higher *pH* values, the PEDOT dispersions change color and become substantially less conductive. After drying the PEDOT:PSS gel particles form a homogeneous transparent layer able to conduct the electrical current.

3.2 CARDIAC MUSCLE CELL

Cardiac muscle cells (cardiomyocytes) are the muscle cells that make up the heart muscle. The cardiomyocytes are about 100 μm long and 10 – 25 μm in diameter. Every cardiomyocyte contains myofibrils. Myofibrils are specialized organelles consisting of long chains of sarcomeres, which are the main contractile units of muscle cells. Cardiomyocytes exhibits striations analogously as in case of skeletal muscle cells.

There are two species of cells in the heart muscle. Cardiomyocytes compose the atria (the chambers in which blood enters the heart) and the ventricles (the chambers where blood is gathered and pumped out of the heart). These cells can shorten and lengthen their fibers, and hence the fibers must be flexible enough to withstand the stretching. The second type of cells is cardiac pacemaker cells which create the impulses that are responsible for the beating of the

heart. They are spread throughout the heart and have several crucial functions. Firstly, they can generate and send out electrical impulses spontaneously. Secondly, they must be able to receive and respond to electrical impulses from the brain and finally, they must be able to transfer electrical impulses from one cell to another [19].

All of these cells are connected via cellular bridges. Intercalated discs create porous junctions between the cells and allow sodium, potassium, and calcium to diffuse from one cell to another freely. The cellular bridges facilitate depolarization and subsequent repolarization in the myocardium. Thanks to these junctions and bridges the heart muscle can operate as a single coordinated unit [20], [21].

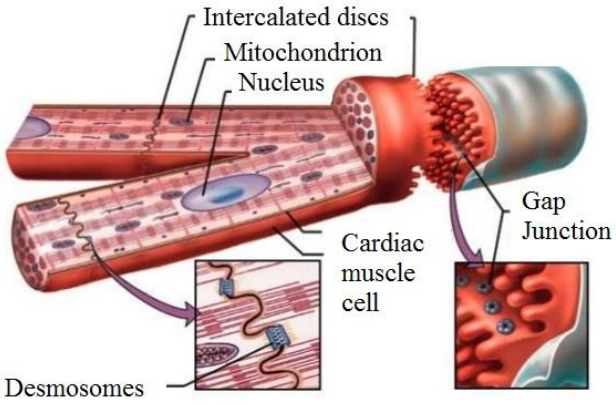

Figure 3 A detailed description of the cardiac muscle cell [21]

3.2.1 Cardiac Action potential

The cardiac action potential (AP) is caused by complex nonlinear interactions between membrane ion channels, the membrane voltage, and the dynamic ionic environment of the cell (Figure 4). These processes define the AP rate-dependent properties and are subject to numerous regulatory mechanisms. The process of normal AP generation is governed by a single type of ion channel, which is the fast sodium channel. This ion channel generates a large and swift inward current, I_{Na}, to depolarize the membrane during the rapid AP upstroke, the rising phase. On the other hand, the AP repolarization phase is a much slower process which is governed by an effort to maintain the balance between inward depolarizing and outward repolarizing membrane currents. These are carried by different kinds of ion channels (Figure 4).

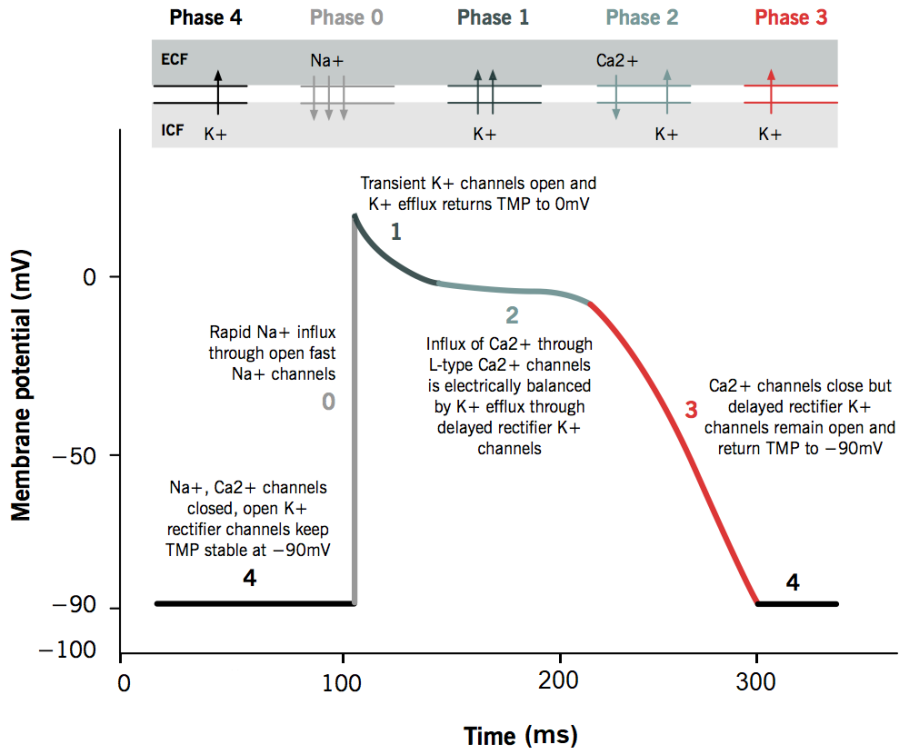

Figure 4 Depiction of the cardiac action potential [22]

AP depolarization is an "all-or-none" process that is executed with a large current reserve (high safety factor), while repolarization is a precisely controlled process that determines with great exactness the rate-dependent AP morphology and duration (APD) [22].

APD shortens with increasing heart rate. This phenomenon is also known as a process termed APD adaptation, which is a characteristic of cardiac AP that is necessary for normal heart function. The repolarization mechanism and its multi-current nature allow for many control points in this process. This results in high utilization of these processes for precise control of APD and its rate dependence. Although, the delicate balance of the AP repolarization can be easily disrupted by disease or drugs that can have an adverse effect on any of the ion channels used.

Most often is AP recorded via patch clamp electrophysiology in current clamp method. Since the AP consists of the ionic currents, that can be measured separately using the voltage clamp, a lot of studies have been conducted in this field in recent years [23], [24]. Changes in one or more of these currents can result in severe dysfunction of the heart. For example, changes in the AP caused by various medicaments results in modulations in Na^+ and Ca^{2+} inward currents or several of the outward K^+ currents, such as the rapidly activated (I_{Kr}) and slow activated (I_{Ks}) currents in human cardiomyocytes (Figure 5).

Values needed to determine the magnitude of AP effects are the AP amplitude (APA; mV), the resting membrane potential (RMP; mV), the maximal rate of depolarization (V_{max}; $V \cdot s^{-1}$) and AP duration at 50 % and 90 % of repolarization (APD_{50}, APD_{90} respectively; ms) [22].

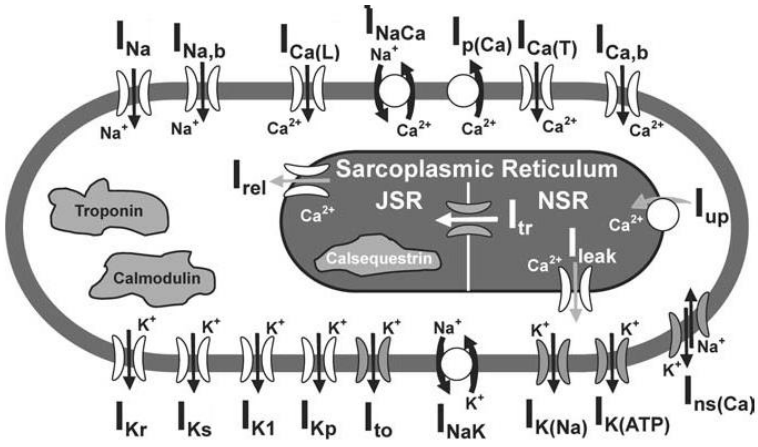

Figure 5 A scheme of the Luo–Rudy dynamic model of a cardiac ventricular cell together with a description of all ionic currents [22]

3.2.2 Cardiac field potential

A non-invasive extracellular recording has developed into an extensively employed standard method in the course of the last 40 years. The semi-permeable lipid bilayer separates different ion concentrations on the inside and outside of the cell membrane. Traditional methods measure the membrane potential that results from the electrochemical gradient directly using an intracellular electrode (patch clamp). The corresponding ions are passing along their electrochemical gradient after ion channels are opened due to chemical or electrical stimulation. Therefore, the resistance of the membrane is lowered, resulting in an inward or outward flow of ions, which can be measured as a transmembrane current. The extracellular gap is also conductive, with low but non zero resistance. The extracellular current gives rise to a small voltage that can be measured employing extracellular electrodes. Extracellular signals are weaker than transmembrane potentials. The magnitude of the signals depends mainly on the distance of the signal source to the electrode. The increase in the distance of the signal source from the electrode results in the decrease in the extracellular signal amplitudes. It is especially important to facilitate a close interface between the electrode and cell membrane for a high signal-to-noise ratio.

The extracellular field potential together with the transmembrane current follows the same time course. The field potential is approximately equal to the first negative derivative of the transmembrane potential. This has been verified for different types of signals derived from neuronal samples as well as cardiac samples. The relationship between the rise time of the cardiac action potential (AP) recordings (with intracellular electrodes) and field potentials (FP) (with extracellular potential) as well as between AP and FP duration is linear. The contribution of individual ionic transmembrane currents can also be determined from the shape of the FP waveform as shown in (Figure 6). For example, the rapid component of the depolarizing sodium current and the slow calcium current can be identified.

Moreover, the delayed rectifying K^+ current (I_{Kr}) manifests either as a positive or negative peak. The polarity of the peak is given by several variables, such as the proximity of the cell layer to the measuring electrode. The field potential duration is equivalent to the action potential duration. The duration is measured from a minimum of the Na^+ peak to the maximum/minimum of the I_{Kr} current peak.

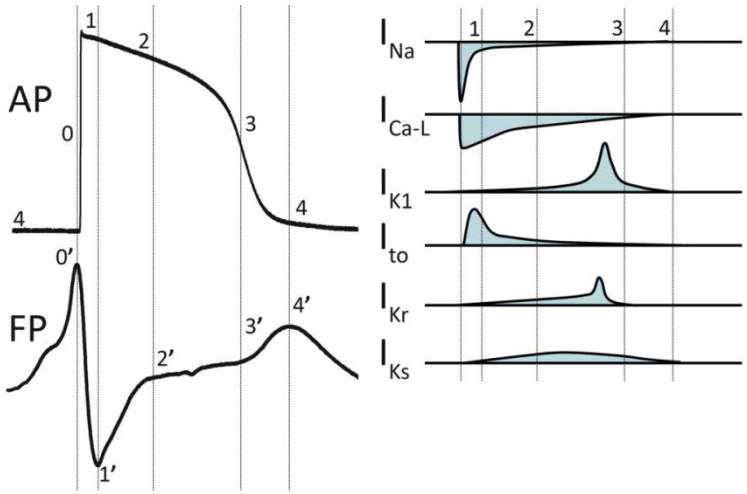

Figure 6 (Left) Comparison of the Action Potential and Field Potential of cardiomyocytes derived from human (induced) pluripotent stem cells (hiPSC-CMs). (Right) Composing active currents depicted schematically [25]

A vast majority of researchers use multi-electrode arrays (MEAs) in recent years in order to measure electrical activity in neural and cardiac cells. MEAs are more and more explicitly used to analyze toxicity of newly developed pharmacological products and compounds or their combinations on cells, mainly cardiomyocytes. MEAs coupled with cardiomyocytes cultivated from human (induced) pluripotent stem cells (hiPSC-CMs) have been published as a tool to examine the ability of several compounds to induce arrhythmias in the heart [25]. These adverse effects represent a main toxic hazard for new drugs in pre-clinical trials [26]. Using patch clamp electrophysiology to detect these effects is feasible but laborious and it requires precise and skillful manipulation in order for the measured parameters to be accurate. This is why using MEA is often more feasible and more accessible for the higher throughput screening, although it records FP and not the AP.

Prolongation or shortening of FP duration (FPD) are routinely measured via MEAs and are considered a measurement of the APD_{90} [26]. Other parameters are difficult to extract from FPs although they may contain a great level of information. In practice, extraction of this information is hindered by a lack of knowledge between the AP and the FP and their underlying relationship (transfer function) [25].

3.3 ORGANIC ELECTROCHEMICAL TRANSISTORS

White et al. firstly demonstrated OECTs, in which the conductivity of a polypyrrole film was modulated by the application of a gate voltage through an electrolyte [27]. Since the invention of OECTs as a variant of the OTFT, it became a promising device for biocompatible sensors in biology and medicine. The growing area of bioelectronics, which links the fields of electronics and biology, holds immense potential for the development of innovative biomedical devices for therapeutics and diagnostics. OECTs can be used as logic elements, as well as incorporated into microfluidics, or coupled to bilayer membranes with ion channels. They can also be used for sensing of water vapour, deoxyribonucleic acid, glucose and lots of other analytes.

Biosensors arose as a promising solution for the investigation of processes in cells and tissue cultures in vitro as well as for diagnostic and therapy in vivo. OECTs are designed to convert the electrochemical processes at cell membranes to electronic signals. Application of organic electronics brings the new approach for sensing in biology and medicine. The central part of the device is a transistor, nowadays mostly based on PEDOT:PSS (poly(3,4-ethylenedioxythiophene) polystyrene sulfonate) conductive polymer.

Electrochemical polymerization of conductive polymer PEDOT was firstly reported back in 1992 by Heywang et al. [28]. The first PEDOT:PSS co-polymer was prepared by the potentiostatic electrochemical polymerization in 1995 by Yamato et al. [29]. PEDOT:PSS has outstanding biocompatibility and potentially high device amplification. Solid or gel electrolyte based devices have been prepared and show similar behaviour to solution based ones.

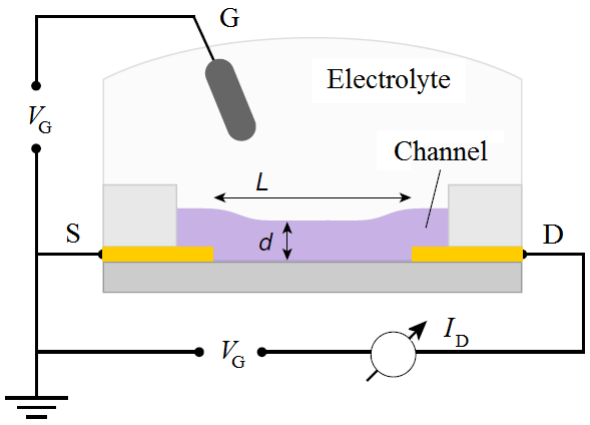

Figure 7 The typical structure of an organic electrochemical transistor (OECT), showing the source (S), drain (D), electrolyte and gate (G) [31]

The semiconducting PEDOT is p‑type doped (oxidized form), which leads to mobile holes that can jump from one chain to another, resulting in a hole current. These holes are compensated by sulfonate anions of PSS, which can be considered as ionized acceptors [30]. In the absence of a gate voltage, a hole current flows in the channel (that is, the ON state), this means that OECTs based on PEDOT:PSS operate in depletion mode. By applying a positive gate bias, cations from the electrolyte are injected into the channel, and the anions are compensated. This is comparable to compensation doping and as a result, the number of holes in the channel decreases. The channel is de-doped as the holes that are extracted at the drain are not replenished at the source. This manifests as a drop in the drain current, and the device reaches the OFF state (Figure 8) [31].

The OECT crucial feature is that doping changes occur over the entire volume of the channel which is in contrast to the field-effect transistors (FETs) where de-doping changes occur only in the interfacial region. OECTs are efficient switches and powerful amplifiers due to the large modulations in the drain current, which can be achieved by applying low-gate voltages [32], [33], [34]. The use of electrolytes results in the tremendous flexibility in device architecture and integration with a range of different substrates, utilizing a variety of form factors and a wide range of fabrication processes. The fundamental adjustability of organic molecules allows further optimization of ion and electron transport and simplifies bio-functionalization. Thanks to these characteristics, OECTs are investigated and tested in

various applications, including neural interfaces [35], [36], chemical and biological sensors [37], [38], printed circuits [39], [40] and neuromorphic devices [41], [42].

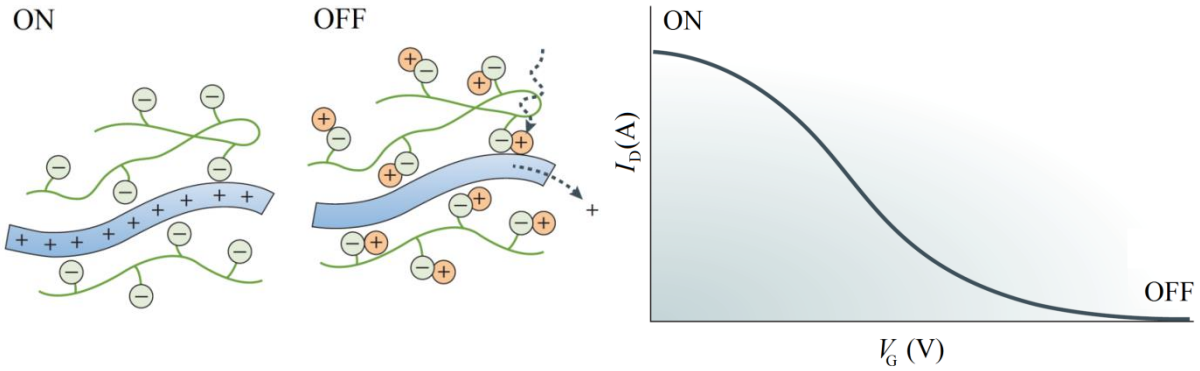

Figure 8 Transfer curve showing the depletion-mode operation of an OECT with a conducting polymer channel [34]

3.3.1 The device physics of OECTs

OECTs transduce small voltage signals applied to the gate into large changes in the drain current. This transduction process is described by a transfer curve, which shows the dependence of the drain current on the gate voltage (Figure 9). The steeper the transfer curve, the more significant the change in drain current for a given gate voltage signal.

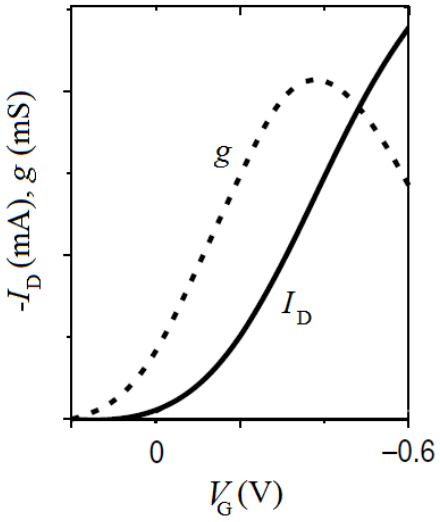

Figure 9 The depiction of the typical OECT transfer curve I_D together with transconductance g [34]

The effectiveness of transduction is determined by the first derivative of the transfer curve and is called transconductance:

$$g = \partial I_D / \partial V_G \tag{1}$$

The most critical parameter for electrochemical transistors to consider and evaluate is transconductance. OECTs have very high transconductance values, on the order of millisiemens (mS) for micrometer-scale devices [32]. This is due to the volumetric nature of

the response of these devices. The basic physical model of OECT operation was described by Bernards [31]. This model captures and describes both steady and transient state of the OECTs. It concludes that ions from the electrolyte enter the channel and change the electronic conductivity throughout its volume. The OECT can be divided into two circuits: electronic, which describes the flow of electronic charge in the source-channel-drain structure according to Ohms law. The second one: the ionic circuit, which describes the flow of ions in the gate-electrolyte-channel structure (Figure 10).

The electronic circuit can be understood as a resistor, in which electronic charge drifts under the influence of the local potential as in the case of MOSFETs (Metal Oxide Semiconductor Field Effect Transistors). The ionic circuit is made of a resistor in series with a capacitor. Resistive part explains the flow of the ions in the electrolyte, and the capacitive part describes the storage of ions in the channel. Using this model, we assume that ions which are injected into the channel do not transfer charge through the OECT film. Hence this model describes utterly capacitive behaviour. Ions electrostatically compensate the opposite charges presented in the conductive channel replacing holes localized on the PEDOT backbone.

We assume that no electrochemical reaction takes place between the electrolyte and the channel. At the steady state, the capacitor is charged, and the gate current approaches zero due to the lack of holes as the charge carriers. Bernard's model gives us a good fit for the output characteristics of OECTs and allows quantitative predictions of the transconductance *g*. Details are discussed in the next chapter. At saturation and for depletion-mode devices, it gives [31]:

$$g = (W/L) \cdot d \cdot \mu \cdot C^* \cdot (V_{\mathrm{Th}} - V_{\mathrm{G}}) \tag{2}$$

Where *W*, *L*, and *d* is the channel width, length, and thickness, respectively; μ is the charge-carrier mobility; C^* is the capacitance per unit volume of the channel, and V_{Th} is the threshold voltage. The voltage terms are inverted in the case of accumulation-mode OECTs. This equation (2) is comparable with the one for FETs, the difference here is that the product $d \cdot C^*$ substitutes the capacitance per unit area of the MOS (Metal Oxide Semiconductor) capacitor, *C'*. This modification characterizes the difference between these two architectures. The physical thickness of the channel does not affect the conductivity of the FET devices.

On the other hand in an OECT, the channel thickness is a parameter that can modify their output. Volumetric gating makes OECTs to perform better regarding amplification in comparison with other transistor types and architectures [32]. The high transconductance of OECTs is unfortunately compensated by their rather large time constants.

From Bernard's model, we can anticipate that the response time will be limited by either the ionic or the electronic circuit. In most cases, the ionic circuit controls the response time, which is determined by the product of the resistance of the electrolyte and the capacitance of the channel. The capacitance of the channel is proportionate to the thickness of the channel. This results in the slower OECT operation as the thickness *d* of the channel is getting bigger [31]. Therefore the thickness of the channel can be used as a variable when deciding between gain and bandwidth [36]. Typical response times of micro-fabricated OECTs with liquid electrolytes are in the range of milliseconds. The application possibilities of OECTs are therefore limited, especially concerning the frequency range with the maximum of tens of kilohertz (kHz). This is sufficient for most biosensor applications, which is quasi-static, and for recording electrophysiological signals [31]. In case of solid or gel electrolytes, the

response time is even larger, but many applications, particularly in the field of printed electronics, do not require fast response times [43].

Bernard's model can be improved by taking into consideration, for example, variable conductivity along the OECT channel, which is nonlinearly dependent on the charge density. This was observed using spatially resolved voltage measurements along the OECT channel [12]. Non-ideal contacts in OECTs introduce additional complications [44]. A more precise characterization of the transfer curve can be done by considering the influence of disorder on hole transport in the channel [45]. Another consideration is that OECTs accounts for the limit at which ions freely enter the volume of the channel. This has been demonstrated in various materials, in which capacitance is proportional to the film thickness [33], [46].

On the other hand, electrolyte-gated FETs account for the other extreme in which ions accumulate at the surface of the channel. Several materials exhibit a response between the two extremes [47]. This suggests the presence of a barrier for ion injection. The physics of electron and hole injection and transport in organic semiconductors has been widely studied in previous decades. Nevertheless, not that much is known about the processes of ion injection and transport in organic semiconductors.

As a result of the electrolyte gating in the OECTs, the fraction of the applied gate voltage that drops across the channel is controlled by the nature and geometry of the gate electrode [48]. Two capacitors are formed in the ionic circuit if a polarizable electrode is used as the gate (Pt or Au). One capacitor represents the electrical double layer formed at the gate–electrolyte interface, and the other capacitor corresponds to the volumetric capacitance of the channel.

The capacitors are connected in series. Therefore the applied gate voltage drops across the smaller one of these two (Figure 10). The capacitance of the gate electrode must be more than ten times larger than the capacitance of the channel to achieve efficient gating. If it is not the case, then a significant fraction of the applied gate voltage will drop at the gate–electrolyte interface. Large gate capacitance can be achieved for example by using thick PEDOT:PSS electrode as the gate electrode.

Another approach is to use a non-polarizable gate electrode (Ag/AgCl). In this case, the voltage drop at the gate–electrolyte interface is insignificant [49]. The type of the electrolyte: liquid, gel or solid and the ion concentration have an impact on the response time of the transistor as well. This is because the electrolyte conductivity determines the resistance of the ionic circuit [50].

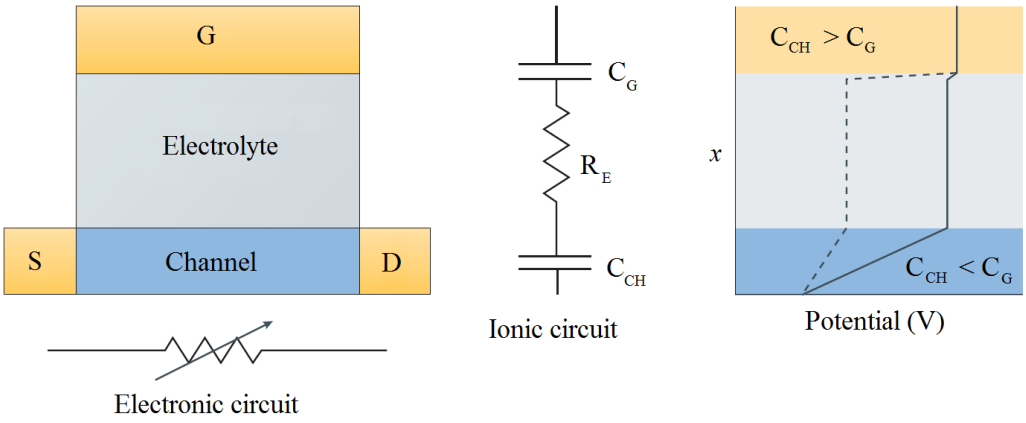

Figure 10 Ionic and electronic circuits used to model OECTs [34]

The electronic circuit, shown below the device design on the left, is modeled as a resistor with a resistance dependent on the applied voltage at the gate electrode. The ionic circuit, depicted in the middle, is composed of the capacitors corresponding to the channel (denoted C_{CH}) and gate (denoted C_G) and a resistor corresponding to the electrolyte (denoted R_E), respectively. The distribution of potential in the ionic circuit is illustrated on the right. The solid line represents the case of effective gating. At this point, ions are driven inside of the channel because most of the applied gate voltage drops at the boundary between the electrolyte and the channel. The dashed lines, on the other hand, represent the case of ineffective gating, where most of the applied gate voltage drops at the gate–electrolyte interface.

3.4 OECT CIRCUIT MODEL

OECTs operating in depletion or accumulation regime can be divided into two separate circuits as was discussed above, an electronic and an ionic circuit. The electronic circuit consists of a p-type organic semiconductor film which is responsible for the hole transport between the drain and the source electrodes. It can be described by Ohm's law, and so the electronic transport is determined by the density and mobility of the holes. The ionic circuit is responsible for transport of ionic charge in the electrolyte. The modulation process in the transistor is commanded by the interaction among the ionic species in the electrolyte and the active area of the organic conductive polymer. This interaction is explained as a combination of linear circuit elements.

3.4.1 Electronic circuit

Using the Ohm's law, we can describe the electronic circuit of an OECT:

$$J(x) = \mathrm{q}\mu p(x)\frac{\mathrm{d}V(x)}{\mathrm{d}x} \tag{3}$$

Where J represents the current flux, q is an elementary charge, μ is the hole mobility, p is the hole density, and dV/dx is the electric field intensity.

For simplification, the hole mobility is supposed to be constant. The de-doping process is used to define the concentration of charge carriers in the semiconductor layer after the positive gate voltage is applied. Cations are inserted from the electrolyte into the semiconductor layer. Every inserted cation replaces one acceptor. This process is similar to the compensation doping of silicon. The difference is that it can be carried out at much lower temperatures (room temperature) and is much quicker.

De-doping is a process which contains two separate steps that preserve electrical neutrality in the organic semiconductor layer at steady-state. For every cation that goes into the organic layer, a hole obtained at the source is not replaced by injection at the drain (assuming $V_D > 0$). In this instance, an expression for the effective dopant concentration in volume v, of semiconductor material is expressed in the equation:

$$p = p_0\left(1 - \frac{Q}{\mathrm{q}p_0 v}\right) \tag{4}$$

Where p is the effective hole concentration, p_0 is the initial hole concentration in the organic semiconductor before the application of a gate voltage, Q is the total charge of the cations injected in the organic film from the electrolyte, and v represents volume.

The introduction of negative ions is assumed not to affect the organic semiconductor. All charge densities are assumed to be uniform across the thickness of the organic semiconductor film, an approximation that limits the validity of this model to thin films.

3.4.2 Ionic Circuit

The ionic circuit is defined by a resistor (R_s) and a capacitor (C_d) connected in series. The resistor describes the conductivity of the electrolyte. It can also be viewed as a scale of the ionic strength of the electrolyte. The capacitor is responsible for polarization at the interface of organic film-electrolyte and gate electrode-electrolyte. This ionic circuit model is based on the assumption that at the gate electrode no chemical reactions take place. Therefore this model is not correct for devices in which oxidation or reduction at the gate electrode is substantial [51].

Another prerequisite is that OECTs operate in the non-Faradaic regime. The model is not accurate enough for the devices operating in the Faradaic regime. This means devices operating at voltages that can result in the electrolysis of aqueous electrolytes [52]. After the gate voltage is applied, the transient behaviour of ionic circuit display properties of a charging capacitor can be described by the equation:

$$Q(t) = Q_{ss}\left[1 - e^{-t/\tau_i}\right] \tag{5}$$

The total charge Q_{ss} which passes through the circuit is expressed:

$$Q_{ss} = C_d \Delta V \tag{6}$$

The ΔV is the voltage applied across the electrolyte. The ionic transit time is described by the equation:

$$\tau_i = C_d R_s \tag{7}$$

Because C_d depends on the area of the device considered, it is convenient to refer to it as in the next equation:

$$C_d = c_d A \tag{8}$$

The c_d is capacitance per unit area, and A is the area of the device under consideration. For simplicity, the concentration and potential dependence of the ionic double layer capacitance are neglected, and a constant value is assumed for the c_d.

3.4.3 Steady-State Behavior

The behavior of the depletion regime OECTs at steady-state had been described by two models. Prigodin et al. presented the first approach from a theoretical solid-state physics point of view [53]. In the organic semiconductor, a decrease in the hole mobility was considered as the mechanism of switching.

Upon the application of a positive gate voltage, the flow of cations is induced from the electrolyte into the organic semiconductor layer. However, this model does not take into account spatial non-uniformity of de-doping. Robinson et al. presented a second model in which variables based on electrostatics and electrochemistry was introduced in order to interpret the details of OECT operation qualitatively. A decline in hole concentration in the organic layer caused by de-doping was considered as a switching mechanism.

The effective hole concentration p in the equation has to be spatially known throughout the organic film in order to solve for organic electrochemical transistor behaviour. The charge in the slice dx in the proximity of position x (Figure 11) at steady-state can be expressed by the equation:

$$Q(x) = c_{\mathrm{d}} \cdot W \cdot \mathrm{d}x\big(V_{\mathrm{G}} - V(x)\big) \tag{9}$$

Where V_{G} represents the gate voltage, $V(x)$ is the spatial voltage profile within the organic film and W is the width of the organic film.

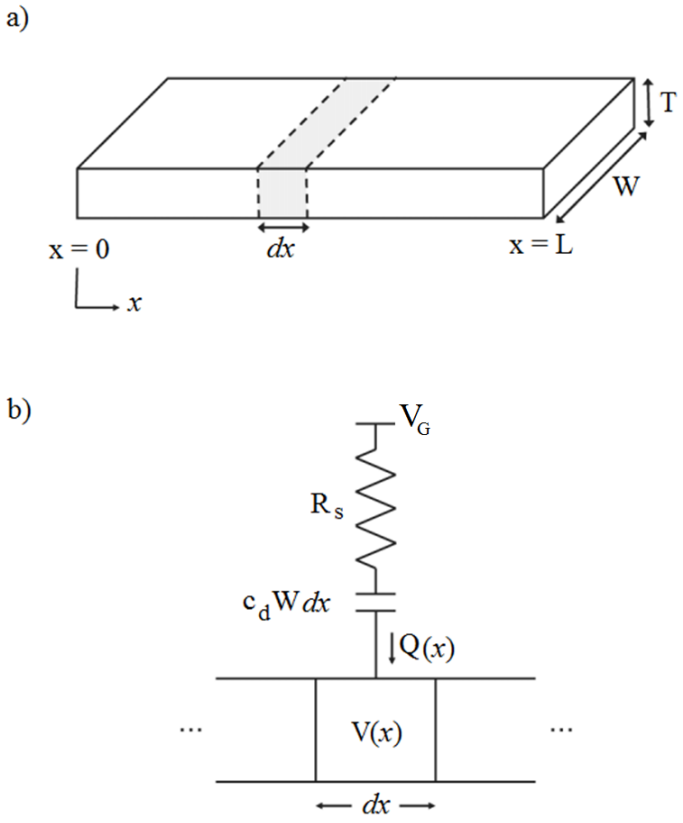

Figure 11 a) The organic semiconductor layer in which the source is located at x = 0 and the drain at x = L. b) Charge (Q) from the ionic circuit is coupled to the voltage in the electronic circuit at a position x along the organic semiconductor [31]

De-doping can take place anywhere within the organic layer and is not limited to regions close to the contacts. De-doping is possible mainly because of the high density of electronic charge within the organic layer that can act as a source or sink for the electronic charge that results from electrochemical de-doping. The governing equation for OECT characteristics at steady-state can be acquired by merging equations 4–7 into a new equation:

$$J(x) = \mathrm{q}\mu p_0 \left[1 - \frac{V(x)}{V_\mathrm{p}}\right] \frac{\mathrm{d}V(x)}{\mathrm{d}x} \tag{10}$$

V_p stands for the pinch-off voltage, defined by equation:

$$V_\mathrm{P} = \mathrm{q}p_0\, d/c_\mathrm{d} \tag{11}$$

Continuity requires the source-drain current density to be spatially constant at the steady-state. Equation (10) can be explicitly solved for different modes of operation (taking into account that $V_\mathrm{G} > 0$). In the first quadrant ($V_\mathrm{D} > 0$) there are two modes which can be distinguished (Figure 12). The first mode, when $V_\mathrm{D} < V_\mathrm{G,}$ de-doping will take place throughout the whole organic layer. By using the previous assumptions, equation (10) can be rewritten in terms of current and then solved explicitly as shown in equation (12). The source can be placed at $x = 0$ and the drain at $x = L$:

$$I = G\left[1 - \frac{V_\mathrm{G} - 1/2V_\mathrm{D}}{V_\mathrm{P}}\right] V_\mathrm{D} \tag{12}$$

Where G represents the conductance of the organic semiconductor layer expressed by the equation:

$$G = \mathrm{q}\mu p_0 W\, d/L \tag{13}$$

The second mode manifests in a case when $V_\mathrm{D} > V_\mathrm{G}$. De-doping will only occur in the region of the device where $V(x) < V_\mathrm{G}$. This mode can be expressed by the equation:

$$I = G\left[V_\mathrm{D} - \frac{V_\mathrm{G}^2}{2V_\mathrm{P}}\right] \tag{14}$$

The current is linear with drain voltage, and the onset of linear behaviour occurs when $V_\mathrm{D} = V_\mathrm{G}$.

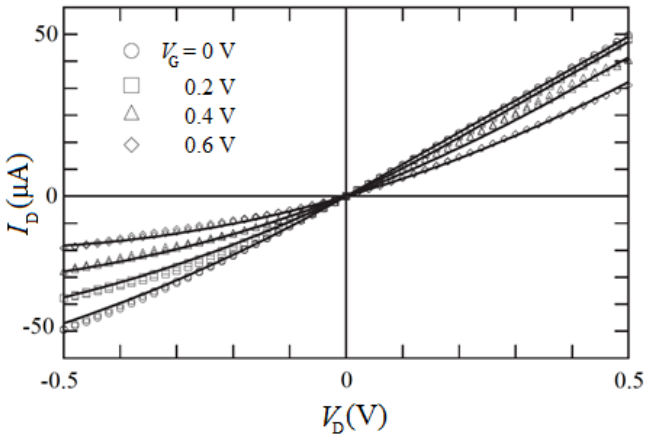

Figure 12 Experimental steady-state current-voltage characteristics (data points) for an OECT fitted to modeled steady-state current-voltage characteristics (solid lines) [31]

Entire de-doping of the organic layer is feasible in the third quadrant when $V_D < 0$. This is true in a case when the local density of injected cations is equivalent to the inherent density of dopant in the semiconducting material. Mathematically this is true if:

$$(V_G - V_D) \geq V_P \tag{15}$$

The critical drain voltage for saturation can be written as:

$$V_D^{sat} = V_G - V_P \tag{16}$$

Locally, the organic semiconductor will be depleted in close proximity of the drain contact. However, holes injected into this region will still be transported to the drain electrode. If the magnitude of V_D increases beyond V_D^{sat}, the extent of the depletion region will move slightly toward the source.

The position of the depleted region nearest the source contact will not change substantially with V_D. The current will continue to increase without saturation in the devices with short source-drain spacing [54]. In the case of long channels, for $V_D \leq V_D^{sat}$, the current will depend on the drain voltage at saturation for appropriate gate voltage as shown in the equation:

$$I = -G \cdot V_D^{sat^2} \cdot \frac{1}{2V_P} \tag{17}$$

3.4.4 OECT transfer characteristic

Tuning the transfer characteristics of the OFETs has been extensively studied and can be accomplished by modifying dopant or trap density and by using different gate electrode materials [55], [56]. Engineering the transfer characteristics in the case of OECTs, however, is not understood that extensively due to the inherently different operating mechanism of these devices.

Transistors convert a modulation in the gate voltage ΔV_G to a modulation in the drain current ΔI_D. The value that controls this conversion is the transconductance, which is defined in equation (2).

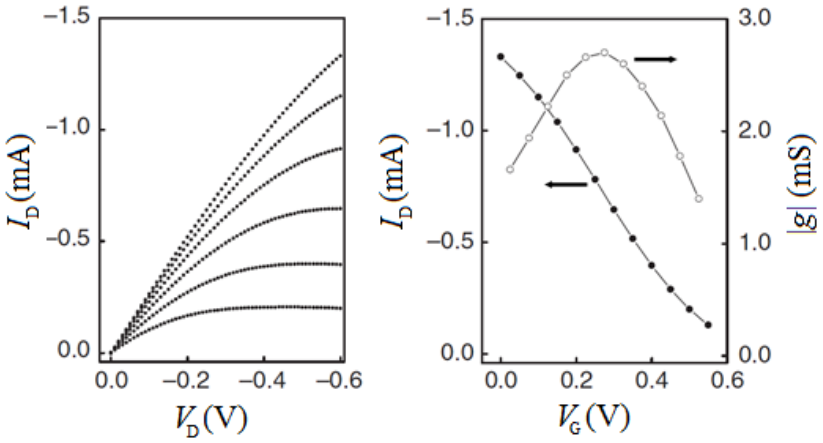

Figure 13 Steady state characteristics. (Left) Output characteristics for V_G varying from 0 (top curve) to 0.5 V (bottom curve) with a step of 0.1 V. (Right) Transfer curve and the associated transconductance [32]

The (Figure 13 Left) depicts the output characteristics of a typical OECT with negative drain bias V_D, and the gate bias V_G in the range from 0 to 0.5 V. These characteristics display the low voltage operation that is typical for electrolyte gated transistors. The corresponding transfer curve for $V_D = -0.6$ V and transconductance is shown in (Figure 13 Right).

The drain current decreases with gate voltage, which is consistent with operation in the depletion mode. This behaviour corresponds with the current understanding of the operation mechanism of OECTs.

The transistor output can be adjusted by modifying the channel volume. Fabrication of the thinner channel can result in a faster response. This is due to the smaller amount of ions which are needed in order to de-dope thinner channel. The drain current and its modulation upon gating decreases which results in the lower transconductance. In addition to these parameters, the gate electrode material and drain bias can also be used to modify transistor characteristics [32].

High transconductance in a compact device that shows a fast response time is desirable and represents a significant step towards less complicated amplifying transducers that offer more simple integration into systems for biomedical applications.

3.5 DIFFERENCE BETWEEN ORGANIC TRANSISTORS

In a FET, an organic semiconductor film (the channel) is separated from a metal electrode (the gate) by a thin insulating layer (the gate dielectric). The field-effect doping of the semiconductor is caused by a voltage applied between the gate and the channel. The result is the accumulation of a mobile electronic charge near the interface with the dielectric (Figure 14 Left). The charge in the channel is balanced by a sheet of charge at the gate electrode. The two sheets of charge form the two plates of a parallel plate capacitor. The amount of charge that is induced in the channel can be expressed as:

$$Q = C \cdot V_G \tag{18}$$

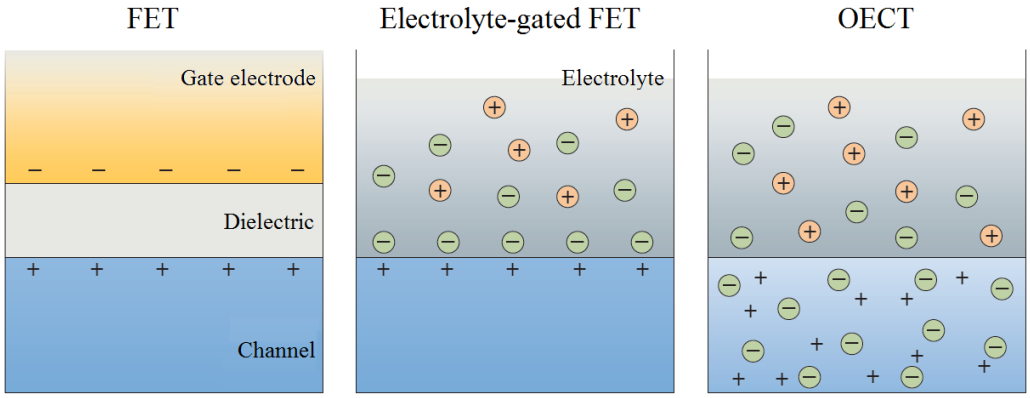

Figure 14 Organic based transistors, a difference between various kinds of organic transistors [34]

Where C represents the capacitance and V_G is the gate voltage. The capacitance is inversely proportional to the distance between the two plates. By minimizing the thickness of the dielectric layer, one can maximize the amount of induced charge and also the drain current of the transistor.

In an electrolyte-gated FET (Figure 14 Middle), a double-layer capacitor is created at the electrolyte-channel interface. A sheet of ionic charge in the electrolyte compensates the induced sheet of electronic charge in the channel. This setup represents a limiting case of FET in which the thickness of the dielectric is reduced to dimensions comparable with the ionic radius, which results in a high capacitance.

In OECT, ions penetrate the semiconductor, leading to changes in the doping state within the channel (Figure 14 Right). This configuration is not characterized by a parallel plate capacitance but rather by a volumetric capacitance (detailed in the next section). Compared to a FET of similar size, the same gate voltage induces a more electronic charge in the channel and thus a larger drain current in an OECT. However, the capacitance, in this case, is not caused by accumulation or depletion of the charge and creating the space charge regions. It is caused by the exchange of the charge carriers holes by positive ions and vice versa, while the total space charge remains zero in the bulk of semiconductor. The channel conductivity changes due to the different mobility of holes and ions.

3.6 VOLUMETRIC CAPACITANCE

The capacitance of PEDOT:PSS films has been reported to scale with the volume of the deposited layer as a linear function with zero offsets. Hence the measured value of capacitance per unit volume of PEDOT:PSS was established at $C^* = 39$ F/cm^3. The ionic charge injected from the electrolyte is evenly distributed within the PEDOT:PSS layer due to the linear dependence between capacitance and deposited volume [36]. No substantial ion accumulation is present at the interface between the polymer and electrolyte, which is confirmed by the zero offsets. PEDOT:PSS films behave as ideal volumetric capacitors. The capacitance per unit area c_d in a double layer that is built between electrons in a metal plate and a solvated layer of ions that accumulates on the plate under the influence of applied potential (Figure 15) is given by Helmholtz model equation:

$$c_{\mathrm{d}} = \frac{C_{\mathrm{d}}}{A} = \frac{\varepsilon \cdot \varepsilon_0}{L_{\mathrm{d}}} \tag{19}$$

Where A represents the area, $\varepsilon \cdot \varepsilon_0$ is the dielectric constant and L_{d} stands for the distance between the center of the ions and the metal plate.

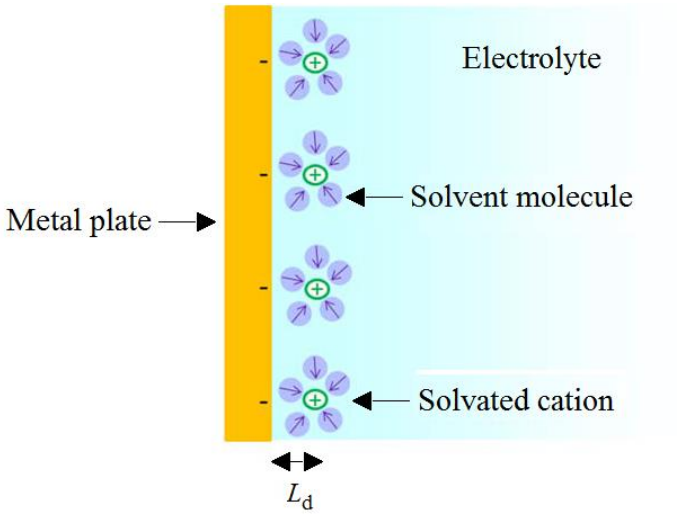

Figure 15 A simplified version of the double layer formed between a metal plate and hydrated ions [57]

Fiber parts with sulfonate anions in (Figure 16) represent the PSS chains, and the rest of the fibers with positive charge represent the PEDOT chains (carrying holes). Applying the bias results in the de-doping of the PEDOT:PSS channel, this is caused by the cations which are injected into the film from the electrolyte. At this point, the holes are extracted through a metal contact on the other side of the film. The capacitor is created by an injected cation and a sulfonate ion which gives rise to the volumetric capacitance. The film contains a defined number of "sites" consisting of sulfonate anion/hole pairs. An injected cation drifts to one of these sites and replaces (electrostatically speaking) the hole. In this case, the site density corresponds to the maximum number of sites that can host holes, which is the maximum hole density in the film [57].

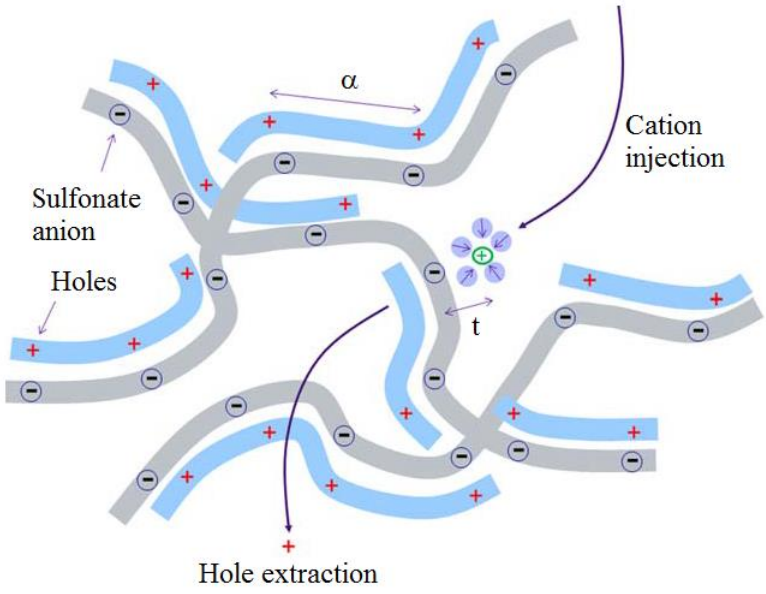

Figure 16 Representation of the de-doping process caused by ion injection, where α is the average site distance [57]

Organizing pairs of sulfonate anion/hole into the lattice with the average distance between two consecutive sites being α as shown in (Figure 17) we create a set of parallel planes. These are perpendicularly oriented to the surface of the film with the area:

$$A = w \cdot d \tag{20}$$

Where w represents the width and d is the thickness of the PEDOT:PSS layer. An electric double layer will be formed at every site after injection of cations from the electrolyte, and therefore each plane can be understood as a plate along which a double layer capacitor is formed similarly to one in (Figure 15).

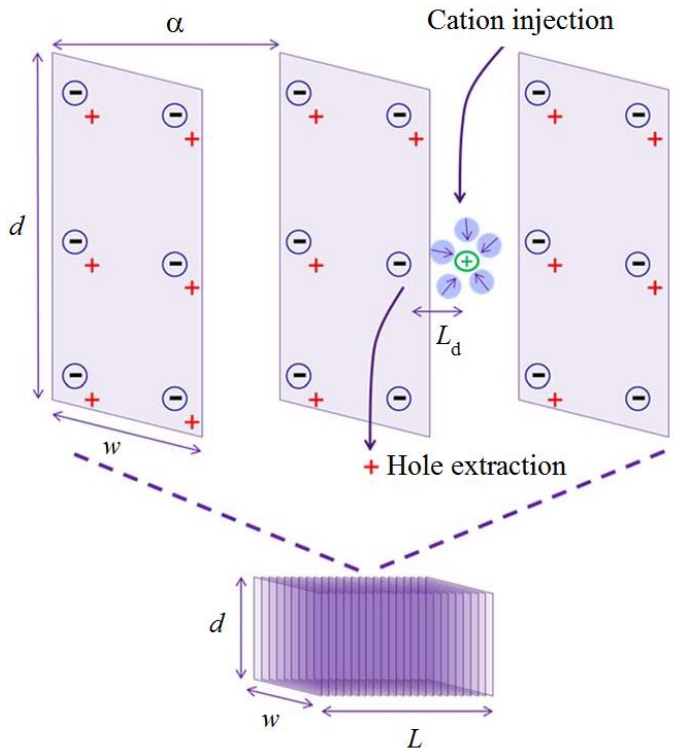

Figure 17 Schematic of a collection of plates against which ions accumulate up to form double layer capacitors [57]

The entire film can then be modelled as *N* capacitors in parallel:

$$N = \frac{L}{\alpha} \tag{21}$$

Where *L* stands for the length of the film. The total capacitance *C* is *N* times that of a double layer capacitor:

$$C = N \cdot \varepsilon \cdot \varepsilon_0 \cdot \frac{A}{L_d} \tag{22}$$

Therefore the capacitance per unit volume is given by:

$$C^* = c_d/\alpha \tag{23}$$

The equation (23) puts in context the capacitance per unit volume with the average distance between sites in the conducting polymer layer. In case of PEDOT:PSS in which one site is located every three to four thiophene rings [58] and a density of 1 g/cm^3, the site density can be estimated to approximately $1.93 \cdot 10^{20}$/cm^{-3}. The average distance between sites of PEDOT:PSS is then calculated to 1.8 nm. Equation (23) predicts a capacitance per unit volume of 6–57 F/cm^3 by fitting c_d values measured for organic electrodes, which is in a good agreement with the experimentally determined value in PEDOT:PSS.

The main drawback of the Helmholtz model is that it fails to capture the full complexity of real double layer, which includes the field and ion density dependence of capacitance.

Also, the distance L_d used in this model may be different from the situation outlined in (Figure 17) due to the different arrangement of ions in real PSS chain. The details of the ion arrangement can be approximated using effective c_d values, and in this case, the model allows the comparison of similar polymers.

From equation (23) we can determine that to increase volumetric capacitance, we should increase the density of sites in which sulfonate anions/holes pairs might occur. This could be accomplished by implementation of dopants that are smaller than PSS, which in turn could result in lower dilution of PEDOT. Another way, how to increase volumetric capacitance is to employ different polymers in which the number of charges increases to one per monomer instead of one every 3–4 monomers as in PEDOT. The utterly different method of how to improve the volumetric capacitance of conducting polymers is to mix them with nanomaterials with an intrinsically higher site density, for example, graphene. Recent measurements on polyaniline composites with graphene show volumetric capacitances on the order of hundreds of F/cm^3 [59].

3.7 OECT GEOMETRY

The volumetric character of the capacitance of the OECTs has a particular effect on a relationship between the transconductance and the device geometry (Figure 18). This is well illustrated by equation (2). From the previous research done by Rivnay et al. it can be deduced that the transconductance at saturation is proportional to the term *Wd/L* [36]. The response time τ is also given by the volumetric response of capacitance and therefore by the device geometry.

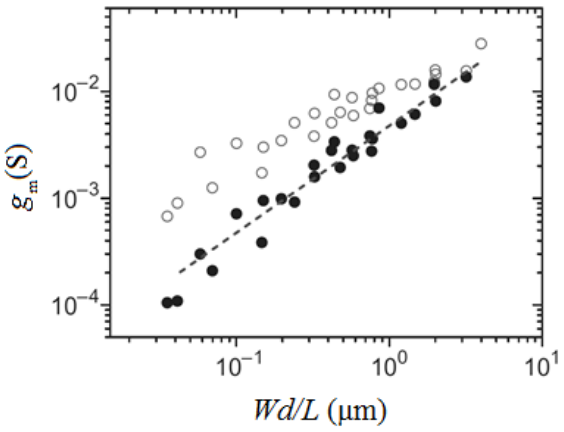

Figure 18 Dependence of the OECT transconductance on the device geometry. Open symbols correspond to peak transconductance, and solid symbols are the transconductance at saturation equation (2) [36]

The most prominent feature of OECTs which distinguishes them from classical FETs is the increase/decrease of transconductance with a higher/lower thickness of the channel respectively. This relationship was proven in devices with layer thickness up to 1 mm. Deviations from this relationship may be assumed for layers with a greater thickness with respect to second-order effects (for example, incomplete film hydration).

This makes OECTs excellent candidates for applications in which channel area is fixed by geometrical constraints, such as recording arrays, where devices must be tightly packed, and lab-on-a-chip systems, where space is very tight [36].

3.7.1 Vertical OECT

OECTs performance is often limited by utilizing rather large channels, which is caused by conventional fabrication methods together with the typical 2D layout. One way how to avoid these limitations is the production of vertical OECTs. PEDOT:PSS based OECTs in the vertical layout have been fabricated (screen printed) on plastic or paper substrates utilizing both sides to mediate connection [60]. Photolithographically prepared vertical OECT shown in (Figure 19) published recently is a state of the art device which can be produced on flexible substrates, achieves high amplification and signal-to-noise ratio. Although, the vertical OECT fabrication process relies on sacrificial layer lithography to pattern PEDOT:PSS channels [61].

The main difference between planar OECT and vertical OECT is the definition of the channel length. In planar OECTs, the length of the channel is given by the distance between a source and drain electrodes deposited in the one layer. The distance is given and ruled by the limitations of a fabrication process, typically no less than 5 μm. This also presents the limit in the device density (number of transistors fabricated in a given area). On the other hand, in the case of vertical OECT is the channel length L given by the thickness of the dielectric layer, which separates the vertically stacked electrodes (source and drain). This results in the possibility of spacing electrodes at only a few hundred nanometers apart (reported lowest value of $L = 450$ nm), therefore in maximizing transconductance of the device. Reported geometry normalized intrinsic transconductance (linear slope) was higher than 800 $S \cdot m^{-1}$ [61].

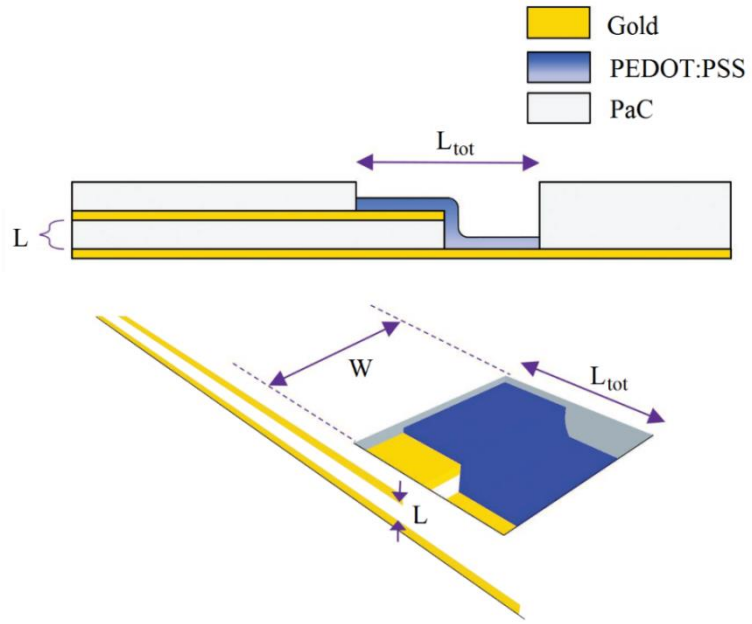

Figure 19 Vertical OECT. Cross-sectional view demonstrating how the parylene C layer thickness defines the channel length [61]

3.8 PEDOT:PSS IN OECT

The conductivity of PEDOT:PSS is given by its redox state. By exchanging ions with the solution it can go from oxidized (doped) to the reduced form (de-doped), and vice versa as shown in the equation:

$$\mathrm{PEDOT^+ : PSS^-} + \mathrm{M^+} + e^- \leftrightarrow \mathrm{PEDOT^0} + \mathrm{M^+ : PSS^-} \tag{24}$$

Where M^+ are positively charged ions in the solution. This reaction is directed by the gate-source and drain-source potentials. An electrolyte in contact with PEDOT:PSS supply positively charged ions (M^+) together with the ion conductivity needed to transport these cations in and out of the PEDOT:PSS. Upon application of a positive gate voltage (V_G), cations (M^+) from the electrolyte enter the PEDOT:PSS channel causing its de-doping according to the following equation (24).

The process is known as de-doping because the cations cause a decrease of the module of drain current (I_D). This is due to the lower concentration of holes available for conduction in PEDOT:PSS channel, as a consequence of cations incorporation into the PEDOT:PSS backbone. According to the equation (24) cations adsorbed in $PEDOT^+$:PSS^- cause a reduction of the oxidized $PEDOT^+$ and induces a decrease in conductivity upon reduction to $PEDOT^0$. This process is reversible, and when V_G is switched off, ion diffusion occurs from the PEDOT:PSS to the electrolyte. This, in turn, increases the number of conducting holes and consequently the drain current I_D (doping). This change is also detectable due to the fact that PEDOT in its oxidized state is light blue and almost transparent but on the other hand in the reduced state is dark blue. This effect is caused by the increase of the band gap energy of PEDOT. Thus a colour gradient from dark blue to nearly transparent will form.

In the case of OECT, with both the channel and gate made of PEDOT:PSS doping/de-doping occur in both of them. This model is shown in (Figure 20). The electrolyte enables under optimal conditions to the two adjacent layers transfer ions but no electrons. Charge transfer among the two neighbouring layers of PEDOT:PSS is mediated through the transport of M^+ ions as a result of the potential difference. Ions flow from the positively biased part via electrolyte into the negatively biased part and pair up with the PSS^- ions. The injected electrons render the negatively biased part non-conductive due to the reduction of $PEDOT^+$ to $PEDOT^0$. The positively biased part further oxidizes and becomes slightly more conductive. As a result, PEDOT:PSS devices are prone to the competitive behaviour of the gate and channel in absorbing ions from the solution [62]. If the reaction (24) takes place, it is fair to assume that the reaction (25) could take place also.

$$\mathrm{PEDOT^+\ PSS^-} + \mathrm{X^-} \leftrightarrow \mathrm{PEDOT^+X^-} + \mathrm{PSS^0} + e^- \tag{25}$$

Where X^- ions represent anions of the electrolyte paired initially up with M^+. This reaction takes place to some degree. The size of the X^- ions will largely decrease their mobility in the PEDOT:PSS layer. Thereby the possibility of the X^- ions entering the film, to complete the reaction (25) is diminished.

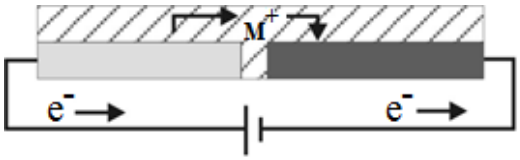

Figure 20 The patterned area illustrates the electrolyte layer on top and in between the two films of PEDOT:PSS [62]

In the OECTs doping and de-doping processes take place through the bulk of the conducting polymer at very low gate bias. The deficiency of a dielectric between the channel and electrolyte in OECTs permits ions to be injected into the channel and results in a response that is given by the volume of the active channel. The modulation of the current in these devices is corresponding to the portion of charge injected into the channel. OECT may be considered as the ideal ion to electron transducers owing to their exceptionally large transconductance [32].

PEDOT:PSS is suitable due to its high amplification defined by OECTs transconductance, short time response and wide frequency range, up to a few kHz used for ECG (Electro Cardiogram) recording. Dimensions of OECT can be optimized for the setting of the working point with maximum transconductance at zero gate bias [63].

3.9 PEDOT REPLACEMENT

PEDOT:PSS (Figure 21) and PEDOT:TOS (poly(3,4-ethylenedioxythiophene)-tosylate, a small molecule variant) (Figure 22) films in OECTs exhibits good properties and performance, although they also have some limitations. The complicated structure of PEDOT:PSS limits its use as a model system for structure-function relationships. Moreover, the bulky structure of PSS affects electrical properties due to its direct influence on the volume fraction of PEDOT in the film and hence its volumetric capacitance [57]. Therefore conjugated polymer structures with higher hole mobility than that of PEDOT has been extensively researched. These polymers often rely on the structure of fused thiophenes [64]. Regarding mechanical properties, Young's modulus of PEDOT:PSS is noticeably higher than that of most biological tissues [65]. This represents a significant limitation for applications in bioelectronics.

On the other hand, polymers or composites with more versatile bio-functionalization than PEDOT which is mostly cytocompatible are also necessary. Finally, from the perspective of solution processing, the acidity of PSS can cause corrosion of the print heads. Replacing of the PSS with less acidic polyanions, such as polymers containing (trifluoromethylsulfonyl)imide side groups, results in OECTs with a similar performance in terms of transconductance and response time as PEDOT:PSS based OECT [66].

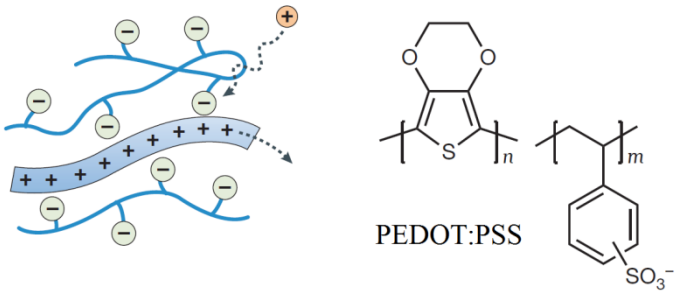

Figure 21 Polyelectrolyte-doped conducting polymer: PEDOT:PSS [34]

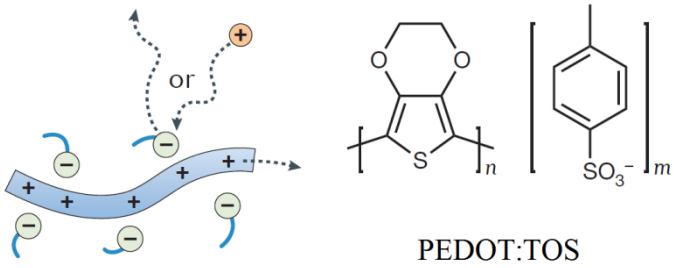

Figure 22 Small-molecule-doped conducting polymer: PEDOT:TOS [33]

Another approach is to remove PSS altogether and instead attach the ionic groups directly on the thiophene backbone by means of the side chains. These types of conjugated polyelectrolytes are semiconductive when the ion is compensated by a counter ion from the electrolyte, or can also be conductive when the ion is compensated by an electronic charge on the conjugated backbone.

High performing accumulation-mode OECTs have been studied utilizing a semiconductor based on polythiophene with a sulfonate group attached to the backbone with a hexyl chain: poly(6-(thiophene-3-yl)hexane-1-sulfonate) (PTHS) (Figure 23) [67]. Depletion-mode OECTs have been designed using a conductor based on PEDOT with a pendant sulfonate group (PEDOT‑S) (Figure 24) poly(4-(2,3-dihydrothieno-(3,4-*b*)-(1,4)dioxin-2-yl-methoxy)-1-butanesulfonic acid, sodium salt). Combining a semiconducting and a conducting conjugated polyelectrolyte provides OECTs that can be adjusted by balancing the stoichiometry of the channel [68].

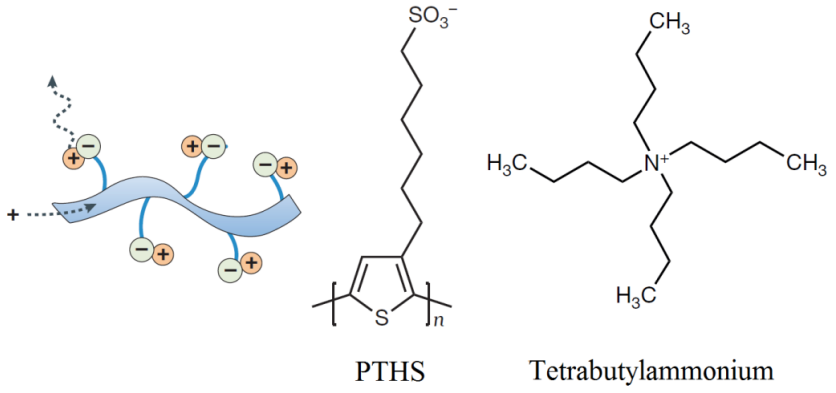

Figure 23 Semiconductive conjugated polyelectrolyte: PTHS together with a counter ion from electrolyte tetrabutylammonium [67]

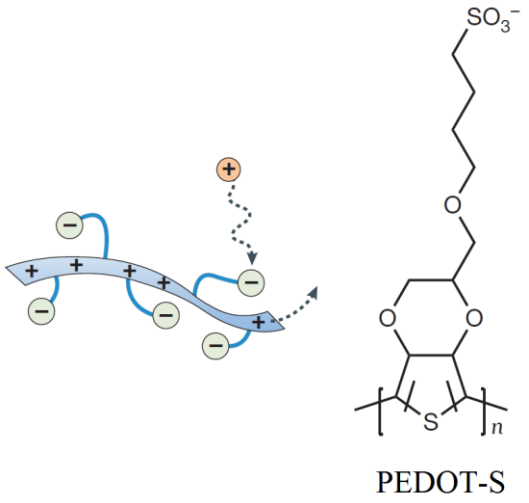

Figure 24 Conductive conjugated polyelectrolyte: PEDOT-S [68]

Completely another approach is based on the use of conjugated polymers with hydrophilic or ion-transporting side chains for the OECTs. OECTs developed from poly(2-(3,3´-bis(2-(2-(2-methoxyethoxy) thiophene) p(g2T-TT), polythiophene with glycolate side chains, display better transconductance values than PEDOT:PSS based OECTs of the same geometry [47] (Figure 25). Employing the same side-chain functionalization, an n-type copolymer poly((ethoxy)ethyl 2-(2-(2-methoxyethoxy ethoxy)acetate)-naphthalene-1,4,5,8−tetracarboxylic diimide co-3,3´-bis(2-(2-(2-methoxyethoxy)ethoxy)ethoxy)-(bithiophene)) p(gNDI-g2T), based on naphthalene-1,4,5,8-tetracarboxylic diimide and bithiophene units, has been used to design ambipolar OECTs [46] (Figure 26).

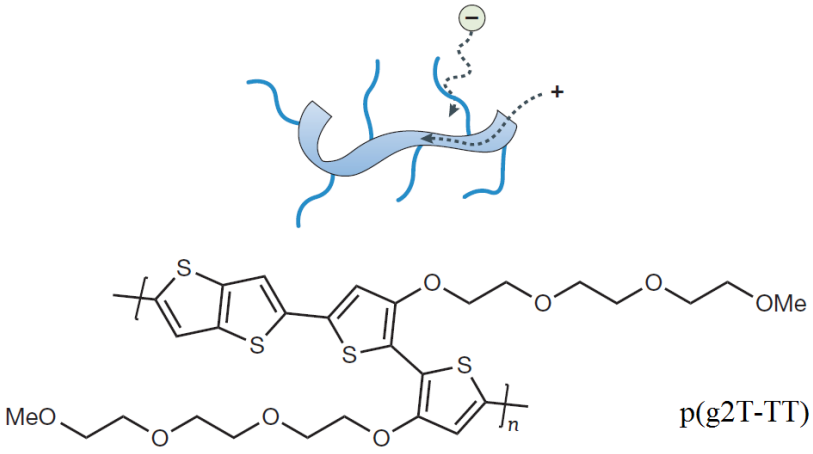

Figure 25 p-type semiconductive polymer p(g2T-TT) [47]

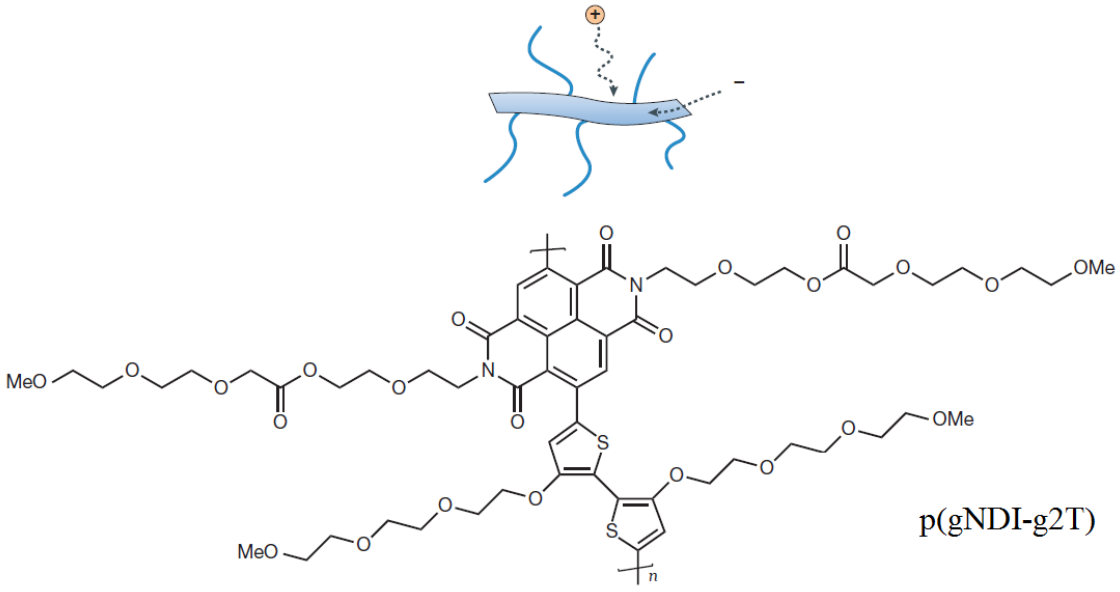

Figure 26 n-type semiconductive polymer p(gNDI-g2T) [46]

It has been also shown that mixing of PEDOT:PSS with poly(vinyl alcohol) (PVA) provides a tool for consecutive silanization. This allows for the covalent linkage of biological moieties onto the films without any detrimental effects on the electrical properties [69].

3.9.1 New materials benchmarking

The OECT channel must be able to execute two tasks at once, transport electronic charge (mobility μ) and store ionic charge (C^*). The transconductance of a particular material is determined by the product of the charge-carrier mobility and volumetric capacitance ($\mu \cdot C^*$) equation (2). For example, PEDOT:PSS with ethylene glycol has a $\mu \cdot C^*$ around 75 $F \cdot cm^{-1} \cdot V^{-1} \cdot s^{-1}$ [36], while p–type materials, such as p(g2T-TT) (Figure 25), can reach $\mu \cdot C^*$ of 228 $F \cdot cm^{-1} \cdot V^{-1} \cdot s^{-1}$ [47]. On the other hand, the n–type material like for example p(gNDI-g2T) (Figure 26), have a $\mu \cdot C^*$ of ~0.1 $F \cdot cm^{-1} \cdot V^{-1} \cdot s^{-1}$ [46]. Decoupling the charge carrier mobility and volumetric capacitance can clear out why one material performs better

than the other. The material mentioned above p(g2T-TT) has, for example, a higher $\mu \cdot C^*$ than PEDOT:PSS due to the six times higher volumetric capacitance, although it has similar hole mobility. Another material p(gNDI-g2T) has the highest reported C^* (~400 $F \cdot cm^{-3}$), but low electron mobility (~$1 \cdot 10^{-4}$ $cm^2 \cdot V^{-1} \cdot s^{-1}$). It seems that even the slightest hydrophilicity of studied materials has enormous benefit to ion transport and therefore is a requirement for OECT materials [70]. However, there are several hydrophobic self-doped conjugated polyelectrolytes and poly(3-hexylthiophene) which can also be used as channel materials in water-based OECTs [71]. Entirely another approach is to employ block copolymers or blends of semiconducting and ion-conducting polymers which can result in the separate control of ion and electron transport [72].

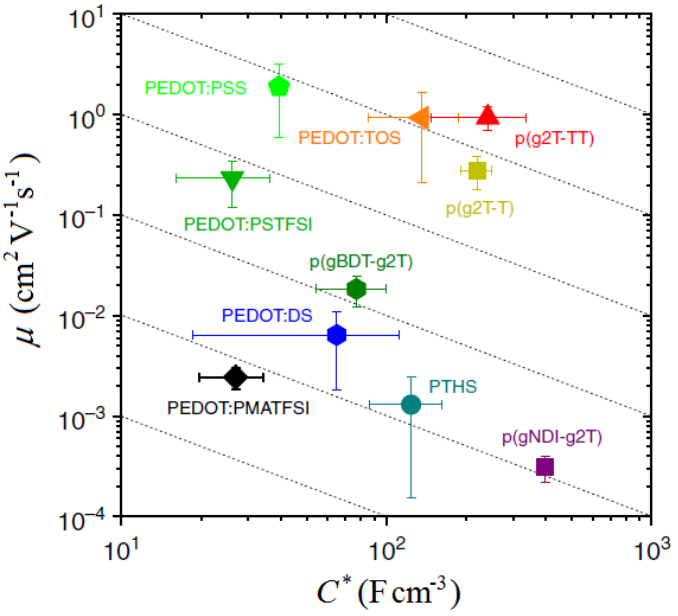

Figure 27 Benchmarking of previously reported materials, a map of mobility vs. volumetric capacitance [73]

3.10 OECTS PREPARATION METHODS

Plenty of different electrolytes, for example gels and solids [74], and the use of various gate electrodes, including traditional polarizable electrodes (such as Pt) and non-polarizable electrodes (such as Ag/AgCl) [75], as well as non-traditional gate materials such as PEDOT:PSS and various forms of carbon, have been used to fabricate OECTs [76].

Electrochemical polymerization was used to fabricate the first OECTs. It is a versatile method for incorporating biomolecules in conducting polymers. Nevertheless, the technique has fallen out of favour due to its dependence on growth from a conducting surface, which is hard to implement in OECTs.

An alternative method is vapour phase polymerization which can also incorporate different biomolecules in the channel of OECTs. In this process, a film cast from a precursor solution containing tosylate (TOS, the pendant group of PSS) moieties is exposed to EDOT vapor to yield the conducting polymer PEDOT:TOS [77] (Figure 22). The combination of different polymers in the precursor solution results in high-quality composites.

Composites of PEDOT:TOS with polyethylene glycol (PEG) have OECT performance comparable with that of pure PEDOT:TOS [78]. Also, gelatine can be incorporated into PEDOT:TOS without changing the electrochemical properties of the conducting polymer or its performance in OECTs . Such composites were found to support bovine brain capillary endothelial cell adhesion and growth in vitro, indicating a functional protein [79].

The type of material is frequently governed by the application or limitations dictated by fabrication methods. The components commonly used were pre-patterned Au source and drain electrodes on a glass substrate, an Ag/AgCl gate electrode and an aqueous solution of NaCl (sodium chloride) or KCl (potassium chloride) as the electrolyte.

3.11 OECT OVERVIEW AND STATE OF THE ART

Microfabricated planar OECTs prepared on rigid substrates published in the recent years exhibits excellent properties and have many benefits. The most prominent among these benefits is the possibility of preparation of sandwich structure, the usage of solid electrolytes [80] and the incorporation of diaphorase enzymes into the channel [81]. OECTs also show high performance in aqueous and non-aqueous electrolytes [82]. The usage of electrolytes as gating media results in enormous flexibility and variability in the OECTs device layouts. This feature is most prominent in terms of positioning of the gate electrode with respect to the channel. Different designs of OECTs with low operating voltage can be manufactured with respect to the gate, electrolyte, channel dimensions, and their relative positions. This is due to the inherent quality of the OECTs thanks to which the entire bulk of the active channel contributes to the charge transport. Hence, for the same channel length of the OECTs, a higher current can be supplied in comparison to the regular OFETs. Charges in the OFETs are transported along the thin sheet of accumulated holes or electrons, located at the semiconductor–gate dielectric interface. This generally results in very low currents in the devices with long active channels. Therefore the use of OFETs as drivers for power consuming components is often not possible. This can be an obstacle in the manufacturing process of the all-printed devices, where only long channels can be reliably printed in large quantities.

Moreover, OECTs can be manufactured using various depositions and patterning procedures on a large number of different substrates, including flexible and stretchable substrates. Development of various OECT structures that are based on PEDOT:PSS and other mixed ionic-electronic polymer conductors are nowadays possible due to the simple production processes. The OECTs with high performance and low operation voltages can be easily manufactured in high volume.

Microfluidic systems manufactured from polydimethylsiloxane (PDMS) [83], when coupled with PEDOT:PSS channels were reported to facilitate OECTs gating through a phospholipid membrane and cells [84].

Polyaniline, polypyrrole, and PEDOT can be grown between platinum electrodes (source and drain) as nanowires and remotely gated through an electrolyte [85]. For tissue culture applications (scaffolds) OECTs based on 3D porous sponges of PEDOT:PSS was developed and published [86].

Conventional and also unconventional methods and approaches in the field of printed electronics have been explored to manufacture OECT devices and circuits on various substrates, most notably plastic foils, and paper. These techniques include screen printing [87] and inkjet printing [88]. For example, vertical electrochromic display cells coupled with

lateral OECTs utilizing PEDOT:PSS were made using printing techniques. These devices were reported as actively addressed smart pixels and displays prepared on a paper substrate.

All screen printed OECT logic circuits, and shift registers have been manufactured on flexible substrate poly(ethylene terephthalate) (PET) [40]. An OECT device prepared on an ultrathin parylene substrate has been published and intended as a sensor in bioelectronics [35]. OECTs prepared on textiles also have their potential, primarily as an application in the field of wearable electronics. PEDOT based OECT was utilized in the preparation of gas sensors on Gore-Tex which served as a "breathable" substrate [89]. Other common types of fabrics, such as woven cotton and Lycra have been used as substrates for screen printed wearable sensors for sensing of the external biological fluid (sweat, saliva, urine) [90].
Several procedures have been explored to build OECTs and even complex circuits on individual or combinations of fibers such as paper, textiles, and polymers [91].

Other OECT applications include polypyrrole based OECT made on a nylon nanofibre as lead-ion detector [92], PEDOT:PSS soaked into natural cotton based OECT channel for saline sensing [93], or PEDOT:PSS in combination with nano-fibrillated cellulose (NFC) as a cladding layer around the fibers [94], Finally, a unique form factor has been achieved by making OECTs from PEDOT derivatives that are infused into living plants [95].

3.12 OECT APPLICATIONS IN BIOELECTRONICS

OECTs represent an essential part of research in the field of bioelectronics, healthcare, and biomedicine [10], [34]. OECTs can be interfaced with various cells, tissues and living organs in the study of their electrical properties (electrophysiology) to measure cell activity. Due to the local signal amplification, the activities of deep brain tissue or epileptic seizures can be observed using microfabricated OECTs, which can be placed directly on the brain of a living rat. In other published works, OECTs have been demonstrated in mediating the contact between the conducting channel and cerebrospinal fluid. This allows using OECTs to inject current and stimulate neurons locally [96]. Another example are OECTs coupled with OFETs which can record myograms with high temporal resolution in rats [97]. Epidermally applied OECTs can for instance record an electrocardiogram when placed on the human skin [98].

Further amplification of electrophysiological signals from the human brain, heart, and muscle employing OECTs has also been explored and published [99]. Moreover, PEDOT:PSS based OECTs can be sterilized by various procedures and therefore be used in clinical applications [100]. OECTs can also be used in association with cell cultures for drug testing and screening. For example, OECT microarrays prepared using photolithography can record action potentials from cardiomyocytes [101] and provide a spatial map of the electrophysiological activity [102]. Non-electrogenic cells (epithelial cells), their cellular health, barrier tissue formation or coverage can also be observed and recorded employing OECTs [103].

An integral part of these measurements is the cultivation of the cell monolayer which covers the channel. This, in turn, results in the formation of a barrier for ion motion and insertion into the channel altering the characteristics of the OECTs [104]. A similar basis can be employed to evaluate ion channels in lipid bilayers assembled on PEDOT:PSS channels [105]. Another advantage of PEDOT:PSS based OECTs is the possibility of simultaneous analysis of optical and electronic signals, due to the fact that PEDO:PSS is optically transparent in the visible part of the electromagnetic spectra [106]. Worth mentioning is also the fact that OECT can operate in various intricate environments, for example, milk where

they can detect the pathogens by measuring transepithelial ion flow [107]. OECTs can be coupled with 3D cell cultures to monitor their integrity and the effect of several toxic compounds on the cell structure. It is also possible to control the location of epithelial cells attachment on the channel by the variation in an applied drain and gate voltage [108]. This offers the opportunity not only to monitor but also control cell behaviour as was shown using porous sponge-like PEDOT:PSS scaffold able to sustain and control cell culture attachment[109].

For the detection of electrolytes and metabolites, such as lactate and glucose, biosensors based on OECTs can also be utilized in the form of transducers. These metabolites are of great importance for monitoring of human health. An integral part of the research is to develop OECTs with high selectivity to different moieties [110]. In the case of detecting metabolites, a variety of approaches have been developed. The selective interaction of a redox enzyme with the metabolite and the following transfer of an electron to the gate electrode is the fundamental mode of operation of OECTs for detecting metabolites.

The concentration of the metabolites depends and therefore can be determined by the subsequent change in the drain current. Various enzymes can be introduced and incorporated directly into the OECT channel or dissolved in the electrolyte [111]. Selectivity and sensitivity of the sensor can be further enhanced by the immobilization of the enzyme on the gate electrode directly [112]. Implementation of the OECTs with microfluidic systems is also common, and it has the potential to fashion multi-analytes sensory platforms [113]. Also, the implementation of the OECTs with textiles and fibers allows for their use in wearable electronics (for example analysis of sweat) [114]. Applications of OECTs have primarily focused on detection of analytes in saline solutions, but on the other hand examples of sensing in a breath, sweat, saliva have also been published [115]. OECT lactate sensors were for example demonstrated to measure the metastatic potential of tumour cells [116].

Fast-scan cyclic voltammetry is another field in which usage of OECTs can enhance and amplify measurements, resulting in more straightforward instrumentation compared to commercially available tools [117]. For example, OECTs allow for the selective detection of dopamine in the presence of an interfering substance. The sensitivities and limits of detection of these devices are comparable to, or better than, those obtained by various electrochemistry techniques (differential pulse voltammetry) [118]. The OECTs detecting the adrenaline has been reported [119] together with several studies in which OECTs have been shown to be suitable for the sensing of DNA (deoxyribonucleic acid) [120] and bacteria [121].

3.13 OECT IN CELL SENSING APPLICATIONS

The integration of OECTs with living cells has concentrated on the sensitivity to the changes in biological ion flux. This indicator is used for monitoring the integrity of mammalian cells. The flow of ions is regulated in tissues and dysregulation is often a sign of disease or dysfunction. OECTs have been used for sensing barrier tissue integrity and changes in paracellular ion flux.

Another way to measure the integrity of cells is to seed the cells directly on a device. This can be done using a top gate device structure, or side-gate structure. The top-gate structure was used by Lin et al. [120], and the device was able to detect cell attachment and detachment by shifting the V_g values. The constant operation of the OECT in cell culture together with the ability to facilitate cell growth was validated by Yao et al. [103].

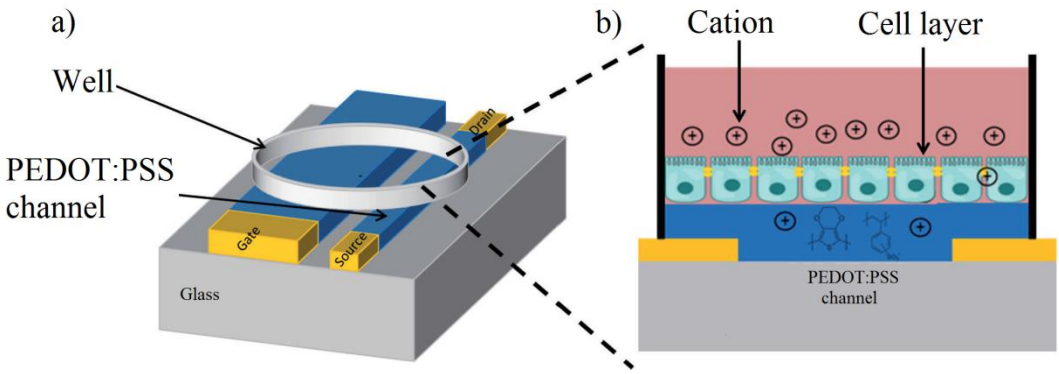

Figure 28 Schematic of the device which consists of a PEDOT:PSS channel and gate patterned onto a glass slide. Cells and media are contained inside a 3D-printed PDMS (polydimethylsiloxane) well [103]

Electrical stimulation and recording of neural activity and nerve tissue have provided invaluable information, mainly in the area of pathological and physiological functions of the body and brain.

The primary technique to record cardiac activity, electrocardiography (ECG), uses electrodes in contact with the skin which provides information about the normal function or abnormalities of the heart. Campana [98] fabricated OECTs on flexible, resorbable PLGA poly(lactic-co-glycolic) acid substrates for ECG recordings.

For the brain, there are three principal electrophysiology recording methods, electroencephalography (EEG), electrocorticography (ECoG), and stereoelectroencephalography (SEEG).

Khodagholy et al. [35] demonstrated and published OECTs for ECoG recordings that can be directly implanted. A conformal device, consisting of integrated electrodes and OECTs array, was placed on the surface of the brain of an epileptic rat. This demonstrated that OECTs could detect low-level activity that was poorly detectable with surface electrodes. This type of devices can be potentially implemented in curing epilepsy, where the identification of zones generating high-frequency oscillations or micro-seizures is critical for diagnosis. In a recent publication the use of an OECT to monitor cardiac rhythm, eye movement, and brain activity in a human volunteer have also been accomplished [99].

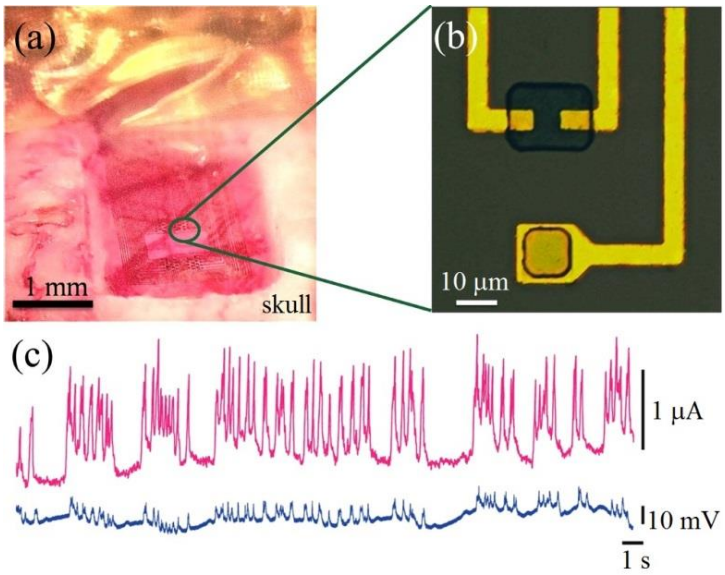

Figure 29 Optical micrograph of an array carrying OECTs and electrodes, placed over the somatosensory cortex (a) and detail of the transistor and electrode structures (b). Recordings from an OECT (top) and an electrode (bottom) show the superior recording ability of the former (c) [10]

Another example is the use of a 16-channel OECT array to map the field potential conduction of a primary rat cardiomyocyte monolayer [102]. Acquisition of the essential parameters in studying cardiac electrophysiology such as the heartbeat frequency, direction, and velocity of the propagation of FPs, the FP duration, and FP rise time has been recorded. These parameters are crucial to quantitatively describe the FP characteristics as was discussed previously.

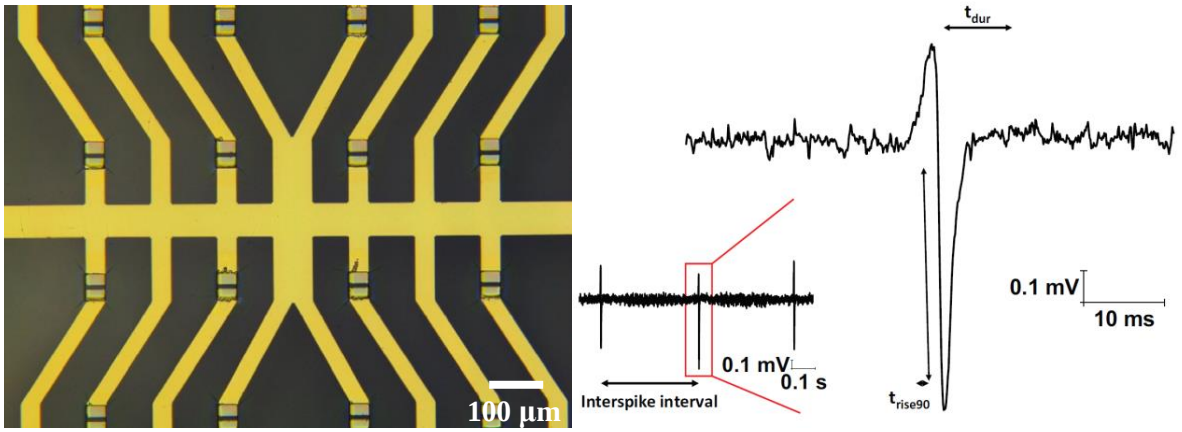

Figure 30(Left) lithographically fabricated multi-OECT device. (Right) The profile of a single field potential of measured cardiomyocytes [102]

4 METHODS

In this chapter, a brief description of the manufacturing methods used in this thesis to produce OECT devices is presented. Specifically described herein are photolithography techniques used to prepare the negative photoresist layer SU-8 and the two printing methods (inkjet printing and screen printing) used to produce conductive, semiconducting and insulating layers.

4.1 PHOTOLITHOGRAPHY

Photolithography (optical lithography or UV lithography) is a method used in microfabrication to pattern sections of a substrate. The fundamental concept behind photolithography is the selective exposure of a photosensitive polymer (photoresist), to ultraviolet light. Illumination of the photoresist through a mask leads to its selective exposure. The mask is usually made from opaque chrome feature on transparent quartz glass, or it can be a foil with precisely printed black patter for less demanding applications.

The exposed parts of the photoresist to the UV light results in the localized chemical reactions which take place within the photoresist and changes its solubility and creates distinct photoresist features. Photoresists are classified as either negative or positive, which depends on their solubility being either increased or decreased by optical exposure, respectively. Photoresists are usually processed in a liquid form, which is accomplished by the addition of solvents, and are coated as thin films onto suitable substrates by means of spin coating. During spin coating, the centrifugal forces exerted by a spinning substrate reduce its thickness to a proportional amount of spin speed and viscosity. Thicknesses ranging from tens of nanometers to hundreds of microns are routinely obtainable [122].

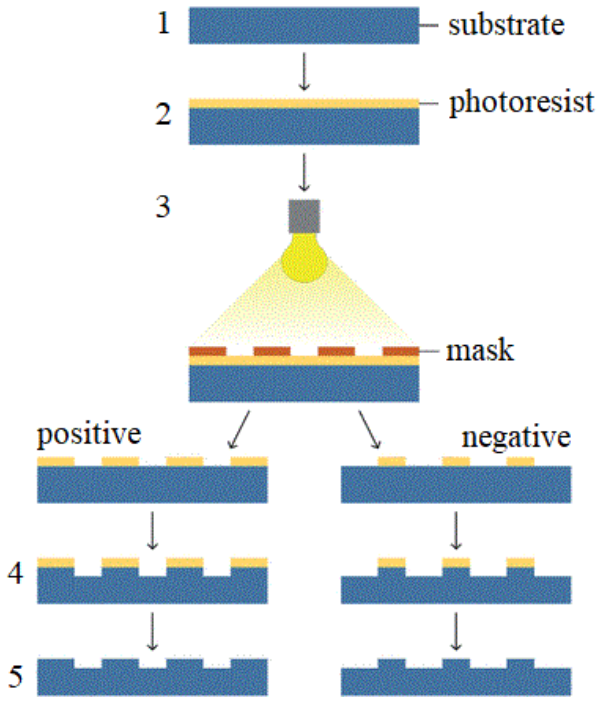

Figure 31 Schematic of the photolithographic process

4.2 PRINTED ELECTRONICS

Printed electronics is a collection of devices fabricated by a material printing technique. Creation of a wide variety of devices, such as transistors, diodes, detectors, sensors or simple conducting structures and circuits is possible using these techniques. Usually, these devices are realized by patterning of thin or thick structures on rigid or flexible substrates. An essential prerequisite is that printed materials are process-able in liquid form as inks.

Printed electronics is the most exciting and promising deposition technology for organic electronics since it takes advantage and employs all the characteristics of the organic molecules to create a competitive counterpart of inorganic electronics [123]. (Figure 32) shows a thorough comparison between printed electronics and conventional electronics properties and performances.

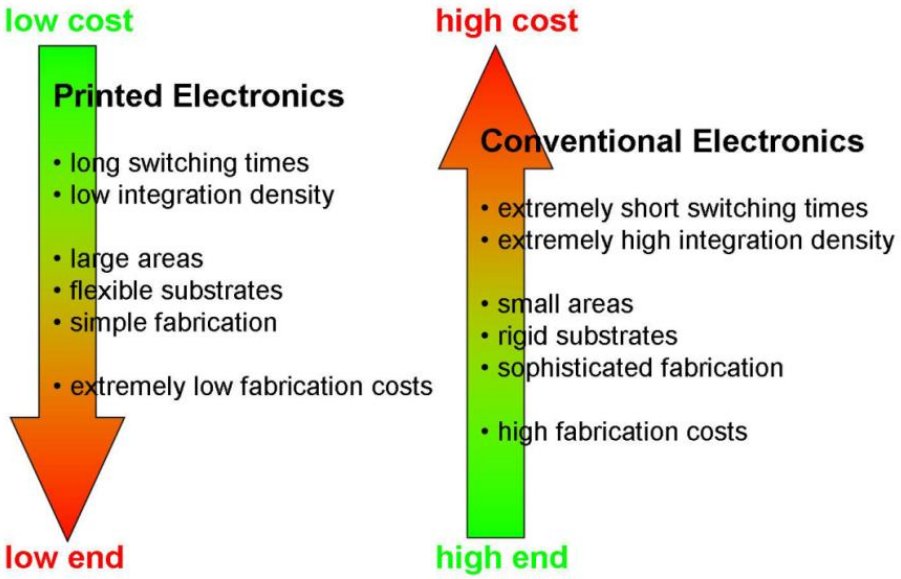

Figure 32 Comparison between printed and conventional electronics [123]

The technology of printed electronics brought the possibility to print biosensor on biocompatible polymer foils such as PET poly(ethylene terephthalate) or PEN poly(ethylene 2,6-naphthalate) enabling processing at higher temperatures. Basirico et al. [123] used inkjet printing technique for the production of fully printed lateral OECTs. Highest achieved amplification at zero gate bias was reached in the case of a much larger gate electrode area compared to the channel. Screen printed OECTs were manufactured in the work of Mannerbro [124] and printed hydrogel electrolyte was also used by many other researchers [6], [37], [62], [69].

Inkjet printing of organic electronic

The basic idea of inkjet printing is to print graphical images by firing tiny droplets of ink onto a substrate. The dry thickness of the inkjet film is given by the number of droplets deposited per area, the individual droplet volume and the concentration of material in the ink as shown in equation (26):

$$d_{\mathrm{dr}} = N_{\mathrm{dr}} V_{\mathrm{dr}} \frac{c}{\rho} \tag{26}$$

Where N_{dr} is the number of droplets deposited per area (cm^{-2}), V_{dr} is the volume of the droplets (cm^3), c is the concentration of the solid content in ink ($g \cdot cm^{-3}$) and ρ is the density of the material in the final film ($g \cdot cm^{-3}$).

The ways to create the droplets and to control where they land on the substrate is done via two main principles: continuous inkjet and drop on demand inkjet. The inks are required to be of low viscosity (4–30 cP) and in the case of continuous inkjet electrostatically charged. Frequently the inks are a complex mixture of several solvents, where one or more of the solvent components are quite volatile.

Inkjet printing can be used as a combined deposition and patterning technique in the area of organic electronics. It is a noncontact, maskless, relatively fast and cheap technique. Inkjet printing has found its best uses in combination with other patterning techniques.

Applications of the inkjet technique include studies focused on the printing of via-hole interconnections in polymer thin film transistor circuits [125], the modification of the sheet resistivity of PEDOT:PSS electrodes [126], the printing of polymer field effect transistors [127], the printing of capacitors and the printing of the pixels in polymer displays. Inkjet printing of conjugated polymers has been done primarily by using advanced inkjet printing devices. On the other hand, several research groups are using simple desktop printers for device fabrication as well.

Screen Printing of organic electronics

The first developments of screen printing date back to the beginning of the 20th century. It is a versatile printing technique that allows for full 2-dimensional patterning of the printed layer. Screen printing is used to manufacture several types of large graphics, posters and also writing on a printed circuit board. It is a simple technique compatible with various materials and surfaces of substrates.

The screen printing device is shown in (Figure 33), and it involves a screen of woven material (synthetic fiber, steel mesh) glued to a frame. The printing pattern is realized by filling the screen printing mesh with a coating emulsion. The area of the printed pattern is kept open, without the emulsion. A squeegee is used to force printing paste through the screen and thus to reproduce the printing pattern onto the substrate.

The wet thickness of the printed pattern is determined by the paste volume of the screen (V_{scr}), which represents the volume amid the threads of the screen and the thickness of the emulsion. The volume of the screen (V_{scr}) is measured in the volume of ink per area of the open screen (cm^3m^{-2}). Some factors, however, are influential on this such that not all the material in the screen is deposited. This varies with the force with which the squeegee is pushed into the screen, the snap-off distance, the speed of the squeegee and the viscosity of the solution. The equation (27) describes the final dry film thickness, d_{dr}, under the assumption that the material in V_{scr} is partially deposited and defined by the pick-out ratio, k_p.

$$d_{dr} = V_{scr} k_p \frac{c}{\rho} \tag{27}$$

Where c is the concentration of the solid material in ink ($g \cdot cm^{-3}$) and ρ is the density of the material in the final film ($g \cdot cm^{-3}$) [128].

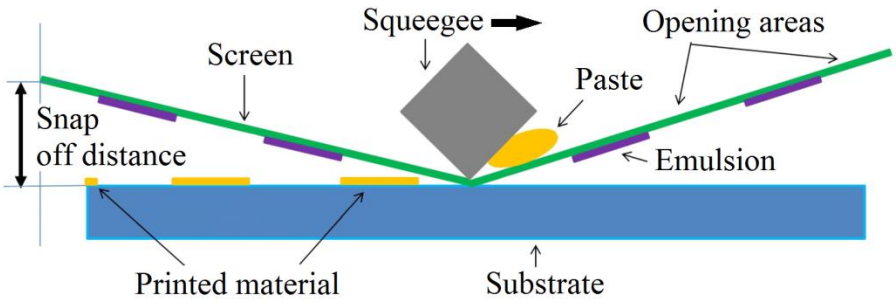

Figure 33 Scheme of the screen printing principle and the equipment involved [128]

Applications of the screen printing in organic electronics include studies done by Bao et al. [129], who have manufactured the first full screen printed organic field-effect transistor. They have found an appropriate organic semiconductor for solution processing, poly-(3-hexylthiophene) (P3HT), and have built on the work of Garnier et al. [130]. The results showed that the characteristics of the films involved were the same as those of spin-coated or cast films. The hole-transfer layer in OLEDs (organic light emitting diodes) has also been fabricated using screen printing technique by Jabbour et al. [131]. Screen printing of highly conductive PEDOT:PSS as an active layer or as conductive electrodes was done by several authors [6], [60], [124]. They all proved that screen printing might be a suitable patterning method for PEDOT:PSS.

5 EXPERIMENTAL PART

In this section, an overview of all materials and chemical used in this thesis is provided. Materials are categorized into separate groups according to their usage: substrates, conductive inks/pastes, semiconductive inks/pastes, dielectrics, and protective materials. A brief description of each material is presented together with relevant chemical and physical properties.

5.1 SUBSTRATES

PET and PEN foils were among the most used materials as actual substrates. Regular glass slides, patterned ITO glass and plain glass substrates from Ossila Ltd. (Solpro, Sheffield, UK) were also frequently used mainly for inkjet printing purposes. Kapton was also employed as a potential substrate, due to its high thermal stability which could be further exploited.

Polyethylene terephthalate

Polyethylene terephthalate (PET) is a thermoplastic polymer of the polyester family. Its monomer, the ethylene terephthalate, is shown in (Figure 34). It is used for a wide variety of applications, primarily as food and liquid container. It has interesting physical properties, such as a tensile strength between 190 and 260 MPa and excellent resistance to most solvents, except alkalines. It was purchased from Goodfellow (Cambridge Ltd., Huntingdon, UK) as a transparent and flexible biaxially-oriented film with two different thicknesses: 250 μm, 125 μm. Its nominal temperature working range is −40 to 115 °C. However empirical experience shows that it can be processed at a maximum of around 90 °C, since for higher temperature it undergoes irreversible deformation. This was an undesired effect for the fabrication of printed OECT based biosensor in which precise alignment of several layers is necessary. Another disadvantage was the high surface roughness, which is an undesired feature for the deposition of thin layers.

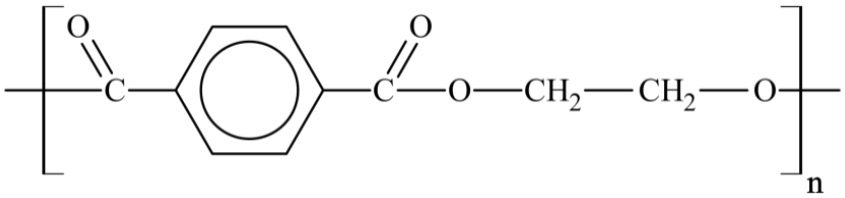

Figure 34 Polyethylene terephthalate monomer structure

Polyethylene naphthalate

Polyethylene naphthalate (PEN) is another thermoplastic polymer quite similar to a PEN. It is intended as a PET replacement, mainly when used as a substrate for flexible integrated circuits. Its monomeric structure is shown in (Figure 35). It has better chemical properties and physical properties since it can be heated up to 180 °C. However, practical experience shows that it can be safely and reliably processed at a maximum of 140 °C since for higher temperature it undergoes slight deformation. This was sufficient for our purposes. It was purchased from Goodfellow (Cambridge Ltd., Huntingdon, England) as a transparent and flexible biaxially-oriented film with two different thicknesses: 250 μm and 125 μm. It had a lower surface roughness in comparison to PET substrates and therefore was more suitable for deposition of thin films. Experimental tests confirmed its thermal resistance within the

required range. Thus it was chosen as the best candidate substrate for post-processing annealing of organic printed layers.

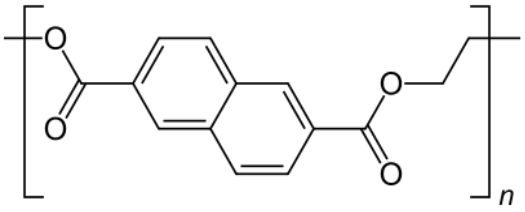

Figure 35 Polyethylene naphthalate monomer structure

Poly(4,4'-oxydiphenylene pyromellitimide)

Poly(4,4'-oxydiphenilene pyromellitimide) is a polyimide film developed by DuPont (DuPont Photopolymer and Electronic Materials, Wilmington, DE, USA) under the name Kapton shown in (Figure 36). Thanks to its wide temperature working range (−270 to 300 °C) and to its radiation resistance, it finds applications in many fields, such as coverage for aircraft, spacecraft, and x-ray instrumentation. It was purchased from Goodfellow (Cambridge Ltd., Huntingdon, England) as transparent and flexible yellowish films with thicknesses of 50 μm. Its yellowish tint and poor transparency in comparison with other substrates made it less desirable for our purposes.

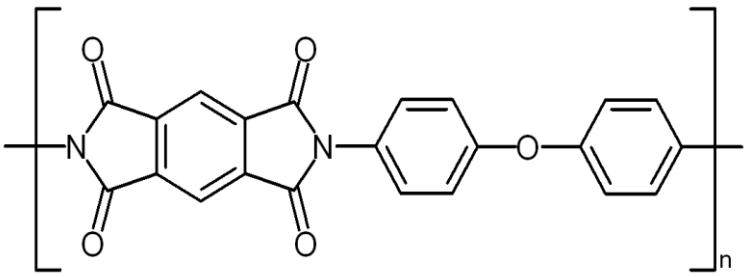

Figure 36 Poly(4,4'-oxydiphenylene pyromellitimide) monomer structure

Regular glass slides

Microscope slides made of soda-lime glass. Substrates were purchased from Knittel Glaser (Waldemar Knittel Glasbearbeitungs – GmbH, Braunschweig, Germany) with dimensions of 25 x 75 mm and a thickness of about 1 mm. These substrates were used mainly for determination of layer thickness of pastes and inks employing standard profilometric measurements.

Ultra-flat Quartz Coated Glass

Substrates made out of ultra-flat soda lime float glass coated with a 20 nm layer of synthetic quartz with superior wettability and flatness were used solely for inkjet-printed and lithographically prepared prototypes. Substrates were purchased from Ossila Ltd. (Solpro, Sheffield, UK) with a size of 20 mm x 15 mm and a thickness of 1.1 mm. The declared flatness was typically 50 nm per 20 mm with a roughness of 1 nm RMS (root mean square).

AKAFLEX® PENCL HT

Akaflex® is a copper laminate on a PEN film backing commonly used for manufacturing of flexible printed circuits. The electrolytic copper foil is laminated on one or both sides of the PEN foil. This substrate was purchased from Krempel Group with a thickness of copper foil 17 μm and thickness of the PEN film 50 μm (PENCL 2-17/50 HT 3) with PEN film of higher dimensional stability. PEN variant was chosen due to its superior stability at high temperatures compared to PET laminates.

5.2 CONDUCTIVE INKS AND PASTES

In this chapter all the conductive materials employed are briefly discussed, those deposited via inkjet printing, those deposited by screen printing and also spin coated materials.

Thermosetting silver conductor CB 115

This screen printing silver paste is used to fabricate circuitry, particularly on rigid printed circuit boards. The material is especially suited for printing fine conductor lines, and for establishing through-hole electrical connections. The conductor can be safely processed using conventional printed circuit board techniques after curing. The paste was purchased from DuPont (DuPont Photopolymer and Electronic Materials, Wilmington, DE, USA) with a sheet resistivity of 25 mΩ/square at 25 μm and recommended curing temperature of 150 °C. This paste was used with printer Rokuprint SD 05.

Flexible silver paste C2131014D3

This is a heat curable silver paste intended for screen printing usage and was purchased from Gwent (Gwent Electronic Materials Ltd, Pontypool, UK). The past is curable at a low temperature of 130 °C at which it forms a thermosetting polymer with a sheet resistance of 100 mΩ/square at 25 μm. This paste had excellent adhesion to substrates (PET, PEN, glass), good chemical and environmental resistance and was used with printer Rokuprint SD 05.

Heat Curable Carbon Paste C2050503P1

This low heat curable carbon paste is intended for screen printing usage and was purchased from Gwent (Gwent Electronic Materials Ltd, Pontypool, UK). It has excellent chemical resistance, excellent adhesion and works in high humidity environments. It cures at low temperature of 150 °C and forms a thermosetting conductive coating that combines good chemical, solvent, and abrasion resistance with a typical sheet resistivity of 50 Ω/square at 25 μm. This paste was used with the printer Rokuprint SD 05.

Metalon® JS-B25HV

An electrically conductive water-based silver ink designed to produce circuits on coated substrates including various photo papers, and inkjet papers. This ink was specially formulated for compatibility and stability with a Dimatix inkjet printer. This ink was purchased from Novacentrix (Novacentrix, Austin TX, USA) with a sheet resistance of 50 mΩ/square.

Silver dispersion (Sigma Aldrich 736465)

This ink is a dispersion of silver nanoparticles in triethylene glycol monoethyl ether with the 30–35 wt. % of silver particles. The ink was purchased from Sigma Aldrich (Sigma-Aldrich

spol. s.r.o, Praha, Czech Republic) with a specific resistivity of 11 μΩ·cm. The ink was used for inkjet printing on plastic films and glass slides with FUJIFILM Dimatix inkjet printer.

Metal® organic solution RL Au 010913 – 15%

Metalon® is a gold resinate solution in the stage of development purchased from Heraeus (Heraeus Precious Metals GmbH & Co. KG, Hanau, Germany). This ink was used with FUJIFILM Dimatix inkjet printer for preparation of printed circuits and electrodes.

5.3 SEMICONDUCTIVE INKS AND PASTES

In this chapter the semiconductive materials employed are briefly discussed, those deposited via inkjet printing and those deposited by screen printing.

PEDOT:PSS pastes

Re-dispersing PEDOT:PSS in high boiling alcohols such as ethylene glycol or 1,2propandiol is the primary technological process in the development and production of printing inks for screen printing techniques. Introduction of high boiling alcohols and consecutive evaporation of excess water leads to the formation of suitable dispersion (pastes). These have a sufficiently high viscosity and slow drying times required for screen printing [132] and have been demonstrated to yield a resolution down to 100 μm. In this thesis, two different pastes both purchased from Heraeus (Heraeus GmbH & Co. KG, Hanau, Germany) were used with properties shown in Table 1. The Clevios™ S pastes for screen-printing are typically used to print electrodes, especially transparent conductive ones that are used in many devices and technically advanced applications.

Table 1 Typical values for Clevios™ screen printing pastes

PEDOT:PSS	Viscosity dPa·s	Sheet resistance Ω/square	Solids content %
Clevios S V3	15–60	350–500	3
Clevios S V4	15–60	200–350	3

PEDOT:PSS inks

To rapidly prototype various device layouts and print even smaller features than those obtainable via screen printing, PEDOT:PSS inkjet dispersions which can be used with FUJIFILM Dimatix printer have been used. The composition of these inks have been modified, and therefore these dispersions show low viscosities and contain water solvent mixtures that dry slowly and avoid the clogging of the inkjet nozzles. In this thesis, two different ink all purchased from Heraeus (Heraeus GmbH & Co. KG, Hanau, Germany) was used with properties shown in Table 2.

Table 2 Typical values for high conductive Clevios™ inkjet grades

PEDOT:PSS	Viscosity mPa·s	Conductivity S/cm	Solids content %	pH
Clevios PH 1000	15–60	850	1–1.3	2–4
Clevios P Jet HC V2	5–20	300	0.8	2–4

5.4 DIELETRICS

In this paragraph the dielectric materials employed are briefly discussed, all the used dielectrics materials were deposited utilizing screen printing technique.

Sylgard® 184

Sylgard® 184 Silicone Elastomer Clear (polydimethylsiloxane elastomer, (Figure 37) is a two-part, room temperature and heat curing encapsulant. It is widely used as a protective coating for LED lighting, power supplies, transformers, sensors, amplifiers, and connectors. When liquid parts are thoroughly mixed (ratio of 10 to 1), the mixture cures to a flexible elastomer. This elastomer is fully suited for the protection of electrical/electronic applications. It provides flowability, flame resistance, and excellent dielectric properties. The Sylgard® 184 was purchased from Dow Corning® (Dow Europe GmbH, Praha, Czech Republic). The silicone elastomer can be employed in the temperature range of −45 °C to 200 °C with the curing time at 150 °C around 10 min. The volume resistivity of the deposited layer is $2.9 \cdot 10^{14}$ Ω·cm.

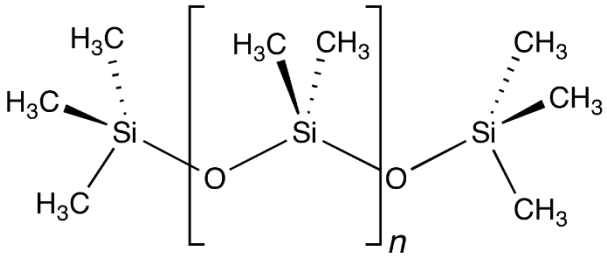

Figure 37 Polydimethylsiloxane monomer structure

SU-8 photoresist

SU-8 is a frequently used epoxy-based negative photoresist. Negative refers to a photoresist in which the parts exposed to UV become cross-linked, while the remainder of the film remains soluble and can be washed away during development. SU-8 was produced by IBM in the late 1980s [133] and is nowadays extensively used in the manufacture of microstructures in electrowetting display and microelectromechanical systems (MEMS) [134].

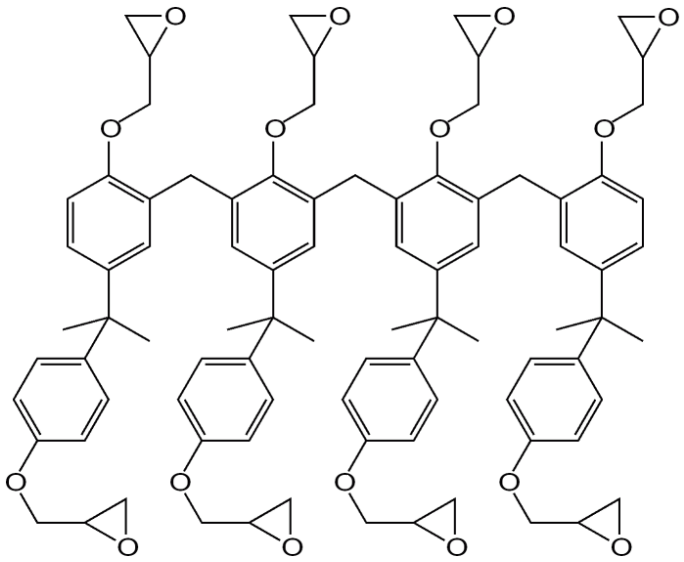

Figure 38 Structure of the SU-8 molecule

SU-8 in the form of a viscous polymer can be spun, printed or spread over with a thickness from below 1 μm up to above 300 μm and used to pattern high aspect ratio structures. Its maximum absorption is in the ultraviolet region with a wavelength of the i-line: 365 nm. When exposed to the UV light SU-8's long molecular chains cross-link causing the polymerization of the material. SU-8 is composed of Bisphenol A Novolac epoxy that is dissolved in an organic solvent gamma-butyrolactone (GBL) or cyclopentanone (Figure 38). SU-8 is mainly used in the fabrication of microfluidics and microelectromechanical systems parts. It is also biocompatible material [135] and is often used in bio-MEMS for life science applications [134]. For the purposes of this thesis, four different thicknesses of the SU-8 (0.5 μm, 7 μm, 15 μm, and 25 μm) were purchased from MicroChem Corp. (Westborough, MA, USA).

The typical and most popular application method of SU-8 is spin-coating. Nevertheless, this approach is somewhat unsuitable for large areas due to edge bead effects [136] and geometric defects due to the solvent evaporation [137]. Increased material consumption renders this technique inadequate for large area production. Screen-printing of SU-8 was reported by J. Klavins et al. [138] to address the aforementioned problems.

5.5 ELECTROLYTE

Phosphate-buffered saline (PBS) is a buffer solution generally used in biological research. This water-based salt solution consists of disodium hydrogen phosphate, sodium chloride and, in some formulations, potassium chloride, and potassium dihydrogen phosphate. The buffer helps to preserve a constant pH value. The ion concentrations and the osmolarity of the solutions closely mimic those of the human body [139]. PBS solution was used with phosphate buffer concentration of 0.01 M and a sodium chloride concentration of 0.154 M and the *pH* 7.4. PBS was purchased from Sigma Aldrich (Sigma-Aldrich, Praha, Czech Republic) and was used as an electrolyte for testing of all OECT sensor and cell culture cultivations.

5.6 EQUIPMENT

In this part, a brief description of the equipment used in this thesis is given. More specifically the printer used in prototyping and manufacturing of OECTs is presented, while in the next section the measuring equipment used to record and interpret the results is described.

Dimatix Materials Printer DMP2831

The inkjet printer used in this thesis for the fabrication of OECTs was the Dimatix Materials Printer DMP2831, a piezoelectric drop-on-demand printer purchased from Fujifilm (Dimatix Inc., Santa Clara, CA, USA). It is a materials deposition system designed for micro-precision jetting of functional fluids onto a variety of surfaces, including plastic, glass, ceramics, and silicon, as well as flexible substrates from membranes, gels and thin films to paper products. All the description below is a summary of the DMP2831 main functionalities. The printer is composed of several main parts, as schematically shown in Figure 39.

Print Carriage is the part of the printer in which the cartridge (reservoir with the ink) is located. The cartridge is a piezo-driven jetting device with an integrated reservoir and heater with usable ink capacity up to 1.5 ml. It is compatible with many water-based, solvent, acidic or basic fluids. The cartridge-based inkjet print head with 10 pl or 1 pl drop volumes consist of 16 nozzles with a spacing of 254 μm aligned in a single row. It is designed for high resolution, non-contact jetting of functional fluids in a broad range of applications. Deposition of features as small as 20 μm is achievable using 1 pl cartridge [140].

Print Carriage is equipped with a fiducial camera, which serves for the alignment using reference marks and the examination of the printed patterns with the precision in the order of micrometers. It allows positioning of a print origin or reference point to match substrate placement, provides a measurement of features and locations and matching drop placement to the previously patterned substrate. Horizontal movement of this element over the substrate represents the basic operation of the printer and allows for printing of detailed and complex patterns. The vertical movement and hence the distance of the substrate and printing nozzles is controlled by the motion of the platen.

Drop Watcher plays an essential role in the calibration and optimization of printed inks using a Dimatix printer. Optimization of the printing parameters is a necessary primary step for satisfactory printing results. Drop Watcher is composed of a camera which serves for observation and immediate modification of ejected drops through the printing head. It is used for identification of misfiring or clogged nozzles and adjustment of the velocity and frequency of the drops. It also supports a retaining container for excess used ink.

Vacuum platen is a positionable metallic plane in which the substrate is fixed during the printing process. Its temperature can be adjusted from ambient temperature up to 60 °C. In most cases, the substrates are too thick for the vacuum to securely hold them in place and therefore an additional adhesive tape is often used. Printable area of substrates with a thickness of fewer than 0.5 μm is 210 mm x 315 mm and in the case of substrates with a thickness of 0.5 μm to 25 μm 210 mm x 260 mm with repeatability of ± 25 μm.

Cleaning Station consists of a single cleaning pad and a small pressure tube. It is used for the cartridge maintenance before, during and after the printing process [140].

The Dimatix printer is equipped and controlled using supplied software. The software monitors all the printing steps and allows the setting of all critical parameters: platen temperature, cartridge height, cartridge temperature, piezo drive waveform, nozzle voltages,

cleaning cycles and other substrate and cartridge related settings. It is also used for the management of the printing patterns, both utilizing a pattern editor and by importing external images (DXF, Gerber, GDSII, OASIS) and converting them to printable files (Bitmaps).

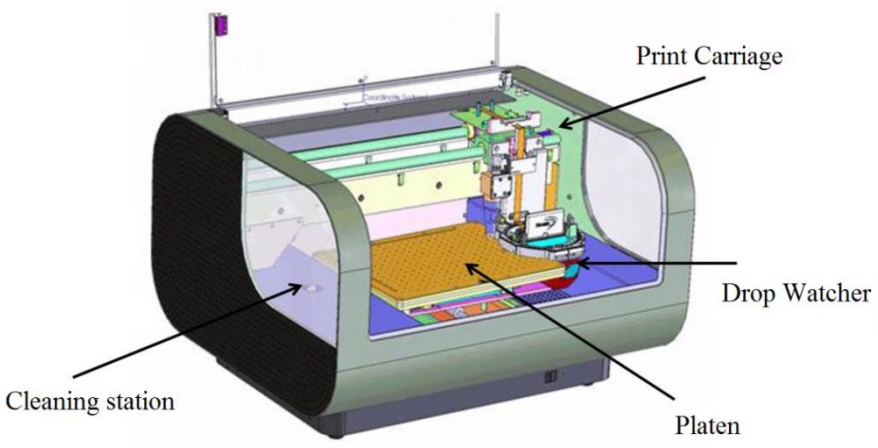

Figure 39 Schematic of the Fujifilm Dimatix Materials Printer [140]

Rokuprint SD 05

Rokuprint SD 05 is a universal semi-automatic screen printing machine (Figure 40) for flat printing with the maximum print format of 320 x 220 mm. It is equipped with a pneumatic thrust mechanism with independently adjustable print and backup spatulas. The printing process can be controlled using programmable printing parameters such as printing speed, starting position, and adjustable squeegee pressure and snap-off distance [141].

Figure 40 Screen printing machine Rokuprint SD 05 [141]

DektakXT Stylus Profiler

There are two types of profilometers: stylus and optical ones. The stylus profilometer uses a physical probe to scan the surface, while the optical profilometer uses light, routinely laser light. In this thesis, the stylus profiler was employed for the thickness assessment of the deposited layers on both glass and foil substrates. The DektakXT stylus profiler is a widely used instrument in the measurement of thin film thickness, surface roughness, waviness, and topology. It consists of a fixed detector (stylus probe), which maps the surface of the sample and the sample stage, which is movable. The radius of the stylus is in the range of 20 nm to 50 μm. The measurement is done mechanically while employing a feedback loop that monitors the force between the probe and the sample. The tracking force of the stylus can be set in the range from less than 1 to 50 mg [142].

Stylus probe scans the surface of the sample during measurement and records the changes in the height, and thus generates analog input. This input is converted into a digital signal which is afterward analysed. Horizontal resolution can be adjusted by adjusting the scan speed. The stylus profilers require force feedback and physical contact with the surface and therefore are quite prone to damage soft and sensitive substrates. Also, the stylus probe can be affected by contaminants from the substrate [143].

Keithley 2400 series SourceMeter

Keithley 2410 Source Measure Unit (SMU) Instruments is designed for test applications that require directly coupled sourcing and measurement. SourceMeter SMU instrument is a highly stable DC power source and instrument-grade 6½-digit multimeter. The power source features incorporate low noise, precision, and read-back. This device can operate as a voltage source, a current source, a voltage meter, a current meter, and an ohmmeter [144]. The Keithley 2410 electrometer with the control software LabTracer 2.9 was used as a core of electrical measurements of OECTs. The electrometer contains in series the controlled power supply for setting proper V_D voltage.

Oscilloscope Tektronix TDS 2024B

Tektronix TDS 2024B is an oscilloscope with 4 channels, 200 MHz bandwidths and sample rate of 2.0 GS/s with removable data storage via front USB port. This oscilloscope was used mainly for the investigation of the OECTs channel current response to the simulated signal of electrogenic cells [145].

6 RESULTS AND DISCUSION

In this section, all the inkjet printing, screen printing and lithographic processes that were developed in our lab are listed together with detailed preparation procedures and measured results.

6.1 INKJET PRITENTED 24-WELL MICROPLATE

SensoPlate™ is a sterile microplate without bottom containing 24 wells with a flattened, raised ring to reduce cross-contamination, chimney well with alphanumeric coding made out of polystyrene. These platforms were used as templates for the development of OECT sensors. Microplates are routinely used for single molecule detection, fluorescence correlation spectroscopy, and confocal microscopy. SensoPlate™ has high optical clarity, low auto-fluorescence, and standard plate geometry – ANSI/SBS Standards (127.76 x 85.48 mm) with working volume per well of 0.5 to 1.5 ml (Figure 41). Micropaltes were purchased from Greiner Bio-One® (Greiner Bio-One North America Inc., Monroe, North Carolina, USA). Our goal was to print one OECT sensor into each well. Our prototypes made using inkjet printing and screen printing were developed to mount into these microplates and are described in the following chapters.

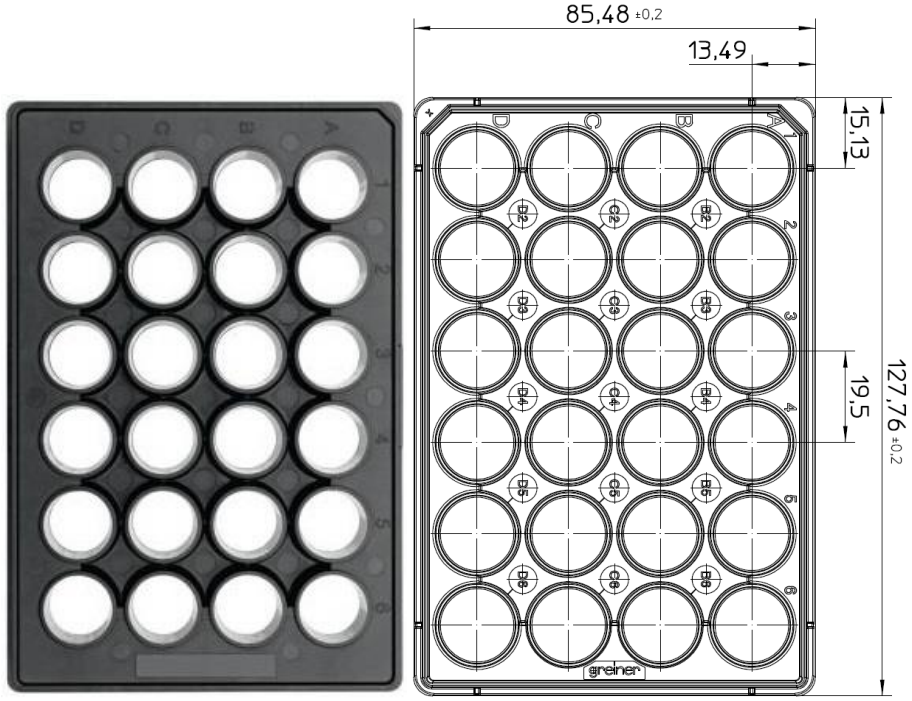

Figure 41 SensorPlate™ microplate with 24 wells, all dimensions are in mm

Fabrication

Inkjet printing of conductive and semiconductive layers was the necessary task to perform in order to manufacture the first prototypes of OECTs. Firstly, several versions of all planar OECT motives were designed. Then a matrix of 24 devices was put together to fit into the SensoPlate™ (Figure 42). First prototypes employed simple electrode system printed using silver ink and a semiconductive part printed with PEDOT:PSS.

In this section, for each ink, the general manufacturing process and a description of the printing is described. The optimization processes needed to produce functional devices have been presented in this chapter too.

The first OECT prototypes were designed to have channel dimensions of 1 cm x 500 µm. The gate electrode with dimensions of 1 cm x 2 mm was set 500 µm apart from the channel (Figure 42 Left). Patterns were designed with AutoCAD and subsequently converted to bitmaps with the required resolution. Both the channel and gate electrode were inkjet-printed with PEDOT:PSS. Circuits printed out of the silver ink were placed outside of the cell cultivation area sealed by the silicone elastomer to avoid contact with the PBS and cells. The circuitry was terminated with five contacts compatible with standard connectors (Figure 42 Right). Transparent and flexible 150 µm thick PET foil was used as a substrate. Prior to the usage of the substrate, the cleaning by the two consecutive ultrasonic bath treatments (15 min each) first in Neodisher® LM3 surfactant (Chemische Fabrik Dr. Weigert GmbH & Co., Muhlenhagen, Germany), and then in deionized water was performed.

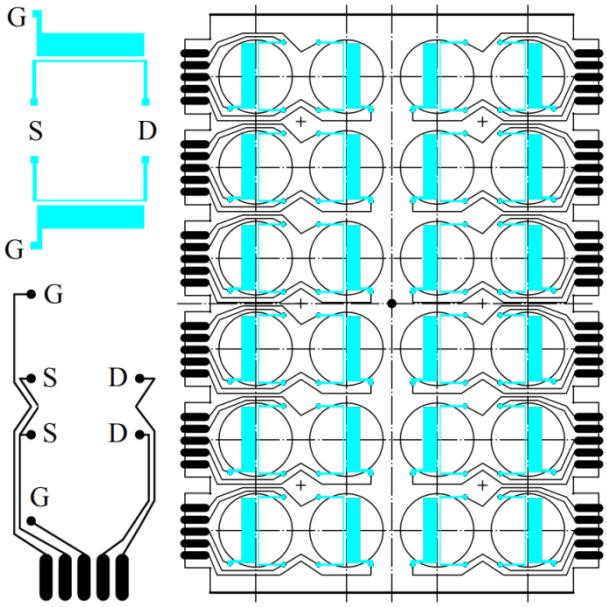

Figure 42 Designed patterns used to print 24 OECT arrays. Left: Close up of printing design of individual OECT sensors. Right: Envisioned 24well microplate array layout

Metalon® JS-B25HV

To print designed conductive contacts we started with printing of Metalon® JS-B25HV Nanosilver ink. It is an aqueous dispersion commonly used for Dimatix printers. The ink was thermally sintered on glass and corundum substrates (Figure 43) to determine the lowest possible curing temperature that would produce sufficiently conductive layers.

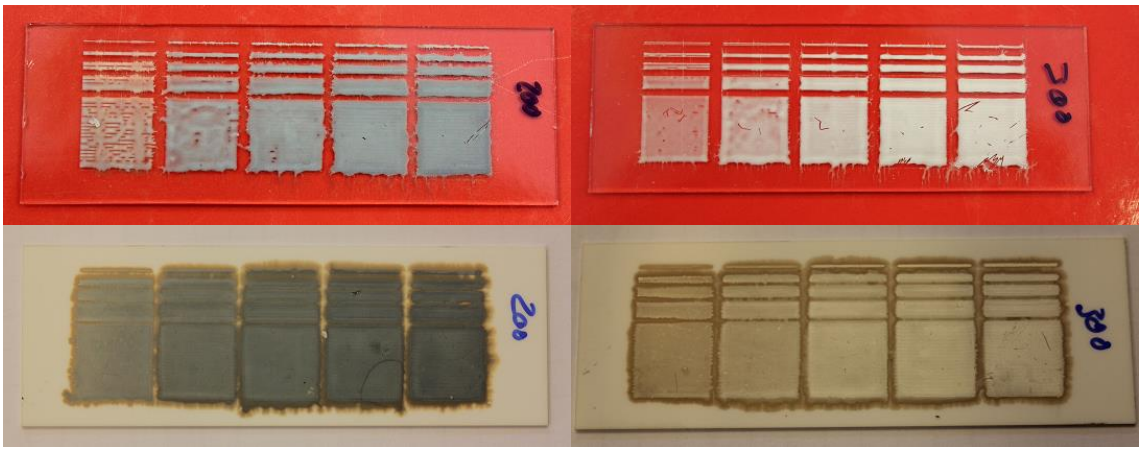

Figure 43 Thermally sintered ink Metalon® JS-B25HV at glass substrates (top) and corundum substrates (bottom) at temperatures of 200 °C and 300 °C, respectively

(Figure 43) shows Metalon® JS-B25HV ink thermally cured at glass substrates (top) at temperatures of 200 °C and 300 °C, respectively. Bottom images show silver ink cured at corundum substrates at 200 °C and 300 °C, respectively. Conductivity measurements show that thermal curing at 200 °C is insufficient (both samples at glass and corundum substrates were nonconductive). The ink was sufficiently cured at 300 °C with resistance values shown in Table 3.

Table 3 Sheet resistances of Metalon® JS-B25HV ink cured at 300 °C

Number of printed layers	**Glass (mΩ/Square)**	**Corundum (mΩ/Square)**
1	-	-
2	815 ± 25	770± 20
3	150 ± 15	91 ± 10
4	73 ± 5	72 ± 5
5	54 ± 5	54 ± 5

Thermal sintering of Metalon® JS-B25HV ink was impossible to use with substrates made of PET or PEN due to its high sintering temperature (at least 300 °C for sufficiently conductive pathways). The sheet resistance of Metalon® JS-B25HV ink as declared in the datasheet was reliably obtained with a higher number of printed layers (Table 3). This was mainly due to the non-compact and inhomogeneous character of the layers at a low layer count (Figure 43). We also explored the possibility to sinter Metalon® JS-B25HV ink using photographic flashes with energies ranging in power from 400 Ws to 1200 Ws. This method of sintering was also insufficient, and the printed layers were non-conductive. Effect of flash sintering can be seen in SEM (scanning electron microscopy) images with a resolution of 40x, 2000x, 10 000x and 40 000x, respectively (Figure 44). From these, it is clear that the layer is inhomogeneous and incomplete which renders it non-conductive. Moreover, the PET and PEN substrates started to melt using flashes with higher energies. Therefore, we decided not

to work with Metalon® JS-B25HV ink because we had not found a simple way to properly sinter it that would be suitable for the use with plastic substrates.

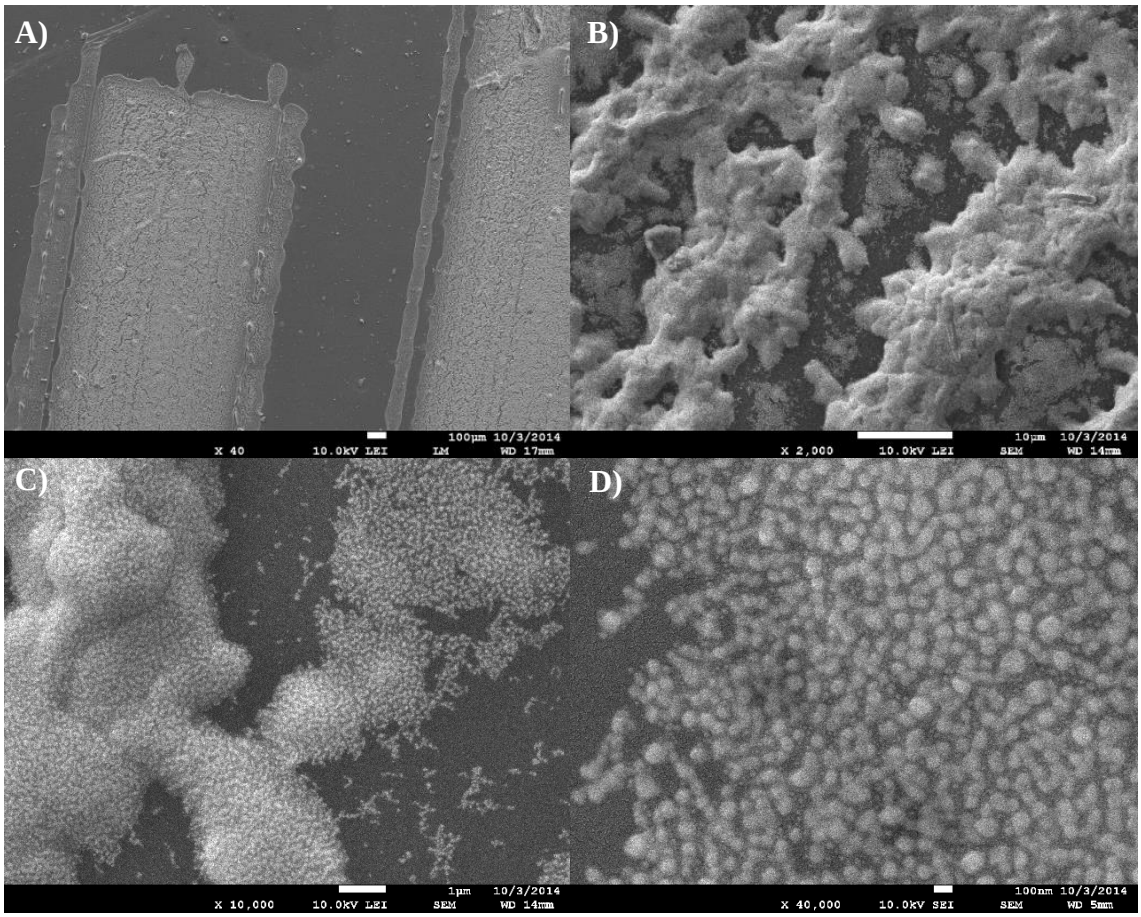

Figure 44 SEM images of flash sintered Metalon®JS-B25HV showing separated grains of insufficiently sintered ink. Resolution of A) 40x, B) 2000x, C) 10 000x and D) 40 000x

Silver dispersion (Sigma Aldrich)

Commercially available silver ink purchased from the Sigma Aldrich was inkjet printed on cleaned PET foils. This ink was based on silver nanoparticles and was curable at low temperatures of 100–150 °C. Therefore it was suitable for printing on plastic sdubstrates. The cleaning process consisted of rinsing foils in a solution of surfactant Neodisher® LM3 (Chemische Fabrik Dr. Weigert GmbH & Co., Muhlenhagen, Germany), and deionized water in ultrasound for 15 min. The next step was rinsing in deionized water for another 15 min and finally in isopropyl alcohol for 15 min. Thermal sintering was done at 150 °C for 90 min. (Figure 45) section A1 and B1 show different parts of the same sample printed with the silver ink on a cleaned substrate without any further modification. The ink was spreading on the substrate and did not form clean lines with the required width. Another two pictures (A2 and B2) show the behaviour of silver ink on the surfactant treated substrate (solution of deionized water and 1 % surfactant). Last two pictures (A3 and B3) show the silver ink pattern on the surfactant treated substrate with the concentration of surfactant about 10 %.

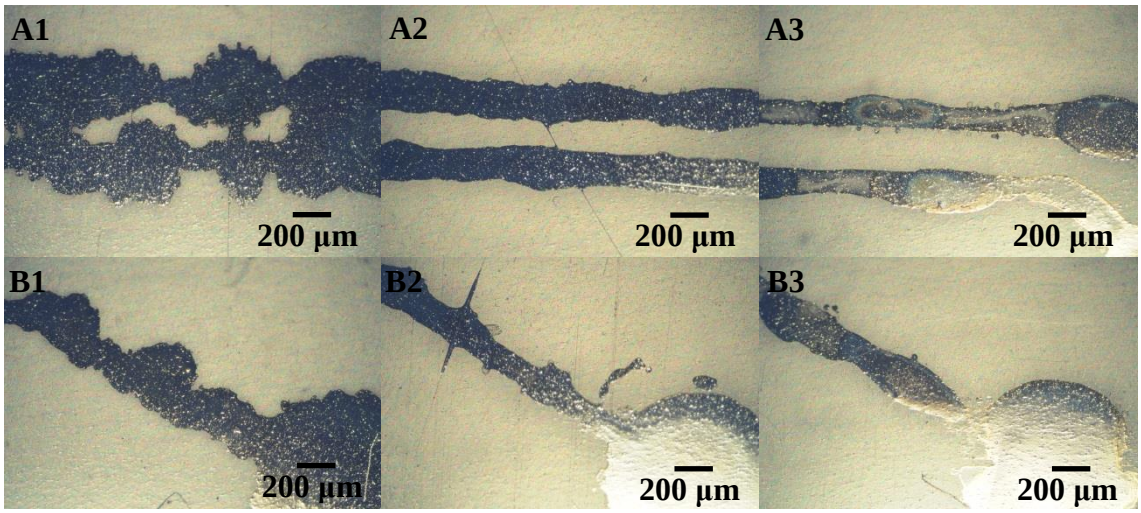

Figure 45 The efect of surfactant addition on layer formation and ink behaviour. A1, B1) without surfactant A2, B2) 1 % of added surfactant A3, B3) 10 % of added surfactant

Clevios™ P Jet HC V2

This water dispersion of PEDOT:PSS was made of sub-micrometer sized gel particles that after thermal annealing formed a continuous and conductive layer. One printed layer of the ink had a thickness of 130 ± 20 nm. Before filling the cartridge, PEDOT:PSS based ink was kept for 15 min in an ultrasonic bath. It was then filtered with 0.45 µm regenerated cellulose filter to avoid nozzle clogging. Another necessity was to modify the surface energy of the substrate so that the PEDOT:PSS ink would form a compact layer. This was done by exposing the substrate to a plasma treatment, and the resulting improvement in layer formation is shown in (Figure 46). These images had been captured using the built-in fiducial camera of the Dimatix Material printer.

PEDOT:PSS channel and the gate electrode was fabricated superimposing two printed layers with a delay of 120 seconds before the deposition of the subsequent layer. A drop spacing of 20 µm was chosen in order to minimize ink spreading on the substrate. Printed layers had been thermally annealed at 125 °C for 15 min.

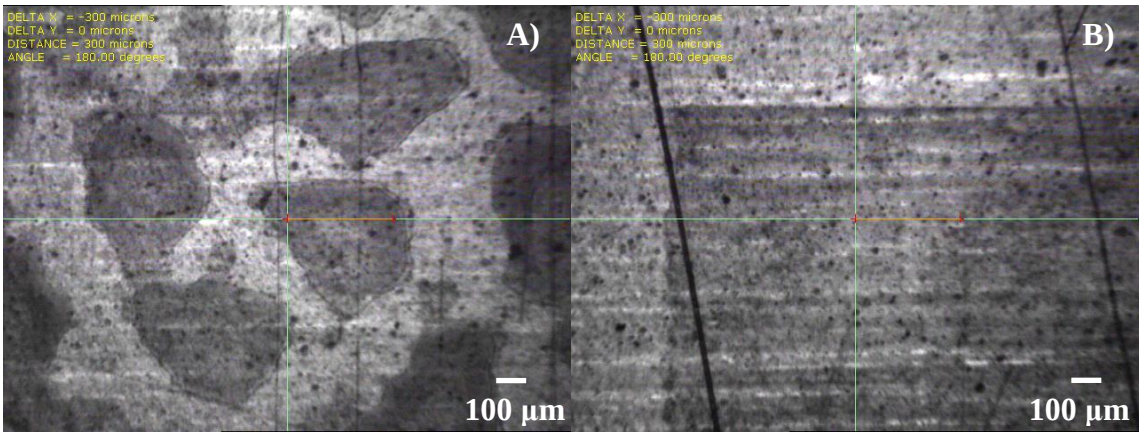

Figure 46 The difference in PEDOT:PSS layer formation in case of plasma treated substrate (Right) and the substrate without plasma treatment (Left)

Printed platform

Resulting platform as shown in (Figure 47) consisted of 24 sensors that were mounted on SensoPlate™ and connected in sets of two to the measurement equipment. Each well was sealed from the top using rubber plugs in order to prevent drying of the electrolyte (PBS) from sensors during prolonged measurements.

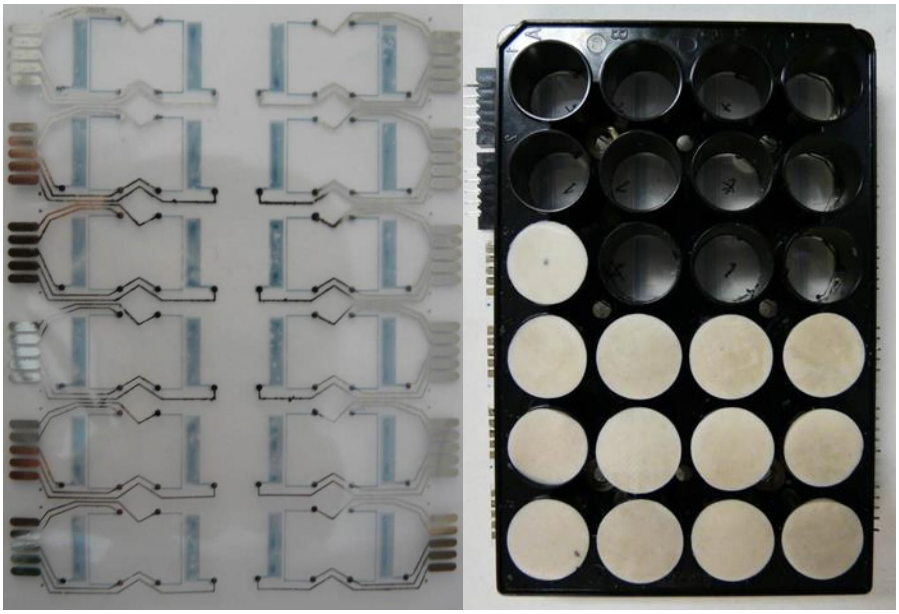

Figure 47 Left) Entirely inkjet printer matrix of 24 OECT sensors on a transparent and flexible substrate. Right) Assembled SensoPlate™ with a rubber plug to minimize electrolyte evaporation

Drawbacks

During the production of a fully inkjet-printed matrix of 24 sensors, we found few shortcomings in our design. Firstly, the PET substrates had insufficient thermal stability and during necessary thermal annealing at 150 °C (silver ink annealing) and even at 125 °C (PEDOT:PSS annealing) softened, waved and changed dimensions slightly.

The silver ink had to be printed on a surfactant treated substrate to achieve a good printing resolution, prevent unwanted ink spreading and pattern joining. Moreover, the silver layer had poor adhesion to the surface and had a tendency to swell and peel off after soaking in water or electrolyte. Furthermore, to print the compact active layer of PEDOT:PSS the substrate with printed silver ink circuits had to be plasma treated to modify surface energy. The process of the fully inkjet-printed matrix of 24 sensors was technologically demanding and lengthy, mainly due to the fact that the reliability of the print was poor. This was caused by the clogging of the nozzles during PEDOT:PSS printing. Moreover, a large number of misprinted samples due to the poor alignment of a substrate in the multi-layer device were caused by substrates dimensional changes.

6.2 SCREEN PRINTED 24-WELL MICROPLATE

In order to overcome the previously mentioned shortcomings, we used different printing technology, namely screen printing. Printing of the whole 24-well OECT matrix had proved to be a much faster and more reliable using screen printing method in comparison to inkjet printing. All screen printed layers had better adhesion to substrates and better reproducibility

than inkjet-printed ones. Screen printing meshes with our own design were custom made (SERVIS CENTRUM a.s., Brno, Czech Republic). Layers of specific materials (screen printing pastes) were designed in three different iterations. First two designs (Figure 48) were very similar to previously used inkjet printing design and only differed in the PEDOT:PSS channel dimensions.

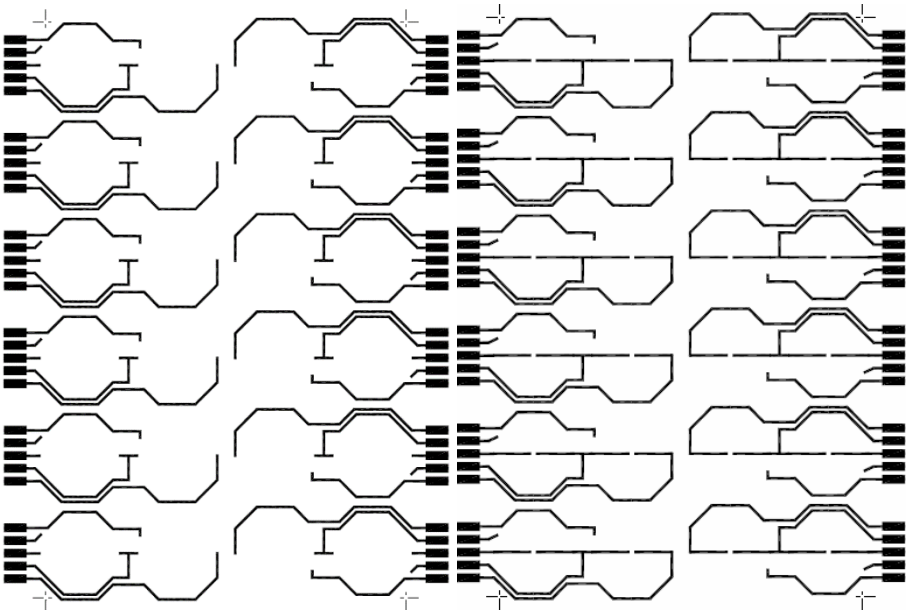

Figure 48 Left) The screen printed design with longer PEDOT:PSS channel (1 cm). Right) Screen printed design with shorter PEDOT:PSS channel (1 mm)

As a next step, we designed and manufactured a circular pattern with a better than before *Wd/L* ratio. In this case, we had to print one additional layer of silicone elastomer Sylgard® 184 to cover all silver/carbon circuitry (Figure 49 Right).

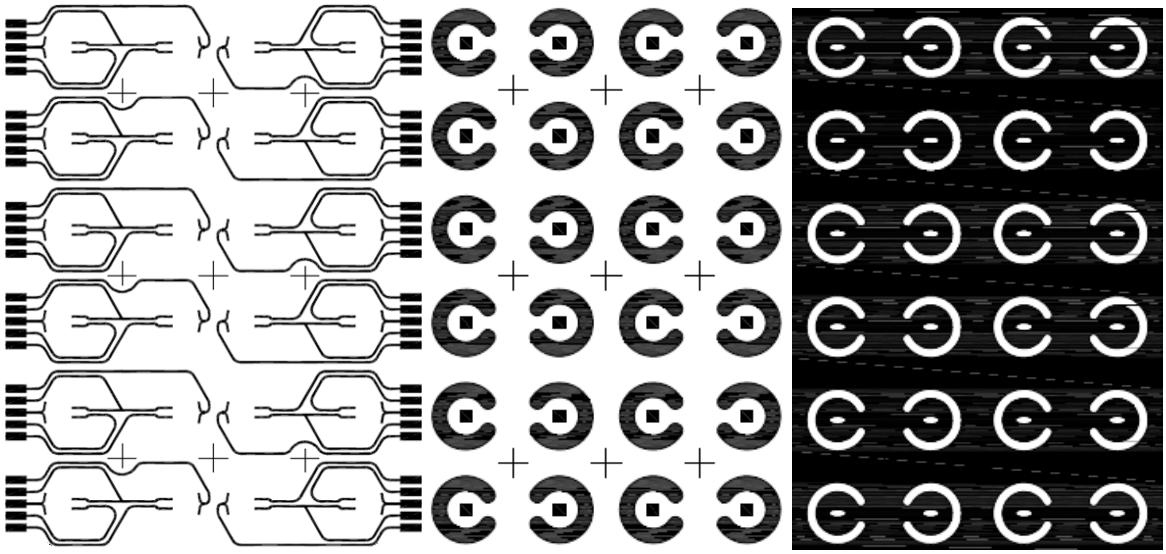

Figure 49 Left) The screen printing pattern of silver circuit layer. Middle) The screen printing pattern of PEDOT:PSS gate and channel. Right) The screen printing pattern of covering layer of silicone elastomer Sylgard® 184

Fabrication

At first, it was necessary to prepare a substrate of the correct shape and to modify its surface properties. Polyethylene naphthalate (PEN) of 30 cm width and thickness of 250 μm (Goodfellow Cambridge Ltd., Huntingdon, UK) was used as a substrate. This was subsequently cut into the final shape compatible with the other parts of the sensor. The cut substrate was cleaned with a series of three ultrasonic baths, each of them lasting for 15 min. The first bath contained distilled water with a Neodisher® LM3 surfactant (Chemische Fabrik Dr. Weigert GmbH & Co., Muhlenhagen, Germany), the second bath contained distilled water and the last bath isopropyl alcohol.

Conductive pathways

The layer of silver conductive paste CB115v2 (DuPont Photopolymer and Electronic Materials, Wilmington, DE, USA) was printed onto a precisely positioned substrate (screen mesh count 77 threads/cm). It created the conductive contact with the paths that were 500 μm in width. The substrate with printed silver circuits was set to sinter at 120 °C on a heated pad for approximately 30 min. After curing the silver lines, the substrate was again aligned to print pattern of the semiconducting material. Other two conductive pastes: Flexible Silver Paste C2131014D3 and Heat Curable Carbon Paste C2050503P1 (Gwent Electronic Materials Ltd, Pontypool, UK) were used following the exact procedure as the CB115v2 paste.

Clevios™ S V3

The PEDOT:PSS layer was printed from commercially available Clevios™ S V3 screen printing pastes (Heraeus GmbH & Co. KG, Hanau, Germany). This paste performed the best from above-mentioned variants in terms of the quality of the print, although it had slightly worse conductivity in comparison to Clevios™ S V4. A detailed study of the influence of the printing parameters on the resulting sheet resistance and the homogeneity of the layers has been given in our previous work [146].

The PEDOT:PSS pattern was printed using a screen mesh count of 140 threads/cm and created a functional OECT gate and channel. The channel dimensions were 5 x 5 mm and the gate electrode was produced by printing a semi-circle that opens on the one side for source and drain contacts.

Sylgard® 184

The device was masked and sealed by the third pattern of the silicone elastomer insulation layer, Sylgard® 184. The silicone elastomer was printed using screens with a mesh count of 120 threads/cm) and insulates the silver conducting paths from the electrolyte environment. It also prevents the tested biomaterial from coming into contact with the non-biocompatible parts and layers of the device. The silicone elastomer was mixed with the initiating agent at a ratio of 10:1 prior to printing. After that, it was printed on the re-aligned substrate and left to polymerize at room temperature for at least 24 h.

Characteristics of 24-well microplate

Screen print of both the organic semiconductor PEDOT:PSS ink as well as silver conducting paste resulted in reliable operating procedure and final function devices. The main characteristics of OECTs are presented as output (Figure 50) and transfer characteristics (Figure 51), the transconductance, and the time-frequency response. The transconductance

g = 100 µS and the time constant τ = 0.07 s at zero gate bias V_G = 0 V and 50 mV input gate signal were achieved (Figure 52).

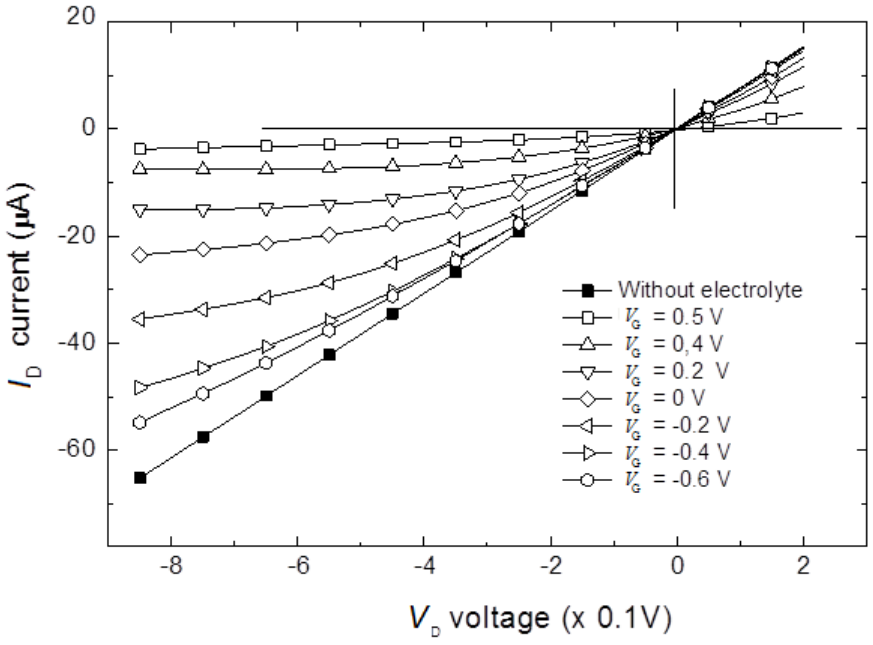

Figure 50 Output characteristics of 24-well microplate OECT

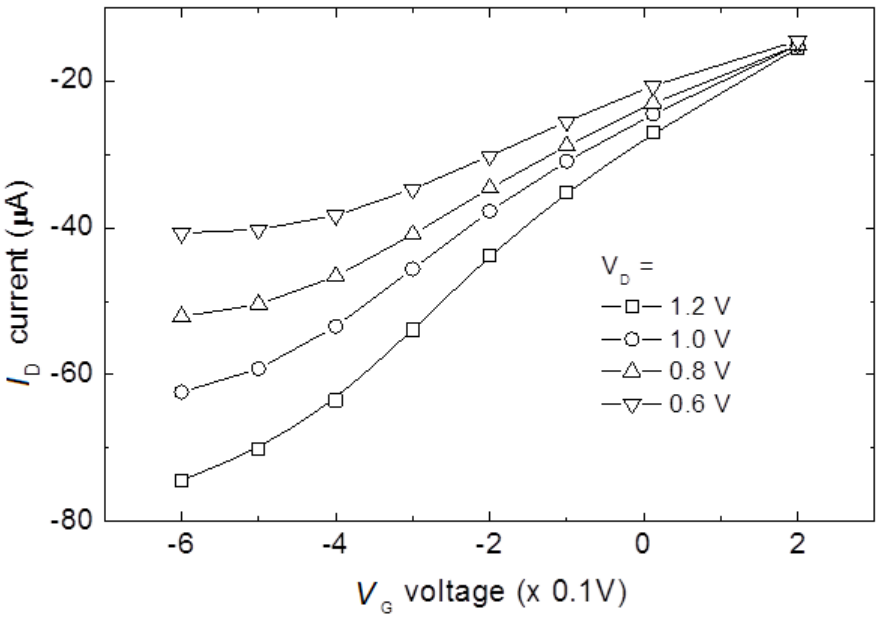

Figure 51 Transfer characteristics of 24-well microplate OECT

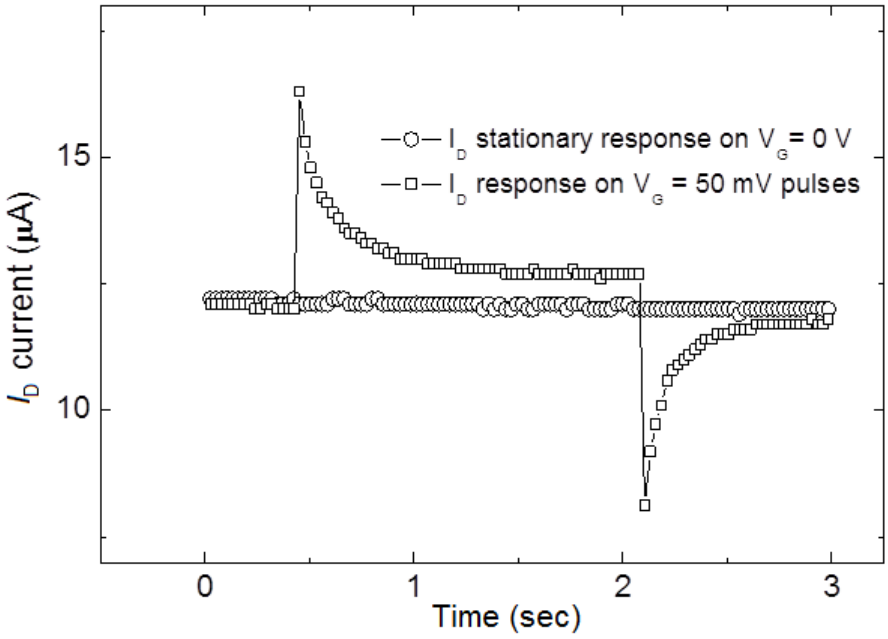

Figure 52 Effect of pulsed gate voltage V_D = 0.5 V

6.3 SCREEN PRINTED 96 WELL MICROPLATE

SensoPlate™ with 96-wells was used as a template for the development of miniaturized OECT sensors. These microplates had standard plate geometry – ANSI/SBS Standards (127.76 x 85.48 mm) with working volume per well of 25 to 340 µl (Figure 53). It was purchased from Greiner Bio-One® (Greiner Bio-One North America Inc., Monroe, North Carolina, USA). Our goal was again to print one OECT sensor into each well. Prototypes were all made using screen printing and also photolithographic methods were developed, and are described in the following chapters. Reliability of devices was dependent on how well the individual layers adhere to the substrate and how they are able to resist in the long term. The reproducibility of the electrical properties of the individual sensors depends on the quality of printing and the ability to print all layers with the highest resolution possible. This is especially true in case of semiconductive material, which has to be as homogenously thick/thin as possible.

The aim of our research at this point was to prepare sensors that are functional, reliable, and have all more or less the same electrical properties. Previous experience with inkjet printing and screen printing of a 24-well microplate has shown that the functionality of sensors is primarily dependent on the continuity of all printed parts and proper multi-layer alignment. The significance of the thickness homogeneity of the PEDOT: PSS layer results from the OECT function. Since the OECT function is influenced by the injection of cations into the polymer layer and subsequent diffusion from the layer, it is important for the layer to have a uniform thickness. The thin parts of the layer would result in faster de-doping, while the thicker parts would still have highly conductive areas in the vicinity of the substrate.

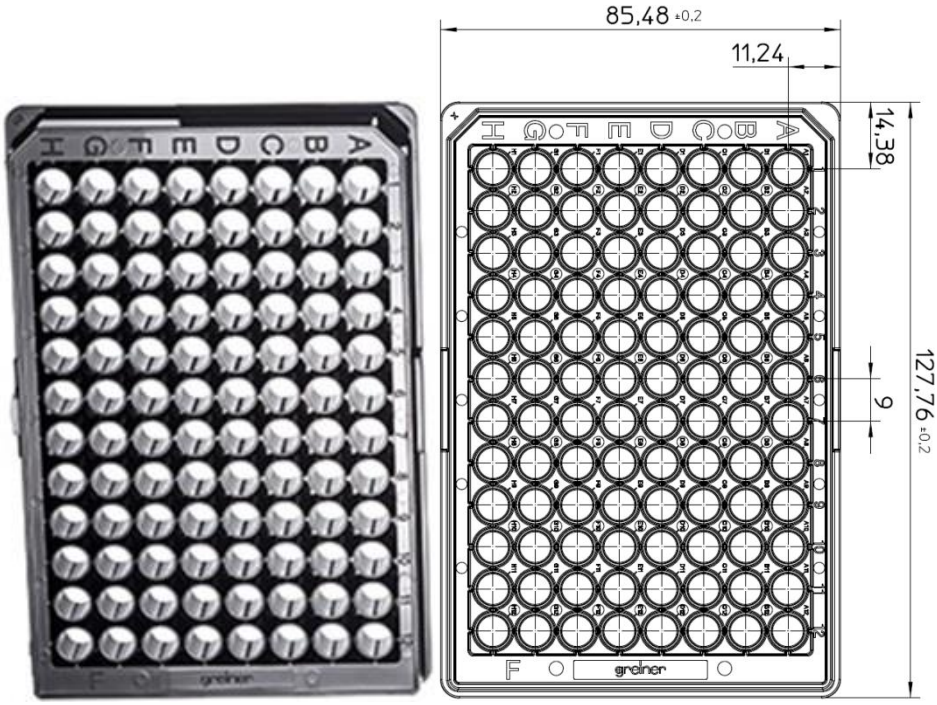

Figure 53 SensorPlate™ microplate with 96-wells, all dimensions are in mm

Fabrication

The fabrication of screen printed devices consisted of a series of processes adjusting the physical and chemical properties of both the surface of the substrate and also the printing pastes. The overall process was divided into several sub-steps, the order of which was experimentally determined and fixed. Replacing the order of these steps, or omitting one or more of them, would result in a faulty sensor. In this chapter, an extended summary of the fabrication process is given. The detailed fabrication steps and necessary printing adjustment are summed up in previous work [147].

At first, it was necessary to prepare a substrate of the correct shape and to modify its surface properties. Polyethylene naphthalate (PEN) of 30 cm width and thickness of 250 μm (Goodfellow Cambridge Ltd., Huntingdon, UK) was used as a substrate. This was subsequently cut into the final shape compatible with the other parts of the sensor. The cut substrate was cleaned with a series of three ultrasonic baths as detailed previously in the 24-well microplate section. All screen printing meshes with our own design were again custom made (SERVIS CENTRUM a.s., Brno, Czech Republic). Layers of specific materials (screen printing pastes) were printed on the cleaned substrate using designed patterns adjusted for a 96-well platform (Figure 54).

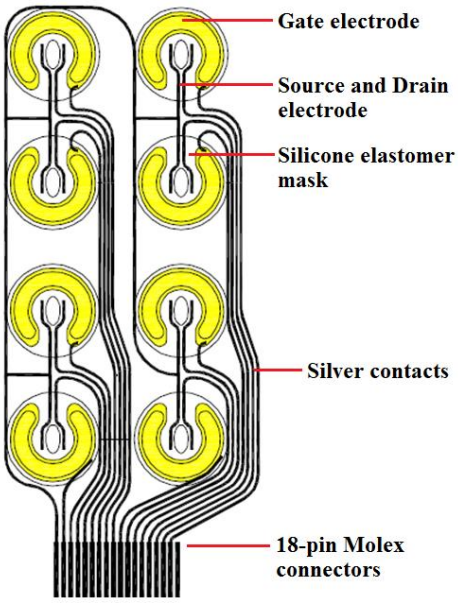

Figure 54 Detail of the printing patterns of 96-well platform

Silver conductive paste CB115v2

Firstly, the layer of silver conductive paste CB115v2 (DuPont Photopolymer and Electronic Materials, Wilmington, DE, USA) was printed onto a precisely positioned substrate (screen mesh count 77 threads/cm). That created a conductive field and the paths with a width of 180 µm. The substrate with printed silver circuits was set to sinter at 120 °C on a heated pad for approximately 30 min. After curing the silver lines, the substrate was again aligned to print pattern of the semiconducting material.

Clevios™ S V3

The PEDOT: PSS layer was printed from commercially available Clevios™ S V3 screen printing pastes (Heraeus GmbH & Co. KG, Hanau, Germany). The PEDOT:PSS pattern was printed using a screen mesh count of 140 threads/cm and created a functional OECT gate and channel. The channel dimensions were 1.5 x 1.5 mm, and the gate electrode was created by printing a semi-circle opened on the one side for source and drain contacts. The substrate with the printed layer was then placed on a heated pad at 120 °C for approximately 30 min until the layer had dried.

The paste was first stirred intensively before printing in order to obtain a lower viscosity and better homogeneity of the resulting film. AN ARG2 rheometer (TA Instruments, New Castle, DE, USA) was used for viscosity measurement at various shear rates at the fixed temperature of 25 °C. The PEDOT:PSS paste of gel consistency exhibited thixotropic behaviour. The static viscosity (at shear rates of 0.1/s) fell from the initial value above 1000 Pa·s down to as low as 15 Pa·s. This was achieved after several days of intensive stirring in a magnetic stirrer at laboratory temperature.

Additionally the stirring of the PEDOT:PSS Clevios™ S V3 was done in magnetic stirrer in a vial at 1000 rpm at elevated temperature of 90 °C. Typical curve depicted in (Figure 55) was obtained for given times of stirring. The stirring at ambient temperature resulted in the rapid change in viscosity that occurred after about 100 h of prior stirring.

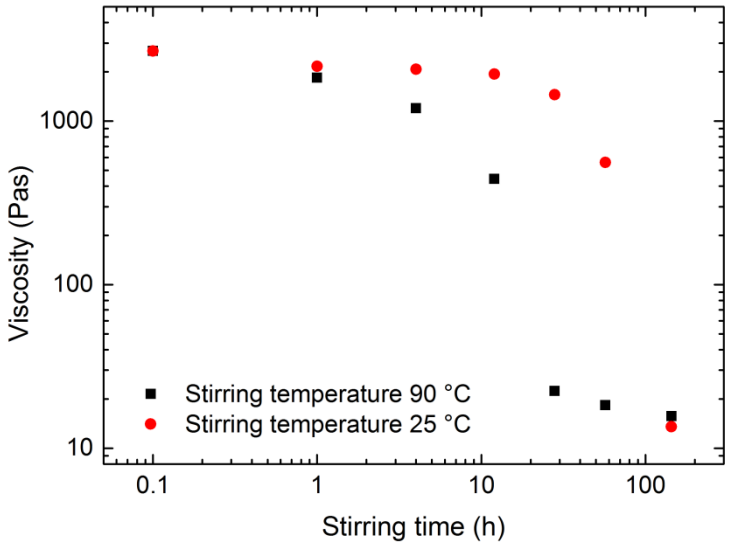

Figure 55 Effect of stirring at an ambient and elevated temperature on viscosity of PEDOT:PSS paste

The stirring at elevated temperature 90 °C shortened the time needed for this change to occur to 24 hours. The viscosity did not decrease further by additional stirring. The viscosity of the paste returned to the initial value in a matter of several hours after the stirring was stopped. Therefore, the printing had to be performed within a few minutes after stirring. Otherwise, the consistency of the paste returned to its initial gel state.

The stirring slightly decreased the resulting thickness of the layer by an average of 20 %, from 250 nm to 200 nm. It also improved the thickness homogeneity and roughness from 25 nm to 18 nm and waviness from 25 nm to 10 nm (Figure 56). These parameters were measured by a DektakXT Stylus Profiler (Bruker, Billerica, MA, USA).

Additionally, the sheet resistance decreased significantly from around 1 kΩ/square to 400 Ω/square. It is considered that intensive stirring acts similarly to alcohol treatment. Furthermore, the core-shell molecular structure changes in a linear fashion as was already reported, and the process is reversible [148]. This can also explain the resistance, roughness, and waviness reduction. The improvement of homogeneity was observed by an optical microscope by the means of round interference fringes on the unstirred PEDOT:PSS layer (Figure 57).

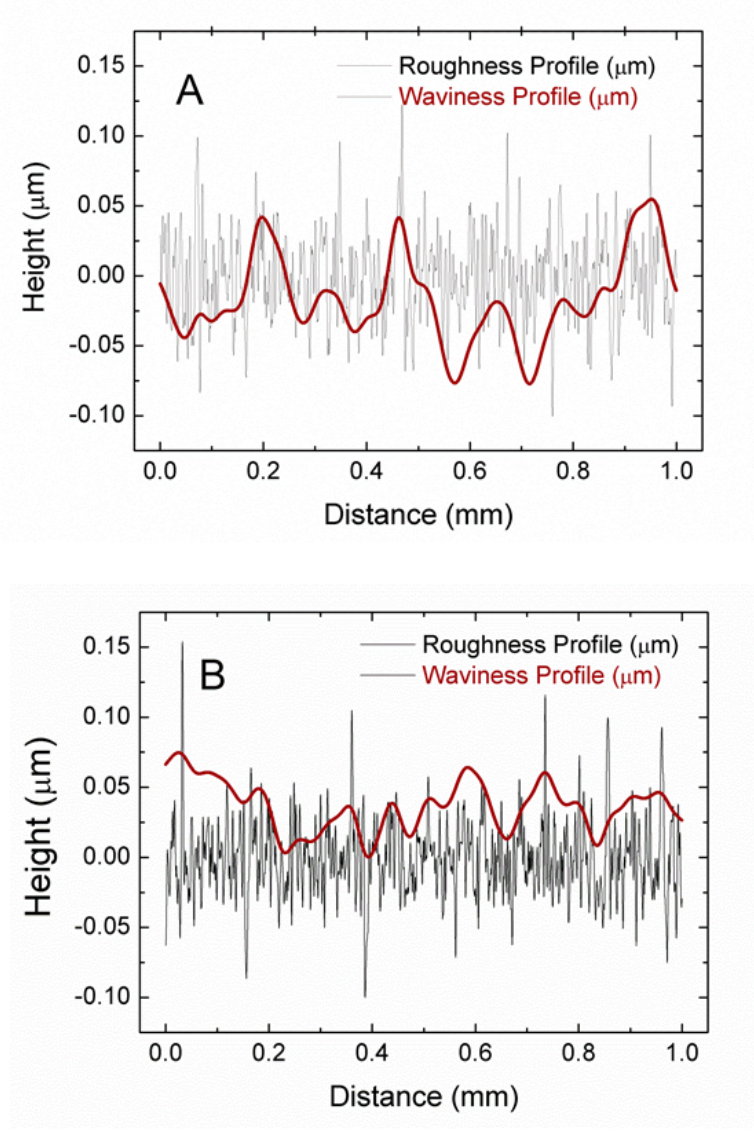

Figure 56 Profile of screen printed PEDOT:PSS layer of Clevios™ S V3. The comparison of the profile of the resulting layer (A) using not stirred (as obtained) and (B) stirred paste.

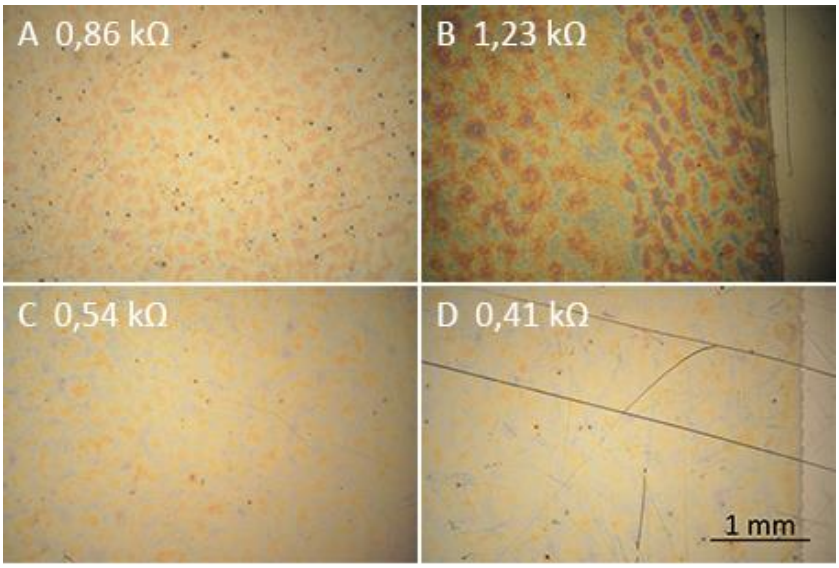

Figure 57 Screen printed layers with channel resistances of stirred PEDOT:PSS paste Clevios™ S V3 (A) stirred for 30 min, (B) non stirred, (C) stirred 24 h at 90 °C (D) stirred 100 h at 25 °C

PEDOT:PSS biocompatibility

To improve the biocompatibility of the Clevios™ S V3 and S V4 screen printing paste they were mixed with increasing concentration of Mouse Collagen, Type IV (BD Biosciences, cat. No. 354233). Resulting composites were tested by the Institute of the Biophysics of the Czech Academy of Sciences. The cell viability (the capability of cells or tissues to maintain or recover the ability to live and develop) was assessed by using MTT test and by the fluorescein diacetate and propidium iodide (FDA/PI) staining. This was tested with 3T3 (3-day transfer, inoculum 3×10^5 cells) fibroblasts (cat. No. CRL-1658, ATCC, Manassas, VA, USA) using the 96-well platform and cultivation time of 48 hours.

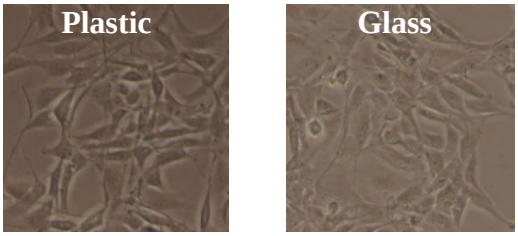

Figure 58 Cultivation of 3T3 fibroblasts using reference cultivation plastic substrate left), glass substrate right)

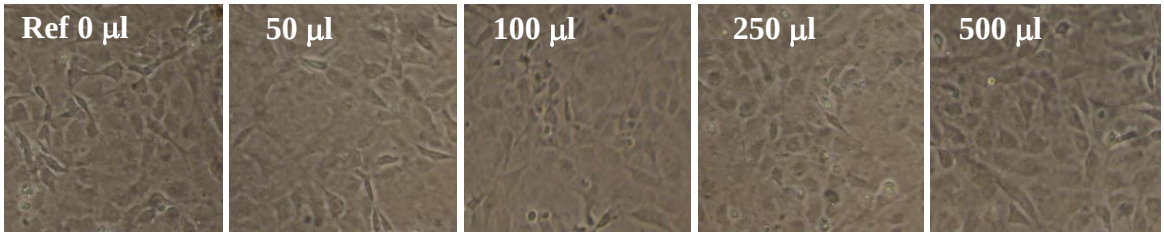

Figure 59 Cultivation of 3T3 fibroblasts using Clevios™ S V3 mixed with increasing concentration of Mouse Collagen IV

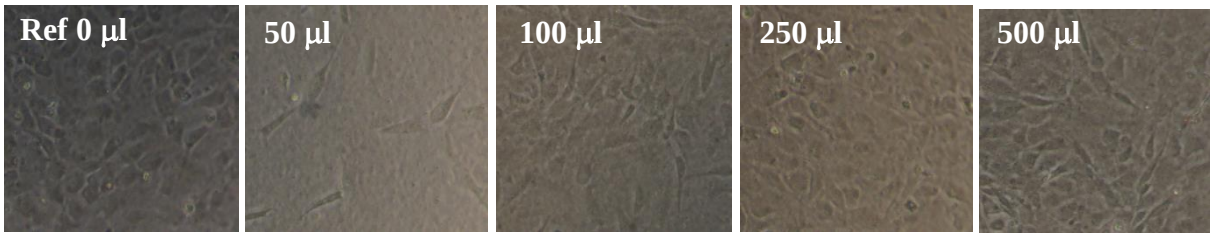

Figure 60 Cultivation of 3T3 fibroblasts using Clevios™ S V4 mixed with increasing concentration of Mouse Collagen IV

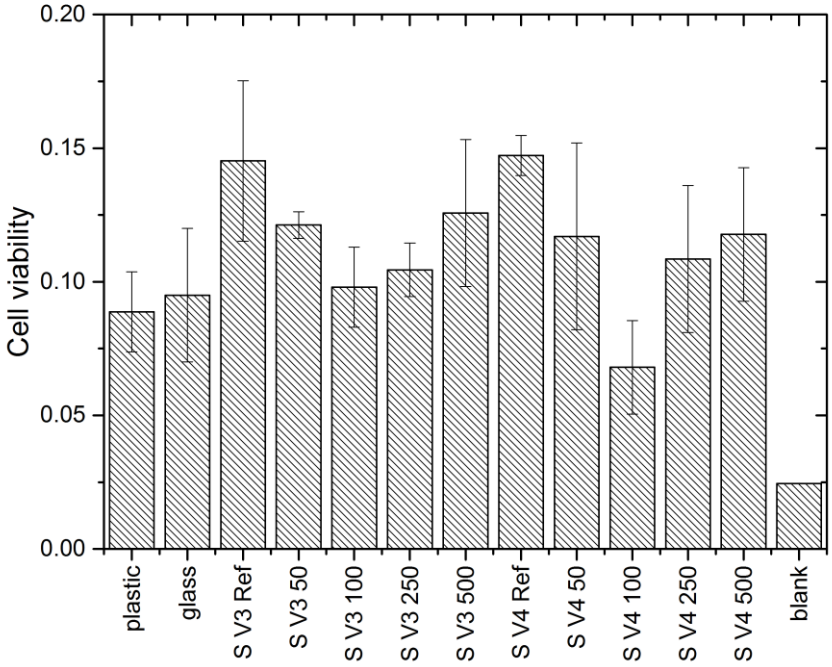

Figure 61 Cell viability MTT test of Clevios™ S V3 and S V4 mixed with increasing concentration of Mouse Collagen IV

The MTT test is a colorimetric assay for evaluating cell metabolic activity. NAD(P)H-dependent (nicotinamide adenine dinucleotide phosphate reduced) cellular oxidoreductase enzymes may, following determined conditions, display the fraction of viable cells present. These enzymes can reduce the tetrazolium dye MTT 3-(4,5-dimethylthiazol-2-yl)-2,5-diphenyltetrazolium bromide to its insoluble formazan, which has a purple color.

It was found out that PEDOT:PSS Clevios™ S V3 and S V4 partially dissolved in the extraction buffer for the MTT test and therefore interfered with the photometric measurements. This fact leads to a false increase in the cell viability that can be seen in (Figure 61) and hence render the data obtained from the MTT test inconclusive.

As an alternative to the inconclusive MTT test, double staining by the fluorescein diacetate and propidium iodide (FDA/PI) was performed as a proof of concept experiment (Figure 62) without any data quantification so far.

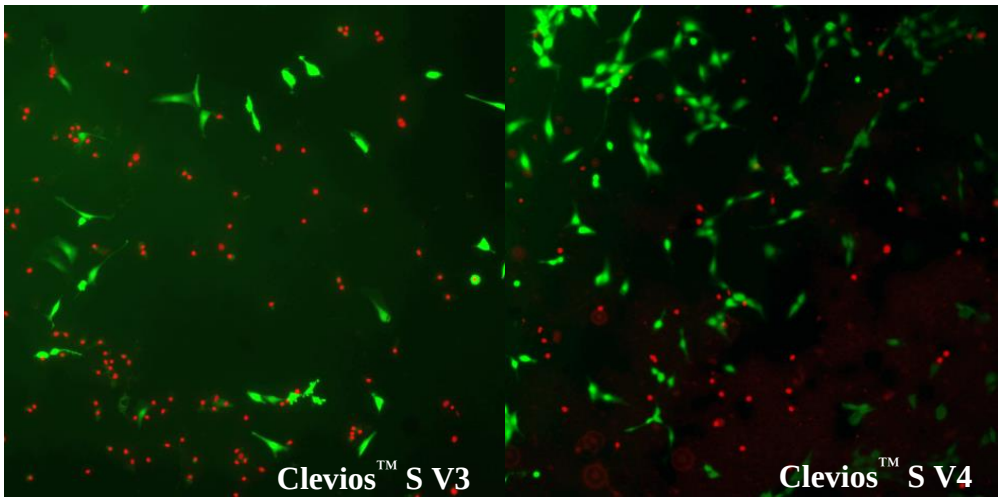

Figure 62 Cell viability test using double staining by the FDA/PI. Green – living cells, Red – dead cells nuclei

Sylgard® 184

The system was masked and sealed by the third pattern of the silicone elastomer insulation layer, Sylgard® 184. The silicone elastomer was printed using screens with a mesh count of 120 threads/cm. This insulates the silver conducting paths from the electrolyte environment and also prevents the tested biomaterial from coming into contact with the non-biocompatible parts of the device. Sylgard ® 184 and every other component and material were tested for biocompatibility by the Institute of the Biophysics of the Czech Academy of Sciences [149].

The silicone elastomer was allowed to react at room temperature for 1 h after being thoroughly mixed with the initiating agent at a ratio of 10:1 prior to printing. After that, the silicone elastomer was printed on the re-aligned substrate. The silicone elastomer pattern was left to polymerize at 60 °C for at least 8 hours before further manipulation. The following screen print has provided a layer of the thickness of 12 µm (Figure 63). A coating to increase biocompatibility was done with Mouse Collagen, Type IV (BD Biosciences, cat. No. 354233), at 10 $\mu g \cdot cm^{-2}$ [150].

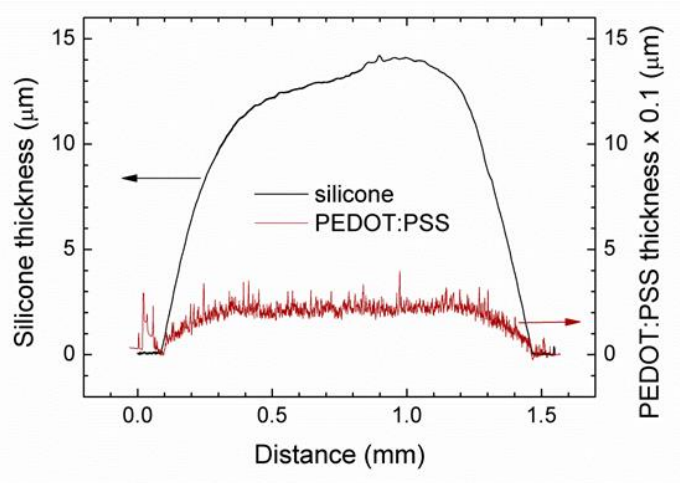

Figure 63 Thickness and roughness of screen printed PEDOT:PSS and silicone elastomer Sylgard® 184 layer

The substrate with all three layers (Figure 64 Left) was used to assemble the whole sensor. The assembly consisted of mounting the sensor matrix into the Greiner Bio-One's SensoPlate™ 96-well platform (Figure 64 Right). The foil was firmly fixed to the polystyrene microplate and bolted down from the bottom utilizing a Plexiglas® plate to enable more comfortable handling and transparency needed for microscope observations [150].

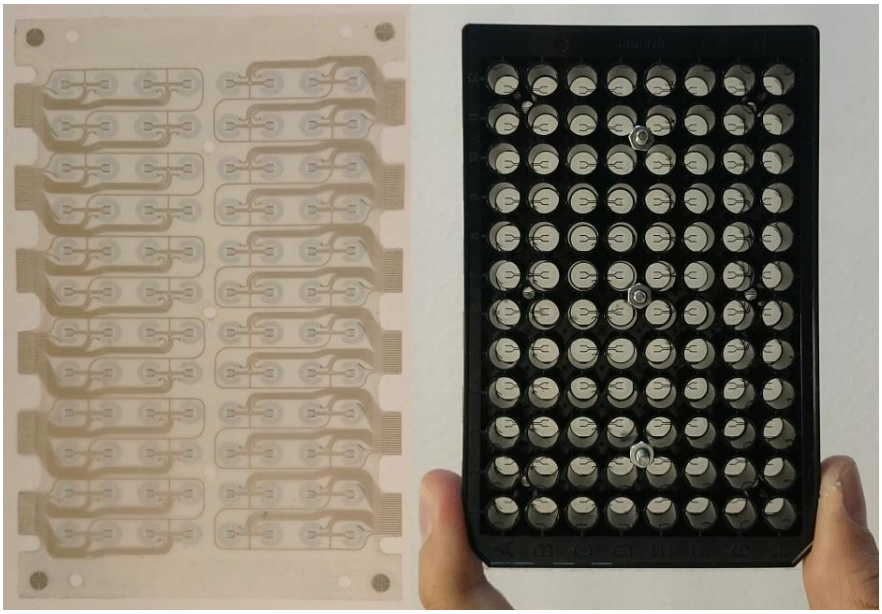

Figure 64 (Left) Screen printed sensor plate with 96 individual sensors on the PEN substrate. (Right) Sensory array mounted on the SensoPlate™ platform

The detail of the sensor with labels S and D indicating the source and drain electrode, and the circular gate electrode G, all made out of PEDOT:PSS is depicted in (Figure 65). The OECT channel visible in (Figure 65), created by a screen-printed rectangular PEDOT:PSS layer on PEN foil, was surrounded by planar circular gate electrode 6 mm in outer diameter. The rotary symmetry should improve the electric field distribution. The electrodes were joined by printed silver conductors 0.2 mm wide. The printed transparent silicone layer covered the surface of the sensing array except for functional PEDOT:PSS interface with the biomaterial and physiological solution. The exposed channel area had length of L = 1 mm and width of W = 1.5 mm, the thickness of the PEDOT:PSS layer was 250 nm on average, and the typical electrical resistance of the channel was 500–700 Ω [147].

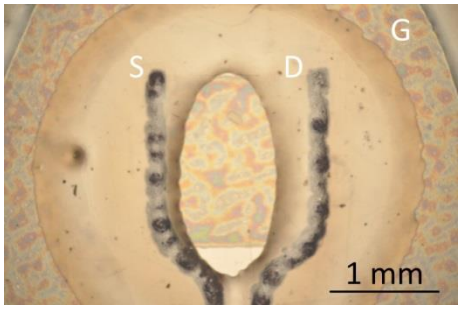

Figure 65 A detailed picture of one screen printed sensor. (S) Source electrode, (D) Drain electrode, (G) Gate electrode

Amplifier and measurement setup

The electrical circuit designed for OECT testing is depicted in a schematic form in (Figure 66). The connect array of the microplate foil was connected by 18-pin Molex connectors and 18-wire ribbon conductors. Eight OECTs were connected by a single connector and each individual OECT could be selected from the array by a proper couple of micro-switches as shown in (Figure 67). Contrary to the majority of researchers, we used the planar arrangement of the electrodes for an easy optical and camera investigation [150].

The gate potential V_G was set from the external source in a range from −0.8 V to 0.8 V to prevent redox reactions at electrodes. Source and drain voltage V_D could be set down to −0.725 V. The source current I_S was converted to voltage in an *I*/*V* converter and recorded by an oscilloscope after further amplification. The offset I_S at a stable working point was compensated by setting the corresponding opposite current at the input of the operating amplifier. The zero Analog OUT voltage was set as an input voltage of $V_G = 0$ V via R_{offset} resistor/potentiometer. The feedback resistor $R_{sense} = 1$ kΩ gives a conversion of 1 mA/1 V. Further amplification was enabled by switching the output jumper [150].

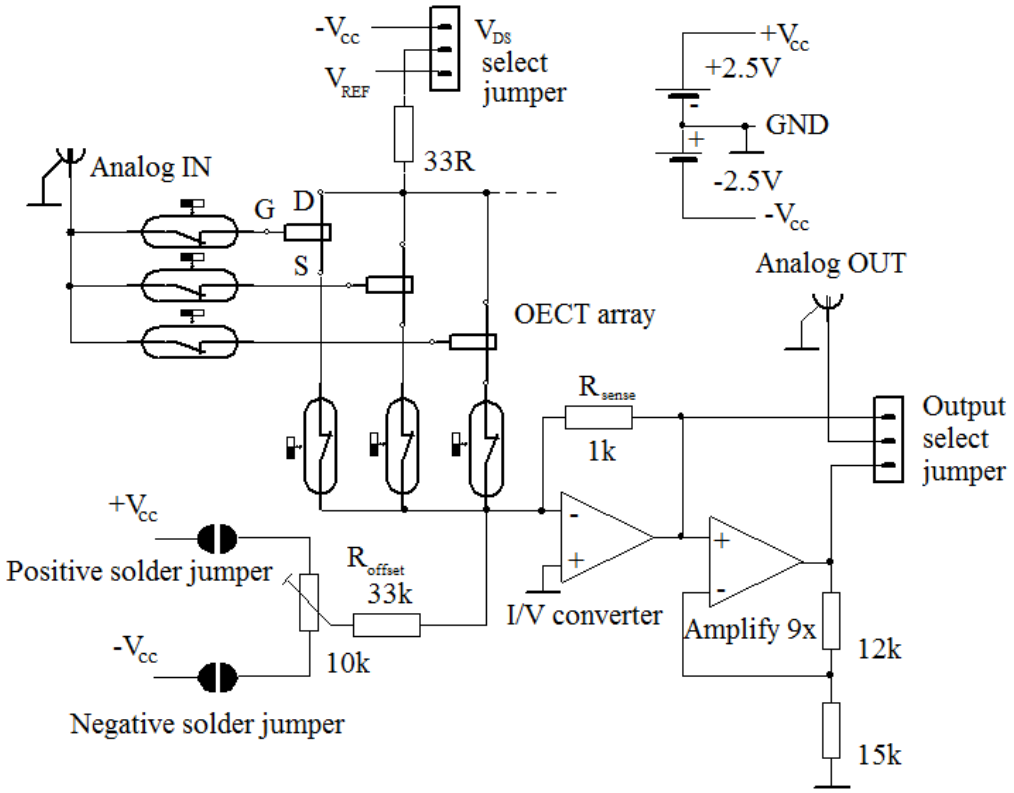

Figure 66 The electrical circuit designed for OECT testing depicted in a schematic form [150]

The electric field strength at the channel vicinity determined the effective ion drift through the channel and consequently the channel conductance. The small channel area at the interface with the electrolyte compared with the large gate electrode area enhanced the electric field. Together with the volumetric capacitance of OECT, it was responsible for the device amplification and speed. The capacitance of the electrode in a physiological solution of phosphate-buffered saline (PBS) based on a 0.15 M solution of NaCl was estimated at

$C = 0.2\ \mathrm{F \cdot mm^{-2}}$. Together with the electrolyte conductance of $g = 1\ \mu\mathrm{S}$, the time constant $t = 0.2\ \mathrm{s}$ was anticipated. The capacitance of the much larger gate electrode could be neglected due to its serial combination with the channel capacitance. The speed of the OECT device was limited by the capacitance of the gate circuit. It was controlled by the effective capacitance of the channel. The label 'effective' here takes into account that the potential at the channel is not uniform but distributed non–linearly along its length from the source to the drain electrode (from 0 to −0.725 V in our case). It was, to some degree, considered a consequence of the channel aspect ratio. Moreover, the geometry of the entire system including the gate electrode and electrolyte could influence the channel potential distribution.

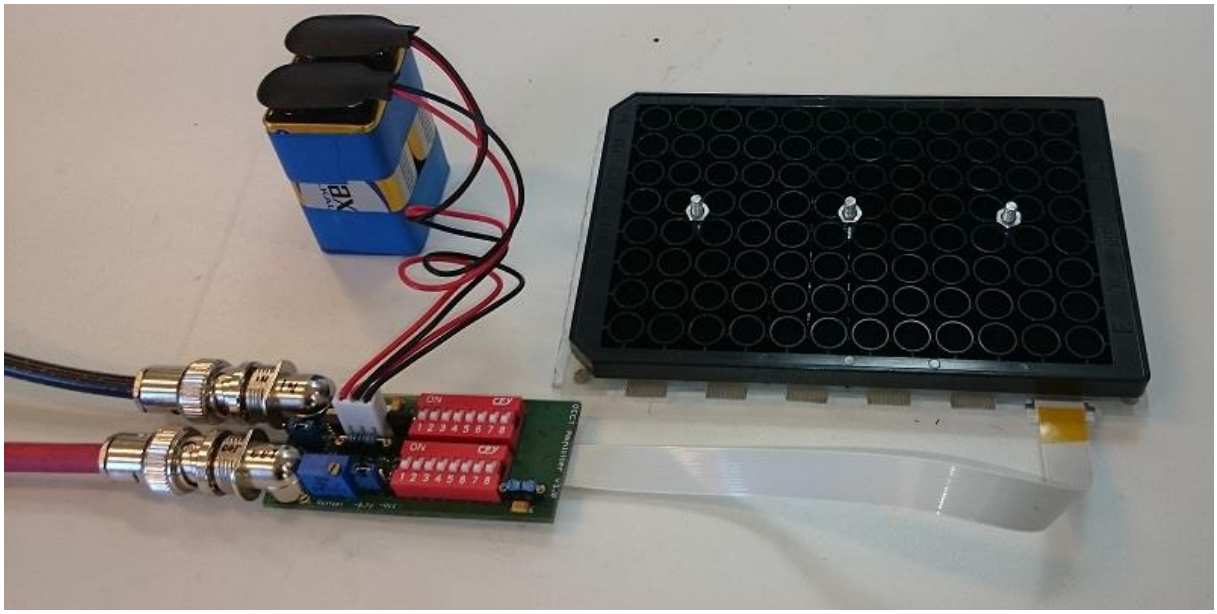

Figure 67 Encapsulated OECT – 96-well microplate with a power source-signal amplifier and current/voltage converter

The gate offset voltage as well the voltage modulation (simulation of the cardiomyocyte pulsing), were delivered from the function generator to the Analog IN input. An OECT was selected by a couple of switches as shown in (Figure 67). The drain was supplied by a negative voltage down to $V_D = -0.735\ \mathrm{V}$. This value was set due to the factory setting. It represented a compromise between the requirement of a safety voltage against electrode redox reactions in the event of a positive gate voltage ($V_G > 0\ \mathrm{V}$) and the necessity of high amplification (transconductance g). Its fixed value enabled comparing the amplification of OECT devices at any point in time. The source was connected to a virtual zero input of the *I/V* converter. The amplified signal was recorded by a digital memory oscilloscope. The offset of the stable channel current was compensated for by a potentiometer R_{offset} so the Analog OUT DC signal component could be eliminated [150].

Cell cultivation

Mouse 3T3 fibroblasts (cat. No. CRL-1658, ATCC, Manassas, VA, USA) were routinely grown in Dulbecco modified Eagle medium, high glucose supplemented with 10 % fetal calf serum, 100 U/ml penicillin, and 0.1 mg/ml streptomycin (all from Gibco, Gaithersburg, MD, USA) in standard 100 mm cell culture dishes (cat. No. 93100, TPP, Trasadingen Switzerland),

as described previously [151]. The inocula for experiments ranged from 8300 to 28,000 cells per 1 cm^2. Viability was routinely checked by employing a cytometer (CASY, Roche Diagnostics Ltd., Rotkreuz, Switzerland). Cells were grown in sensors for 48 h. In order to provide proof of sensor function, cells that during the experiment were washed with physiological buffered saline two times and 200 µl of 0.25 % trypsin (cat. No. R001100, Gibco, Gaithersburg, MD, USA) was added [150].

Results

The first experiment tested the OECT parameters such as the transfer characteristics and the derived transconductance *g*. The fix drain potential was set to $V_D = -0.735$ V, and the output source current was measured continuously at the triangular, symmetric gate voltage V_G in a range of 0.2 to −0.8 V. The results can be found in (Figure 68). As can be seen from (Figure 69), due to relaxations, the transfer characteristics and transconductance *g* included are strongly dependent on the sweep rate of the testing gate voltage V_G and its direction. The sharp transconductance maximum was observed first by Rivnay et al. [36]. Its position on the V_G axis depends on the channel geometry, but no sweep rate influence was reported. The transfer characteristics in our case show significant hysteresis. In the case of a short period of about $T = 1$ s, the volumetric capacitance charging delays the output current I_S, so the hysteresis is oriented counter-clockwise. In the case of a long period of $T = 20$ s, slow relaxations of the polymer network in the channel, reducing the output current I_S, dominate so that the hysteresis is oriented clockwise. In the case of a medium period of $T = 5$ s, both effects are compensated.

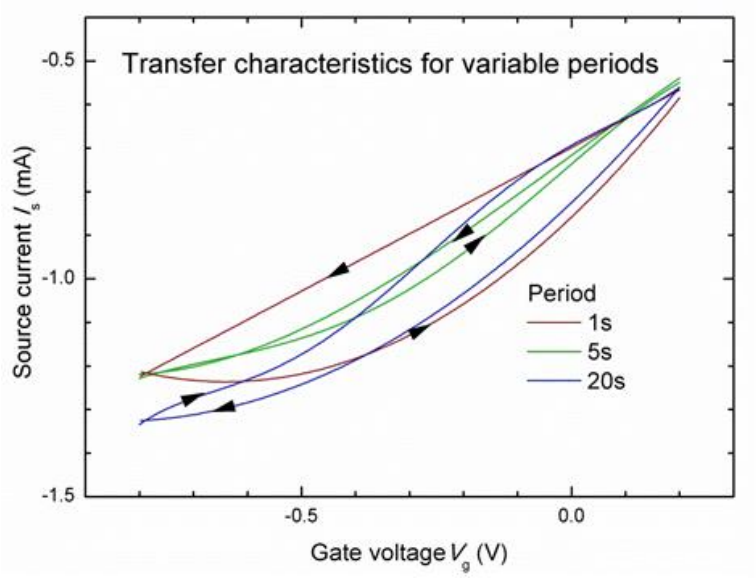

Figure 68 Transfer characteristics measured at the triangular gate periodic voltage at various periods [150]

The second experiment, investigating the response of an OECT's channel current on a simulated signal of electrogenic cells, was conducted (Figure 68). The standard PBS solution was used as an electrolyte. In looking for the optimum working point of the OECT with the highest transconductance, the gate voltage V_G from the function generator was modulated by rectangular pulses of 10 mV_{pp} at a 5 s period. This was superposed on the offset voltage, as

can be seen in (Figure 69). While the response on the offset setting showed negative relaxation with a time constant of approximately 25 s, the amplification of the pulsing signal did not change significantly according to the offset. This means that the transconductance remains constant across a wide range of gate offset, in our case a transconductance of $g = 1$ mS deduced from the plot. However, this value is limited by the frequency band pass $f = (0.2 \sim 8)$ Hz corresponding to the time constants of the gate circuit and slow relaxation processes.

The measured time constant $\tau = 0.12$ s achieved by the simple exponential fitting corresponds to charging-discharging the channel volumetric capacitance $C = 0.1$ μF, and the entire gate circuit resistance of $R = 1.2$ MΩ. The potential on the capacitance varies and it also controls the ion doping and de-doping process. The measured circuit current, charging the gate, reached 1 μA in accordance with the circuit resistance. It is theoretically possible to lower the time constant by decreasing the channel area and hence its capacitance or by reducing the gate-channel distance and thus its resistance. The resistivity of the electrolyte is determined by its physiological function, and so it cannot be varied. The speed of the device is then limited by the screen-printing resolution. The lithographic technique enables the development of much smaller dimensions and quicker devices. This is necessary for recording the shape of the electrogenic cell (cardiomyocyte) signal.

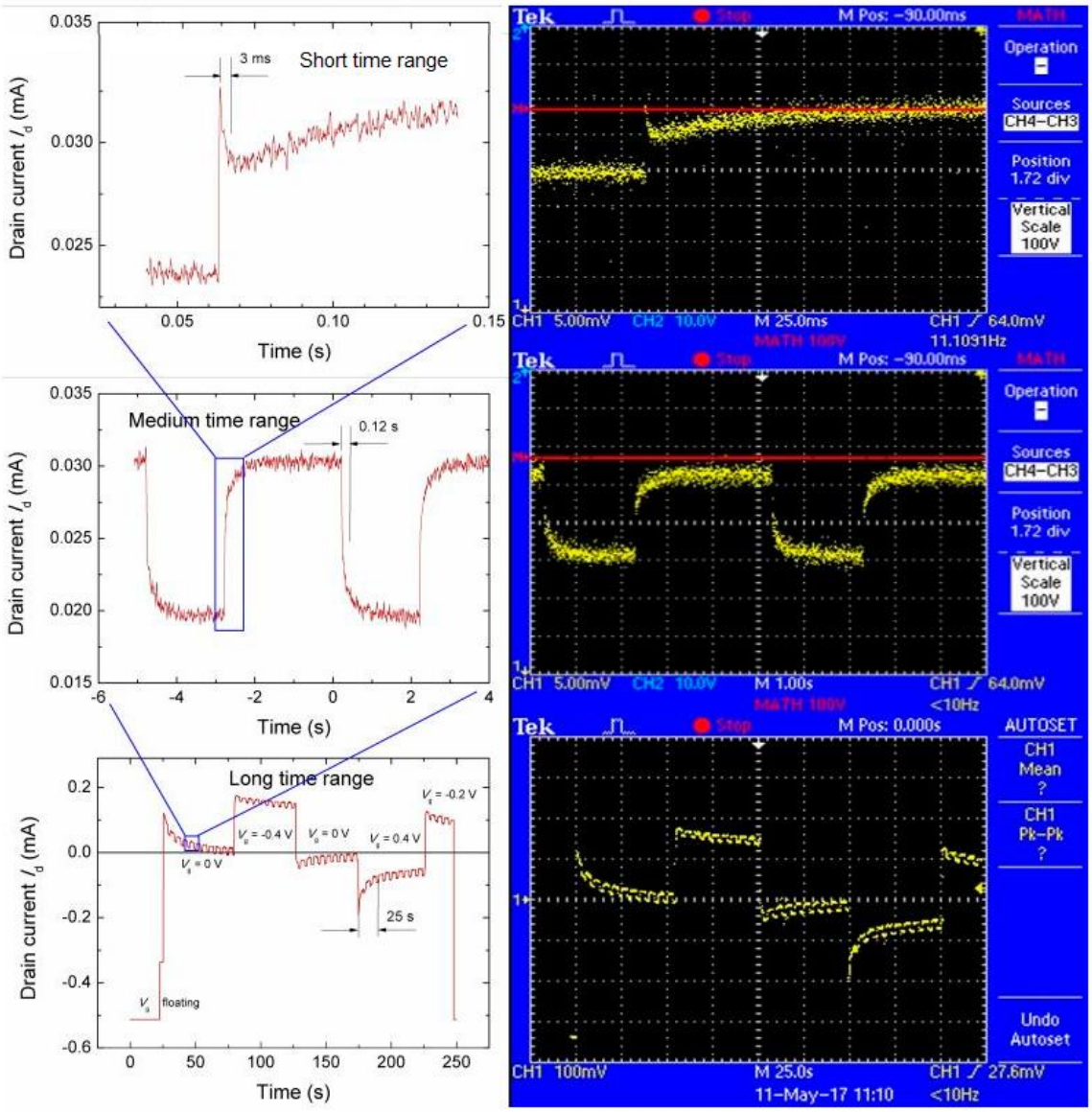

Figure 69 The response of output voltage of the preamplifier – I/V converter (calibrated in drain-current units) on gate input voltage at $V_D = -0.735$ V and the variable gate voltage V_G modulated by rectangular pulses of 10 mV_{pp} voltage and a 5 s period [150]

Using a short time range display, we found one more time constant, namely the time constant of 3 ms caused by hole extraction and injection into the channel [31]. This might play a more significant role at a smaller channel area with lower capacitance and time constant.

The faster rectangular modulation applied to the V_G simulated a signal of electrogenic cells (cardiomyocytes). The period of 5 s was set to get the source current I_S to a sufficiently steady state (Figure 69, medium time range) for the deduction of the time constant τ of the gate circuit. The medium current response was almost not influenced by material relaxation. The ΔI_S response on the modulation represented a consequence controlled by charging and discharging of the volumetric capacitance at the electrolyte-PEDOT:PSS interface. At the moment of the gate pulse edge, a short source current I_S spike appeared with an exponential decay that reached the steady state at around 3 ms. This is considered as the effect of the hole

extraction/injection process in the PEDOT:PSS channel, as was already described by Bernards and Malliaras [31].

The aging of the OECT structure under the voltage load described above was performed over a period of 28 h (Figure 70). A gradual, approximately 25 % decrease of I_S and the transconductance g was recorded.

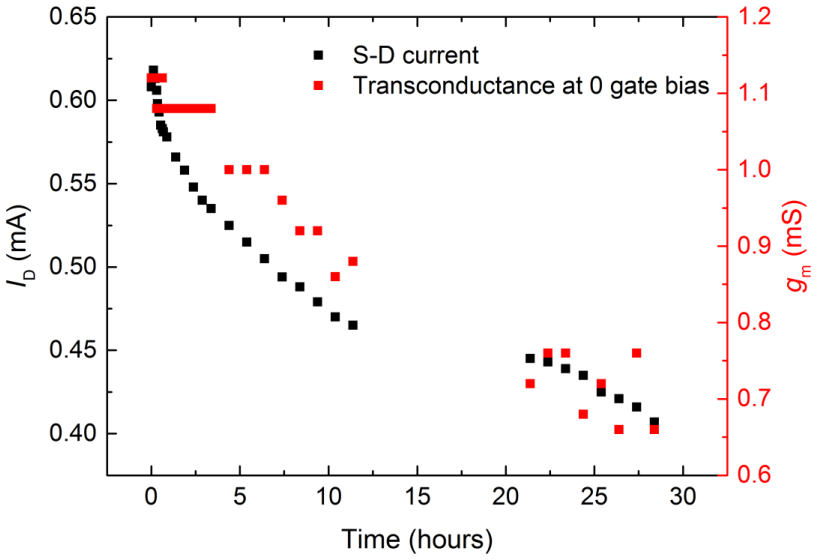

Figure 70 OECT degradation at V_D = −0.735 V and V_G = 0 V in PBS solution

The biocompatibility of the sensor was tested by 3T3 fibroblasts. Cells were able to grow on sensors to the same extent as on control substrates (standard cell culture plastics). The cell viability was comparable to that of control substrates, and it typically reached 90 – 95 %. This indicated that a high level of biocompatibility was reached. Indeed cells were able to form a confluent layer within 48 h (Figure 71 A). A proof of concept experiment for the sensor function was carried out. Due to extensive ion exchange, the cells grown at the transistor channel modulate the current within it. Therefore the removal of cells resulted in changes in the channel current. Thus, the confluent layer of cells within the sensor was treated with trypsin, an approach to detach cells from their support [150], [152]. Indeed, the absolute value of the current decreased in parallel to the trypsin-mediated detachment of cells (Figure 71 B).

Finally, the function of the sensor was verified through a spike of KCl (Lachema, Brno, Czech Republic), which resulted in a significant dropdown of the absolute current value. The main idea of the final proof of concept experiment with cells was to demonstrate that the sensor can host the living cells efficiently and an electrogenic event related to cell physiology could be recorded.

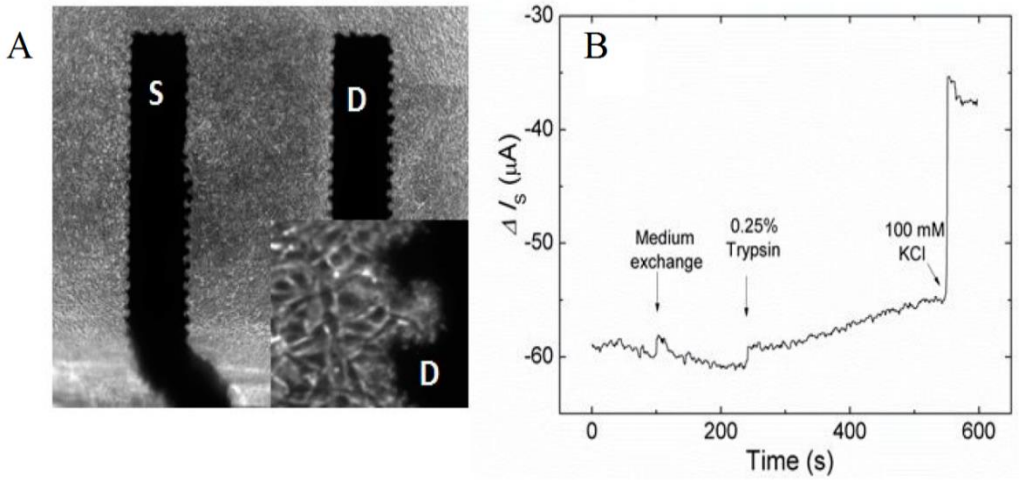

Figure 71 (A) OECT with a confluent layer of 3T3 fibroblasts: S – source, D – drain (B) The electrical response to cell release due to trypsin. 100 mM KCl spike served as a positive control of transistor function [150]

6.4 SU-8 PHOTOLITHOGRAPHY

In good agreement with previously published works improvement of the transconductance and time constant of prepared devices can be achieved by decreasing the OECT dimensions [152]. The increase in parameters mentioned above is done by shortening the gate-channel distance and minimizing the channel-electrolyte volumetric capacitance by reducing the channel area. The miniaturization and optimization were done via photolithography using SU-8 photoresist.

Fabrication process

The combination of photolithographic techniques together with screen-printing method was employed for the device assembly. The copper laminates on a PEN-film backing with a thickness of 50 μm (AKAFLEX PENCL HT provided by Gatema a.s, Boskovice, Czech Republic), was used to photolithographically pattern flexible circuits. The PEN variant was chosen due to its superior stability at high temperatures compared to PET laminates and enabled processing at a temperature of up to 150 °C. On top of the patterned electrolytic copper foil (thickness of 17 μm) was galvanically applied a thin layer of gold (10–100 nm) with an interlayer of nickel for better adhesion. The PEDOT:PSS layer was printed from commercially available Clevios™ S V3 screen printing pastes (Heraeus GmbH & Co. KG, Hanau, Germany). The PEDOT:PSS pattern created a functional OECT gate and channel. PEDOT:PSS was screen-printed in the form of a rectangular channel connecting two parallel gold electrodes with a width of 250 μm and 200 μm gap between them. The channel was surrounded by a planar circular gate electrode also printed using PEDOT:PSS with an outer diameter of 6 mm (Figure 72).

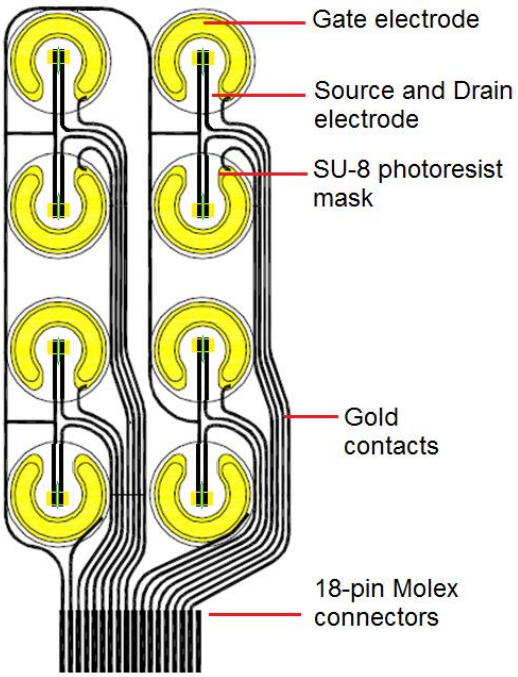

Figure 72 The detail of the designed OECT array

Screen printing of SU-8

The device was sealed by the layer of photoresist SU-8 (MicroChem Corp. Westborough, MA, USA). This layer insulated the gold conducting paths from the electrolyte environment and created a narrow active channel.

For screen printing the RokuPrint Screen printing machine, SD 05 was used together with custom-made polyethylene screens 36/31 (36 µm – size of mesh opening, 31 µm – the size of thread diameter) for screen printing of Clevios S V3 PEDOT:PSS and 140/65 screen for screen printing of SU-8 photoresist. The layers of approximately 200 nm of PEDOT: PSS and 30 µm of SU-8 were obtained. To this end, the SU-8 2015 with a viscosity of 1250 cSt had to be diluted by cyclopentanone to the viscosity of approximately 250 cSt (Figure 73). An ARG2 rheometer (TA Instruments, New Castle, DE, USA) was used for viscosity measurement at the fixed temperature of 25 °C.

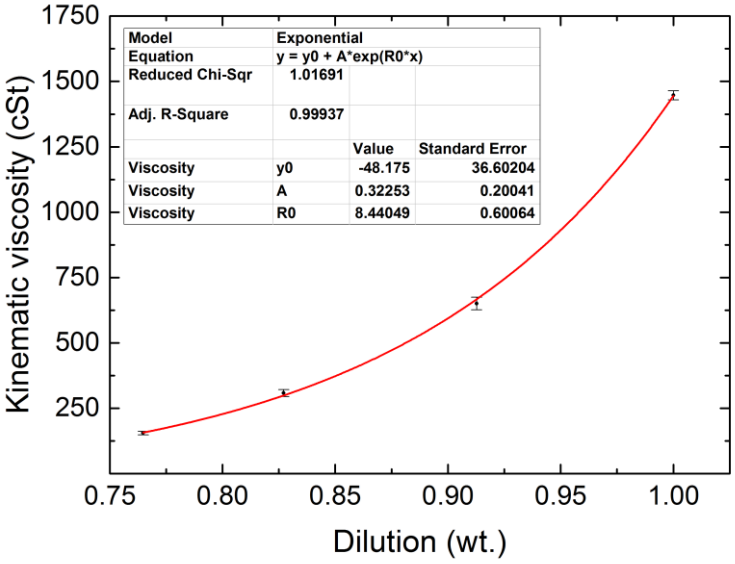

Figure 73 SU-8 kinematic viscosity dependence on cyclopentanone content

The prepared screen-printed layer was firstly dried on a hot plate at 95 °C for 5 min (soft bake). This step was necessary in order to minimize the amount of solvent in the layer of SU-8 before exposure. The resulting photoresist layer was 30 µm thick. The unexposed photoresist substrate was then aligned under a microscope with a chrome photomask made by electron-beam lithography and placed in the Suss Microtech MA6/BA6 adjuster (Institute of Scientific Instruments, The Czech Academy of Sciences, Brno). The photoresist was exposed to UV radiation of 5.6 mW/cm^2 for 120 s. This step was followed by another heat curring on a hot plate for 5 min at 100 °C (post exposure bake). This step was necessary for the development of the desired pattern. Subsequently, the photoresist was submerged for 1 min in the developer, rinsed with isopropyl alcohol and dried in nitrogen flow.

Photolithography exposition of SU-8 layer

The difference between the usage of the foil with a printed pattern and the photomask made by electron-beam lithography to photolithographically produce 50 µm thin channel which is shown in (Figure 74) (collaboration with the Institute of Scientific Instruments of Czech Acadamy of Science, Brno). Using the foil, we were not able to produce adequately exposed patterns due to the random scattering of the incident UV light passing through the foil and due to the inherently not well-defined edges. The usage of foil led to underexposed edges in the vicinity of several micrometers around our designed channel and even to the outright short circuit due to the exposed golden Source and Drain electrodes. Switching to the chrome photomask solved this problem.

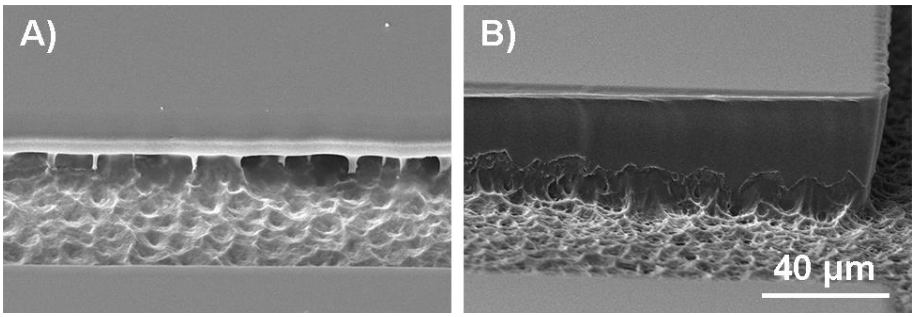

Figure 74 The difference between using printed pattern on the foil A) and chrome photomask B) to produce the photolithographic pattern

The screen printed and the photolithographically patterned layer of SU-8 covers the surface of the whole OECT sensing array as can be seen in (Figure 75).

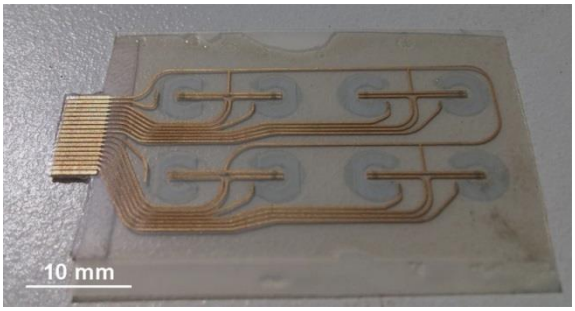

Figure 75 Screen-ptinted and photolithographically patterned OECT sensor array

Only parts of the sensor that comes in contact with the electrolyte (active channel and gate electrode) are exposed. The exposed channel area had the dimension of L = 50 µm and a width of W = 600 µm as shown in (Figure 76). The typical resistance of the channel was 200–300 Ω.

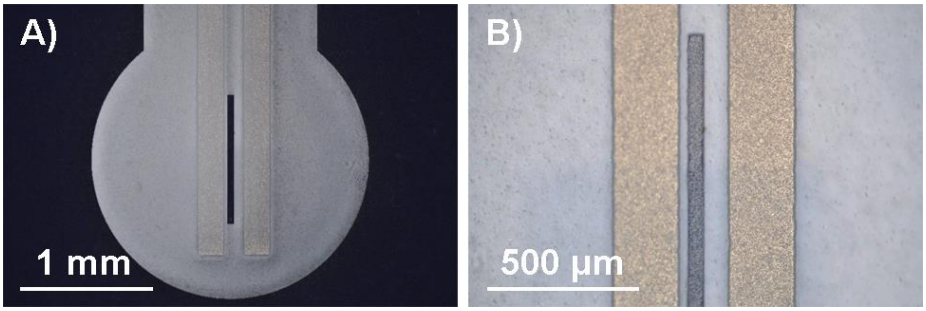

Figure 76 The detail of one sensor channel patterned using SU-8 photoresist

The electrical circuit designed for OECT remained the same as previously and is depicted in (Figure 66). The connector array at the microplate foil was contacted by 18-pin Molex connectors and 18-wire ribbon conductors so that a single connector connected eight OECTs. Individual OECT could be selected from the array by a proper couple of microswitches.

Results

The initial test determined the OECTs parameters such as output characteristics (Figure 77) and transfer characteristics (Figure 78), and from them, the highest derived transconductance g = 2.5 mS which was comparable or even better than state of the art fully lithographically prepared devices. The next experiment investigated the response of an OECT's channel current on a simulated signal of electrogenic cells. The standard PBS solution was used as an electrolyte. In looking for the optimum working point of the OECT with the highest transconductance, the gate voltage V_G was set to 0.2 V and the voltage between Source and Drain electrode was set to $V_D = -0.4$ V. The rectangular pulses of 1 mV_{pp} at a 1 s period were modulated. Typical response on such pulse together with filtered data using FFT (fast Fourier transform) bandpass from 0 to 25 Hz and determined value of the time constant can be seen in Figure 79. 3T3 fibroblasts were used to test the biocompatibility of the sensor. Cells were able to grow on top of the sensor to the same degree as in control substrate (standard cell culture plastics). The cell viability was similar to the control and was typically around 90 – 95 %. The unimpaired viability indicated that a high level of biocompatibility was reached. All the biocompatibility tests were done by the Institute of the Biophysics of the Czech Academy of Sciences.

Su-8 printing summary

The screen printing process of commercially available and biocompatible photoresist SU-8 was optimized and successfully implemented into previously adapted OECT sensors based on PEDOT:PSS. Using the photolithographic process the pattern of 50 mm thin active channel was achieved. Signal amplification was shown employing an electrogenic cell pulsation simulation, where the constant gate offset potential was modulated by a 1.0 Hz, 1.0 mV_{pp} rectangular signal. The resulting Source-Drain current response I_D was 2.5 µA, and the corresponding achieved transconductance 2.5 mS. The upper-frequency limit 7 Hz was concluded from the OECT gate circuit time constant of 0.15 s.

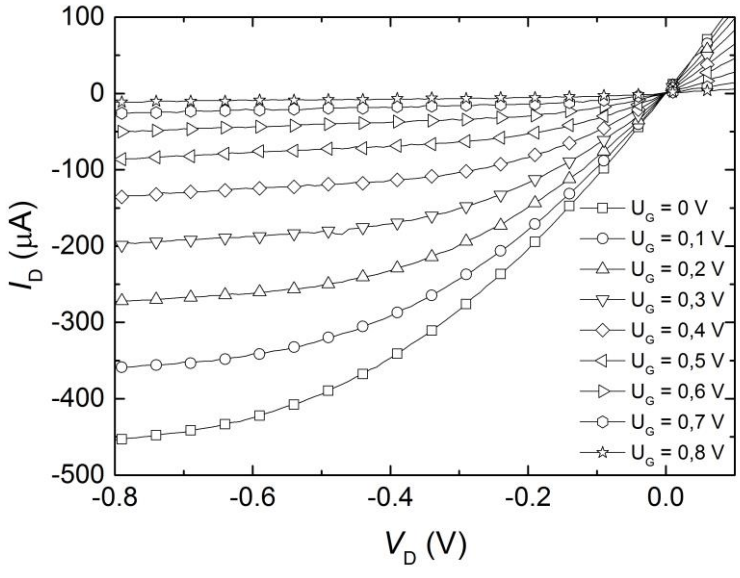

Figure 77 Output characteristics of 96-well OECT with SU-8 as covering layer

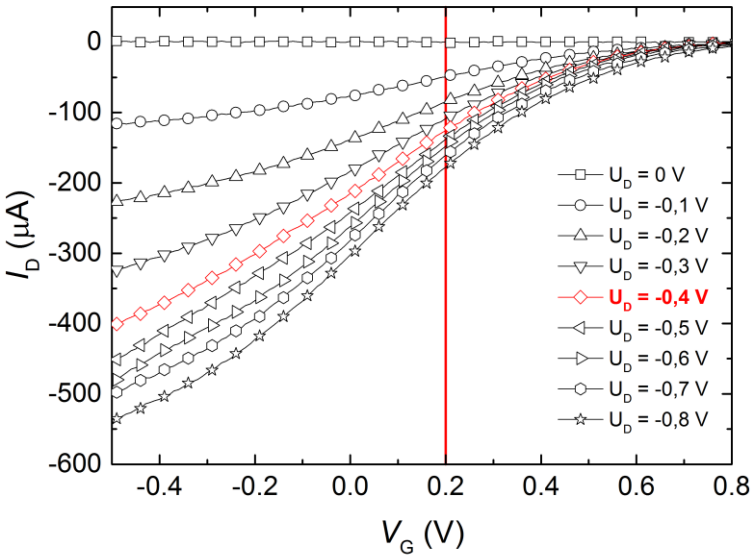

Figure 78 Transfer characteristics with the illustration of set point and the slope dependent on the drain potential

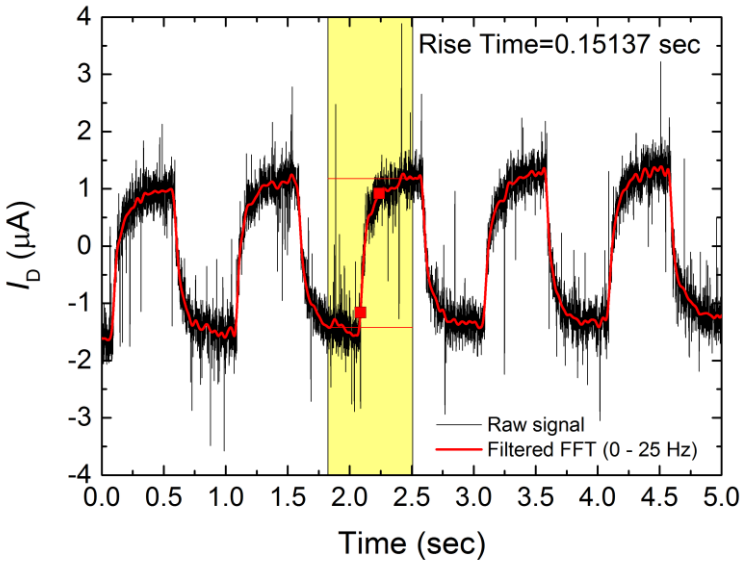

Figure 79 Response of OECT to 1 mV_{pp} gate rectangular signal at setting point $V_D = -0.4$ V, $V_G = 0.2$ V

7 CONCLUSION

The main goal of this dissertation thesis was to compile a comprehensive overview of organic electrochemical transistors, fabrication of such a device using conventional printing techniques and their subsequent use as a bioelectronic sensor. The manufacturing process was done in several iterations consisting of multiple steps. Firstly the inkjet printing of conductive and semiconductive layers was the necessary task to perform in order to manufacture the very first prototypes of OECTs. Several versions of all planar OECT motives were designed to be mounted into a matrix of 24 devices of SensoPlate™. First prototypes employed simple electrode system printed using silver ink and a semiconductive PEDOT:PSS. The first OECT prototypes were designed to have channel dimensions of 1 cm x 500 μm. The gate electrode with dimensions of 1 cm x 2 mm was set 500 μm apart from the channel. Patterns were designed with Autodesk AutoCAD. Both the channel and gate electrode were inkjet-printed using PEDOT:PSS. Circuits printed out of silver ink were placed outside of the cell cultivation area sealed by the silicone elastomer Sylgard® 184 to prevent contact with the PBS and living cells. The circuitry was terminated with five contacts compatible with standard connectors. Transparent and flexible 150 μm thick PET foil was used as a substrate.

During the production of a fully inkjet-printed matrix of 24 sensors, we found out few shortcomings in our design. Firstly, the PET substrates had insufficient thermal stability and during necessary thermal annealing at 150 °C (silver ink annealing) and even at 125 °C (PEDOT:PSS annealing) softened, waved and changed dimensions slightly. The silver ink had to be printed on a surfactant treated substrate in order to achieve good printing resolution, prevent unwanted ink spreading and pattern joining. Moreover, the silver layer had poor adhesion to the surface and had a tendency to swell and peel off after soaking in water or electrolyte. Furthermore, to print the compact active layer of PEDOT:PSS the substrate with printed silver ink circuits had to be plasma treated to modify its surface energy. The process of the fully inkjet-printed matrix of 24 sensors was technologically demanding and lengthy, mainly due to the fact that the reliability of the prints was poor. This was aggravated by the constant clogging of the nozzles during PEDOT:PSS printing. On top of that, a large number of misprinted samples due to the poor alignment of a substrate in the multi-layer device were caused by substrates dimensional changes.

In order to overcome previous shortcomings, we used screen printing technology to print the whole 24-well OECT matrix. It had proved to be a much faster and more reliable technique. All screen printed layers had better adhesion to substrates and better reproducibility than inkjet-printed ones. Layers of specific materials were designed in three different iterations.

Previous experience with inkjet printing and screen printing of a 24-well microplate has shown that the functionality of sensors is primarily dependent on the continuity of all printed parts and proper multi-layer alignment. The significance of the thickness homogeneity of the PEDOT: PSS layer results from the OECT function. Since its function is influenced by the injection of cations into the polymer layer and subsequent diffusion from the layer, it is important for the layer to have a uniform thickness over its entire surface.

The homogeneity of the PEDOT:PSS was addressed by the intensive stirring of the paste. The stirring slightly decreased the resulting thickness of the layer by an average of 20 %, from 250 nm to 200 nm and also improved the thickness homogeneity and roughness from 25 nm to 18 nm and waviness from 25 nm to 10 nm.

The PEDOT:PSS paste of gel consistency exhibited thixotropic behaviour. The static viscosity after stirring fell from the initial value of above 1000 Pa·s down to as low as 15 Pa·s. This was achieved after several days of intensive stirring in a magnetic stirrer at laboratory temperature or at an elevated temperature of (90 °C) in a matter of hours.

To further improve device performance we opted to decrease crucial OECT dimensions. That meant shortening the gate-channel distance and minimalizing the capacitance by reducing the channel area. To this end an all screen printed 96-well array of OECTs for cell culture electrical response monitoring was developed.

We also developed an electrical circuit designed for OECT testing with the connector array at the microplate foil connected by 18-pin Molex connectors and 18-wire ribbon conductors. In this way, the eight OECTs were connected by a single connector and individual OECTs could be selected from the array by a proper couple of micro-switches. The gate potential V_G was set from the external source in a range from −0.8 V to 0.8 V to prevent redox reactions at electrodes. Source and drain voltage V_D could be set down to −0.725 V. The source current I_S was converted to voltage in an I/V converter and recorded by an oscilloscope after further amplification.

Due to relaxations, the transfer characteristics and transconductance g included were strongly dependent on the sweep rate of the testing gate voltage V_G and its direction. The sharp transconductance maximum and its position at the V_G axis dependent on the channel geometry was reported in the literature, but no sweep rate influence was previously mentioned. The transfer characteristics also showed significant hysteresis.

To improve the biocompatibility of the PEDOT:PSS screen printing paste it was mixed with increasing concentration of Mouse Collagen, Type IV. Resulting composites were tested by the Institute of the Biophysics of the Czech Academy of Sciences. The cell viability was assessed by using MTT test and by the fluorescein diacetate and propidium iodide (FDA/PI) staining. All tests were done employing 3T3 fibroblasts using the 96-well platform.

To further miniaturize manufacturing process of OECT biosensor production based on PEDOT:PSS the screen printing process of commercially available and biocompatible photoresist SU-8 was optimized and successfully implemented. Using the photolithographic process the pattern of 50 mm thin active channel was achieved. Signal amplification was shown employing an electrogenic cell pulsation simulation, where the constant gate offset potential was modulated by a 1.0 Hz, 1.0 mV_{pp} rectangular signal. The resulting Source-Drain current response I_D was 2.5 μA, and the corresponding achieved transconductance of 2.5 mS. The upper-frequency limit 7 Hz was concluded from the OECT gate circuit time constant of 0.15 s.

3T3 fibroblasts were used to test the biocompatibility of the sensors. Cells were able to grow on top of the sensors to the same degree as in control substrates (standard cell culture plastics). The cell viability was similar to the control and was typically around 90 – 95 %. The unimpaired viability indicated that a high level of biocompatibility was reached.

To conclude, we were successfully able to produce microelectronic arrays of OECT sensors using standard printing techniques employing only commercially available materials. This approach is cheap, accessible and easy to implement during routine cell culture assessments. All our devices were manufactured without the need for cleanroom facilities, quickly, reliably and in large quantities. OECT sensors were biocompatible and able to measure the simulated response of the cardiac cells to the required extent.

8 LIST OF SYMBOLS AND ABBREVIATIONS

Symbols

α	Average lattice distance
ΔV	Voltage difference across the electrolyte
μ	Hole mobility
μ_i	Ionic mobility
A	Area
C	Capacitance
c	Concentration of the solid content in ink
C^*	Capacitance per unit volume
C'	Capacitance per unit area of the MOS capacitor
c_d	Capacitance per unit area
C_d	Series capacitor
d	Channel thickness
d_{dr}	Dry thickness of the printed film
$\mathrm{d}V/\mathrm{d}x$	Electric field intensity
G	Conductance
g	Transconductance
I_D	Drain current
I_{Kr}	Rapid outward current of K^+
I_{Ks}	Slow outward current of K^+
I_{Na}	Inward current caused by Na^+ cations
J	Current flux
k_p	Pick-out ratio
L	Channel length
L_d	Distance between the center of the ions and the metal plate
N	Number of capacitors
N_{dr}	Number of droplets deposited per area
p	Hole concentration
p_0	Initial hole concentration
pH	Potential of hydrogen
Q	Electrical charge
q	Elementary charge
Q_{SS}	Total charge
R_s	Series resistor
t	Time
T	Time period
v	Volume of semiconductor
$V(x)$	Spatial voltage profile
V_{dr}	Volume of the droplets
V_D^{sat}	Drain voltage at saturation
V_G	Gate voltage
V_G	Gate voltage
V_{max}	Maximal rate of depolarization
V_P	Pitch-off voltage
V_{scr}	Volume of ink per area of the open screen

V_{Th}	Threshold voltage
W	Channel width
ΔI_D	Modulation of the drain current
ε	Permittivity
ε_0	Vacuum permittivity
μ	Charge-carrier mobility
π	Bonding band
π^*	Antibonding band
ρ	Density of the material
τ	Response time
τ_i	Ionic transit time

Abbreviations

2D	Two dimensional
3D	Three dimensional
3T3	3-day transfer, inoculum 3×10^5 cells
Ag/AgCl	Non-polarizable electrode
Ag/AgCl	Silver/silver chloride reference electrode
ANSI	American National Standards Institute
AP	Cardiac action potential
APA	Amplitude of action potential
APD	Action potential duration
APD_{50}	Action potential duration at 50 % of repolarization
APD_{90}	Action potential duration at 90 % of repolarization
Au	Gold
C_{CH}	Capacitors corresponding to the channel
C_G	Capacitors corresponding to the gate
CPs	Conductive polymers
D	Drain electrode
DNA	Deoxyribonucleic acid
ECG	Electro Cardiogram
ECoG	Electro corticography
EEG	Electro encephalography
FDA	Fluorescein diacetate
FET	Field-effect transistor
FFT	Fast Fourier transform
FP	Cardiac field potential
G	Gate electrode
hiPSC-CMs	Human (induced) pluripotent stem cells
Kapton	Poly(4,4'-oxydiphenilene pyromellitimide)
KCl	Potassium chloride
kHz	Kilohertz
M^+	Positively charged ions
MEAs	Multi-electrode arrays
MEMS	Microelectromechanical system
MHz	Megahertz

MOS	Metal-oxide-semiconductor
MOSFET	Metal Oxide Semiconductor Field Effect Transistor
NaCl	Sodium chloride
NAD(P)H	Nicotinamide adenine dinucleotide phosphate reduced
NFC	Nano-fibrillated cellulose
OECT	Organic electrochemical transistors
OLED	Organic light emitting diode
OTFT	Organic thin film transistors
p(g2T-TT)	Poly(2-(3,3′-bis(2-(2-(2-methoxyethoxy) thiophene)
p(gNDI-g2T)	Poly((ethoxy)ethyl 2-(2-(2-methoxyethoxy ethoxy)acetate)-naphthalene-1,4,5,8−tetracarboxylic diimide co-3,3′-bis(2-(2-(2-methoxyethoxy)ethoxy)ethoxy)-(bithiophene))
P3HT	Poly(3-hexylthiophene-2,5-diyl
PANi	Polyaniline
PBS	Phosphate-Buffered Saline
PDMS	Polydimethylsiloxane
PEDOT	Poly(3,4-ethylenedioxythiophene)
PEDOT:PSS	Poly(3,4-ethylenedioxythiophene) polystyrene sulfonate
PEDOT:TOS	Poly(4-(2,3-dihydrothieno-(3,4-*b*)-(1,4)dioxin-2-yl-methoxy)-1-butanesulfonic acid, sodium salt)
PEG	Polyethylene glycol
PEN	Poly(ethylene 2,6-naphthalate)
PET	Poly(ethylene terephthalate)
PI	Propidium iodide
PLGA	Poly(lactic-co-glycolic) acid
PPy	Polypyrrole
Pt	Platinum
PTh	Polythiophene
PTHS	Poly(6-(thiophene-3-yl)hexane-1-sulfonate)
PVA	Polyvinyl alcohol
R_E	Resistor corresponding to the electrolyte
RMP	Resting membrane potential
RMS	Root mean square
S	Source electrode
SBS	Society for Biomolecular Screening
SEEG	Stereo electroencephalography
SEM	Scanning electron microscopy
SMU	Source Measure Unit
USB	Universal super bus
UV	Ultraviolet light
X^-	Anions of the electrolyte

9 LITERATURE

[1] MALLIARAS, George a Richard FRIEND. An organic electronics primer. *Physics Today* [online]. 2005, 58(5): 53-58 [cit. 2015-07-14]. DOI: 10.1063/1.1995748. ISSN 0031-9228.

[2] TARABELLA, Giuseppe, Gaurav NANDA, Marco VILLANI, Nicola COPPEDÈ, Roberto MOSCA, George G. MALLIARAS, Clara SANTATO, Salvatore IANNOTTA a Fabio CICOIRA. Organic electrochemical transistors monitoring micelle formation. *Chemical Science* [online]. 2012, 3(12): [cit. 2015-07-14]. DOI: 10.1039/c2sc21020g. ISSN 2041-6520.

[3] PEI, Q., G. YU, C. ZHANG, Y. YANG a A. J. HEEGER. Polymer Light-Emitting Electrochemical Cells. *Science* [online]. 1995, 269(5227): 1086-1088 [cit. 2015-07-14]. DOI: 10.1126/science.269.5227.1086. ISSN 0036-8075.

[4] MORTIMER, Roger J., Aubrey L. DYER a John R. REYNOLDS. Electrochromic organic and polymeric materials for display applications. *Displays* [online]. 2006, 27(1): 2-18 [cit. 2015-07-14]. DOI: 10.1016/j.displa.2005.03.003. ISSN 01419382.

[5] BERNARDS, D. A., S. FLORES-TORRES, H. D. ABRUNA a G. G. MALLIARAS. Observation of Electroluminescence and Photovoltaic Response in Ionic Junctions. *Science* [online]. 2006, 313(5792): 1416-1419 [cit. 2015-07-14]. DOI: 10.1126/science.1128145. ISSN 0036-8075.

[6] BERGGREN, M. and A. RICHTER-DAHLFORS. Organic Bioelectronics. *Advanced Materials* [online]. 2007, 19(20): 3201-3213 [cit. 2015-07-14]. DOI: 10.1002/adma.200700419. ISSN 09359648.

[7] SVENNERSTEN, Karl, Karin C. LARSSON, Magnus BERGGREN a Agneta RICHTER-DAHLFORS. Organic bioelectronics in nanomedicine. *Biochimica et Biophysica Acta (BBA) - General Subjects* [online]. 2011, 1810(3): 276-285 [cit. 2015-07-14]. DOI: 10.1016/j.bbagen.2010.10.001. ISSN 03044165.

[8] OWENS, Róisín, Peter KJALL, Agneta RICHTER-DAHLFORS a Fabio CICOIRA. Organic bioelectronics — Novel applications in biomedicine. *Biochimica et Biophysica Acta (BBA) - General Subjects* [online]. 2013, 1830(9), 4283-4285 [cit. 2019-01-08]. DOI: 10.1016/j.bbagen.2013.04.025. ISSN 03044165.

[9] BUZSÁKI, György, Costas A. ANASTASSIOU a Christof KOCH. The origin of extracellular fields and currents — EEG, ECoG, LFP and spikes. *Nature Reviews Neuroscience* [online]. 2012-5-18, 13(6): 407-420 [cit. 2015-07-14]. DOI: 10.1038/nrn3241. ISSN 1471-003x.

[10] RIVNAY, Jonathan, Róisín M. OWENS a George G. MALLIARAS. The Rise of Organic Bioelectronics. *Chemistry of Materials* [online]. 2013, 26(1): 679-685 [cit. 2015-07-14]. DOI: 10.1021/cm4022003. ISSN 0897-4756.

[11] SCHUMACHER, Soeren, Jörg NESTLER, Thomas OTTO, et al. Highly-integrated lab-on-chip system for point-of-care multiparameter analysis. *Lab Chip* [online]. 2012, 12(3), 464-473 [cit. 2019-01-08]. DOI: 10.1039/C1LC20693A. ISSN 1473-0197.

[12] ROBINSON, Nathaniel D., Per-Olof SVENSSON, David NILSSON a Magnus BERGGREN. On the Current Saturation Observed in Electrochemical Polymer Transistors. *Journal of The Electrochemical Society* [online]. 2006, 153(3) [cit. 2015-07-14]. DOI: 10.1149/1.2172534. ISSN 00134651.

[13] HEEGER, Alan J. Semiconducting and Metallic Polymers: The Fourth Generation of Polymeric Materials. *The Journal of Physical Chemistry B* [online]. 2001, 105(36), 8475-8491 [cit. 2015-08-20]. DOI: 10.1021/jp011611w. ISSN 1520-6106.

[14] JIMISON, Leslie H., Jonathan RIVNAY a Róisín M. OWENS. Conducting Polymers to Control and Monitor Cells. *Organic Electronics* [online]. Weinheim, Germany, 2013, 2013-08-23, 27-67 [cit. 2019-01-08]. DOI: 10.1002/9783527650965.ch02. ISBN 9783527650965.

[15] STAVRINIDOU, Eleni, Pierre LELEUX, Harizo RAJAONA, Dion KHODAGHOLY, Jonathan RIVNAY, Manfred LINDAU, Sébastien SANAUR a George G. MALLIARAS. Direct Measurement of Ion Mobility in a Conducting Polymer. *Advanced Materials* [online]. 2013, 25(32): 4488-4493 [cit. 2015-11-11]. DOI: 10.1002/adma.201301240. ISSN 09359648

[16] JONAS, Friedrich, Werner KRAFFT a Bavo MUYS. Poly(3, 4-ethylenedioxythiophene): Conductive coatings, technical applications and properties. *Macromolecular Symposia* [online]. 1995, 100(1): 169-173 [cit. 2015-11-11]. DOI: 10.1002/masy.19951000128. ISSN 10221360.

[17] SØNDERGAARD, Roar, Markus HÖSEL, Dechan ANGMO, Thue T. LARSEN-OLSEN a Frederik C. KREBS. Roll-to-roll fabrication of polymer solar cells. *Materials Today* [online]. 2012, 15(1-2): 36-49 [cit. 2015-11-23]. DOI: 10.1016/S1369-7021(12)70019-6. ISSN 13697021

[18] ELSCHNER, Andreas, Stephan KIRCHMEYER, Wilfried LOVENICH, Udo MERKER a Knud REUTER. *PEDOT: principles and applications of an intrinsically conductive polymer*. Boca Raton, FL: CRC Press, 2010. ISBN 978-142-0069-112.

[19] MARTINI, Frederic, *The Fundamentals of Anatomy and Physiology: Chapter 10 Cardiac Muscle Tissue*. *SlidePlayer* [online]. [cit. 2018-09-25].

[20] GÖKTEPE, Serdar, Oscar John ABILEZ, Kevin Kit PARKER a Ellen KUHL. A multiscale model for eccentric and concentric cardiac growth through sarcomerogenesis. *Journal of Theoretical Biology* [online]. 2010, 265(3), 433-442 [cit. 2019-01-08]. DOI: 10.1016/j.jtbi.2010.04.023. ISSN 00225193.

[21] OLIVETTI, G. Aging, Cardiac Hypertrophy and Ischemic Cardiomyopathy Do Not Affect the Proportion of Mononucleated and Multinucleated Myocytes in the Human Heart. *Journal of Molecular and Cellular Cardiology* [online]. 1996, 28(7), 1463-1477 [cit. 2019-01-08]. DOI: 10.1006/jmcc.1996.0137. ISSN 00222828.

[22] RUDY, Yoram. Molecular Basis of Cardiac Action Potential Repolarization. *Annals of the New York Academy of Sciences* [online]. 2008, 1123(1), 113-118 [cit. 2019-01-08]. DOI: 10.1196/annals.1420.013. ISSN 00778923.

[23] SPLAWSKI, I., K. W. TIMOTHY, N. DECHER, P. KUMAR, F. B. SACHSE, A. H. BEGGS, M. C. SANGUINETTI a M. T. KEATING. Severe arrhythmia disorder caused by cardiac L-type calcium channel mutations. *Proceedings of the National Academy of Sciences* [online]. 2005, 102(23), 8089-8096 [cit. 2019-01-08]. DOI: 10.1073/pnas.0502506102. ISSN 0027-8424.

[24] WOOD, Alastair J.J. a Dan M. RODEN. Drug-Induced Prolongation of the QT Interval. *New England Journal of Medicine* [online]. 2004, 350(10), 1013-1022 [cit. 2019-01-08]. DOI: 10.1056/NEJMra032426. ISSN 0028-4793.

[25] TERTOOLEN, L.G.J., S.R. BRAAM, B.J. VAN MEER, R. PASSIER a C.L. MUMMERY. Interpretation of field potentials measured on a multi electrode array in pharmacological toxicity screening on primary and human pluripotent stem cell-derived cardiomyocytes. *Biochemical and Biophysical Research Communications* [online]. 2018, 497(4), 1135-1141 [cit. 2019-01-08]. DOI: 10.1016/j.bbrc.2017.01.151. ISSN 0006291X.

[26] BRAAM, Stefan R., Leon TERTOOLEN, Anja VAN DE STOLPE, Thomas MEYER, Robert PASSIER a Christine L. MUMMERY. Prediction of drug-induced cardiotoxicity using human embryonic stem cell-derived cardiomyocytes. *Stem Cell Research* [online]. 2010, 4(2), 107-116 [cit. 2019-01-08]. DOI: 10.1016/j.scr.2009.11.004. ISSN 18735061.

[27] WHITE, Henry S., Gregg P. KITTLESEN a Mark S. WRIGHTON. Chemical derivatization of an array of three gold microelectrodes with polypyrrole: fabrication of a molecule-based transistor. *Journal of the American Chemical Society* [online]. 1984, 106(18): 5375-5377 [cit. 2015-07-24]. DOI: 10.1021/ja00330a070. ISSN 0002-7863.

[28] HEYWANG, Gerhard a Friedrich JONAS. Poly(alkylenedioxythiophene)s—new, very stable conducting polymers. *Advanced Materials* [online]. 1992, 4(2), 116-118 [cit. 2019-01-08]. DOI: 10.1002/adma.19920040213. ISSN 0935-9648.

[29] YAMATO, Hitoshi, Masaki OHWA a Wolfgang WERNET. Stability of polypyrrole and poly(3,4-ethylenedioxythiophene) for biosensor application. *Journal of Electroanalytical Chemistry* [online]. 1995, 397(1-2), 163-170 [cit. 2019-01-08]. DOI: 10.1016/0022-0728(95)04156-8. ISSN 15726657.

[30] KOPOLA, P., T. AERNOUTS, S. GUILLEREZ, H. JIN, M. TUOMIKOSKI, A. MAANINEN a J. HAST. High efficient plastic solar cells fabricated with a high-throughput gravure printing method. *Solar Energy Materials and Solar Cells* [online]. 2010, 94(10), 1673-1680 [cit. 2019-01-09]. DOI: 10.1016/j.solmat.2010.05.027. ISSN 09270248.

[31] BERNARDS, D. A. a G. G. MALLIARAS. Steady-State and Transient Behavior of Organic Electrochemical Transistors. *Advanced Functional Materials* [online]. 2007, 17(17): 3538-3544 [cit. 2015-07-14]. DOI: 10.1002/adfm.200601239. ISSN 1616301x

[32] KHODAGHOLY, Dion, Jonathan RIVNAY, Michele SESSOLO, et al. High transconductance organic electrochemical transistors. *Nature Communications* [online]. 2013, 4(1) [cit. 2019-01-09]. DOI: 10.1038/ncomms3133. ISSN 2041-1723.

[33] NIELSEN, Christian B., Alexander GIOVANNITTI, Dan-Tiberiu SBIRCEA, et al. Molecular Design of Semiconducting Polymers for High-Performance Organic Electrochemical Transistors. *Journal of the American Chemical Society* [online]. 2016, 138(32), 10252-10259 [cit. 2019-01-09]. DOI: 10.1021/jacs.6b05280. ISSN 0002-7863.

[34] RIVNAY, Jonathan, Sahika INAL, Alberto SALLEO, Róisín M. OWENS, Magnus BERGGREN a George G. MALLIARAS. Organic electrochemical transistors. *Nature Reviews Materials* [online]. 2018, 3(2) [cit. 2019-01-09]. DOI: 10.1038/natrevmats.2017.86. ISSN 2058-8437.

[35] KHODAGHOLY, Dion, Thomas DOUBLET, Pascale QUILICHINI, et al. In vivo recordings of brain activity using organic transistors. *Nature Communications* [online]. 2013, 4(1) [cit. 2019-01-09]. DOI: 10.1038/ncomms2573. ISSN 2041-1723.

[36] RIVNAY, Jonathan, Pierre LELEUX, Marc FERRO, et al. High-performance transistors for bioelectronics through tuning of channel thickness. *Science Advances* [online]. 2015, 1(4) [cit. 2019-01-09]. DOI: 10.1126/sciadv.1400251. ISSN 2375-2548.

[37] STRAKOSAS, Xenofon, Manuelle BONGO a Róisín M. OWENS. The organic electrochemical transistor for biological applications. *Journal of Applied Polymer Science* [online]. 2015, 132(15), [cit. 2016-02-15]. DOI: 10.1002/app.41735. ISSN 00218995.

[38] LIN, Peng a Feng YAN. Organic Thin-Film Transistors for Chemical and Biological Sensing. *Advanced Materials* [online]. 2012, 24(1), 34-51 [cit. 2019-01-08]. DOI: 10.1002/adma.201103334. ISSN 09359648.

[39] NILSSON, D., N. ROBINSON, M. BERGGREN a R. FORCHHEIMER. Electrochemical Logic Circuits. *Advanced Materials* [online]. 2005, 17(3), 353-358 [cit. 2019-01-08]. DOI: 10.1002/adma.200401273. ISSN 0935-9648.

[40] HUTTER, Philipp C., Thomas ROTHLANDER, Gregor SCHEIPL a Barbara STADLOBER. All Screen-Printed Logic Gates Based on Organic Electrochemical Transistors. *IEEE Transactions on Electron Devices* [online]. 2015, 62(12), 4231-4236 [cit. 2019-01-08]. DOI: 10.1109/TED.2015.2491342. ISSN 0018-9383.

[41] GKOUPIDENIS, Paschalis, Dimitrios A. KOUTSOURAS a George G. MALLIARAS. Neuromorphic device architectures with global connectivity through electrolyte gating. *Nature Communications* [online]. 2017, 8 [cit. 2019-01-09]. DOI: 10.1038/ncomms15448. ISSN 2041-1723.

[42] VAN DE BURGT, Yoeri, Ewout LUBBERMAN, Elliot J. FULLER, et al. A non-volatile organic electrochemical device as a low-voltage artificial synapse for neuromorphic computing. *Nature Materials* [online]. 2017, 16(4), 414-418 [cit. 2019-01-09]. DOI: 10.1038/nmat4856. ISSN 1476-1122.

[43] BERGGREN, M., D. NILSSON a N. D. ROBINSON. Organic materials for printed electronics. *Nature Materials* [online]. 2007, 6(1), 3-5 [cit. 2019-01-09]. DOI: 10.1038/nmat1817. ISSN 1476-1122.

[44] KAPHLE, Vikash, Shiyi LIU, Akram AL-SHADEEDI, Chang-Min KEUM a Björn LÜSSEM. Contact Resistance Effects in Highly Doped Organic Electrochemical Transistors. *Advanced Materials* [online]. 2016, 28(39), 8766-8770 [cit. 2019-01-09]. DOI: 10.1002/adma.201602125. ISSN 09359648.

[45] FRIEDLEIN, Jacob T., Jonathan RIVNAY, David H. DUNLAP, Iain MCCULLOCH, Sean E. SHAHEEN, Robert R. MCLEOD a George G. MALLIARAS. Influence of disorder on transfer characteristics of organic electrochemical transistors. *Applied Physics Letters* [online]. 2017, 111(2) [cit. 2019-01-09]. DOI: 10.1063/1.4993776. ISSN 0003-6951.

[46] GIOVANNITTI, Alexander, Christian B. NIELSEN, Dan-Tiberiu SBIRCEA, et al. N-type organic electrochemical transistors with stability in water. *Nature Communications* [online]. 2016, 7(1) [cit. 2019-01-09]. DOI: 10.1038/ncomms13066. ISSN 2041-1723.

[47] GIOVANNITTI, Alexander, Dan-Tiberiu SBIRCEA, Sahika INAL, et al. Controlling the mode of operation of organic transistors through side-chain engineering. *Proceedings of the National Academy of Sciences* [online]. 2016, 113(43), 12017-12022 [cit. 2019-01-09]. DOI: 10.1073/pnas.1608780113. ISSN 0027-8424.

[48] HÜTTER, Philipp C., Thomas ROTHLÄNDER, Anja HAASE, Gregor TRIMMEL a Barbara STADLOBER. Influence of geometry variations on the response of organic electrochemical transistors. *Applied Physics Letters* [online]. 2013, 103(4) [cit. 2019-01-09]. DOI: 10.1063/1.4816781. ISSN 0003-6951.

[49] BARD, Allen J a Larry R FAULKNER. *Electrochemical methods: fundamentals and applications*. 2nd ed. New York: Wiley, c2001. ISBN 978-0-471-04372-0.

[50] KOUTSOURAS, Dimitrios A., Paschalis GKOUPIDENIS, Clemens STOLZ, Vivek SUBRAMANIAN, George G. MALLIARAS a David C. MARTIN. Impedance Spectroscopy of Spin-Cast and Electrochemically Deposited PEDOT: PSS Films on Microfabricated Electrodes with Various Areas. *ChemElectroChem* [online]. 2017, 4(9), 2321-2327 [cit. 2019-01-09]. DOI: 10.1002/celc.201700297. ISSN 21960216.

[51] ANDERSSON, P., D. NILSSON, P.-O. SVENSSON, M. CHEN, MALMSTRÖM a T. REMONEN. Active Matrix Displays Based on All-Organic Electrochemical Smart Pixels Printed on Paper. *Advanced Materials* [online]. 2002, 14(20): 1460-1464 [cit. 2018-09-26]. DOI: 10.1002/1521-4095(20021016)14:20<1460::AID-ADMA1460> 3.0.CO;2-S.

[52] LIN, Fuding a Mark C. LONERGAN. Gate electrode processes in an electrolyte-gated transistor: Non-Faradaically versus Faradaically coupled conductivity modulation of a polyacetylene ionomer. *Applied Physics Letters* [online]. 2006, 88(13): [cit. 2018-09-26]. DOI: 10.1063/1.2190077. ISSN 00036951

[53] PRIGODIN, V.N., F.C. HSU, Y.M. KIM, J.H. PARK, O. WALDMANN a A.J. EPSTEIN. Electric Field Control of Charge Transport in Doped Polymers. *Synthetic Metals* [online]. 2005, 153(1-3): 157-160 [cit. 2018-09-26]. DOI: 10.1016/j.synthmet.2005.07.180. ISSN 03796779.

[54] ALAM, Maksudul M., Jun WANG, Yaoyao GUO, Stephanie P. LEE a Hsian-Rong TSENG. Electrolyte-Gated Transistors Based on Conducting Polymer Nanowire Junction Arrays. *The Journal of Physical Chemistry B* [online]. 2005, 109(26): 12777-12784 [cit. 2018-09-26]. DOI: 10.1021/jp050903k. ISSN 1520-6106.

[55] KERGOAT, L., L. HERLOGSSON, B. PIRO, M. C. PHAM, G. HOROWITZ, X. CRISPIN a M. BERGGREN. Tuning the threshold voltage in electrolyte-gated organic field-effect transistors. *Proceedings of the National Academy of Sciences* [online]. 2012, 109(22), 8394-8399 [cit. 2018-09-26]. DOI: 10.1073/pnas.1120311109. ISSN 0027-8424.

[56] MADDALENA, F., E. J. MEIJER, K. ASADI, D. M. DE LEEUW a P. W. M. BLOM. Doping kinetics of organic semiconductors investigated by field-effect transistors. *Applied Physics Letters* [online]. 2010, 97(4), [cit. 2018-09-26]. DOI: 10.1063/1.3466903. ISSN 00036951.

[57] PROCTOR, Christopher M., Jonathan RIVNAY a George G. MALLIARAS. Understanding volumetric capacitance in conducting polymers. *Journal of Polymer Science Part B: Polymer Physics* [online]. 2016, 54(15), 1433-1436 [cit. 2019-01-09]. DOI: 10.1002/polb.24038. ISSN 08876266

[58] ZOTTI, G., S. ZECCHIN, G. SCHIAVON, et al. Electrochemical and XPS Studies toward the Role of Monomeric and Polymeric Sulfonate Counterions in the Synthesis, Composition, and Properties of Poly(3,4-ethylenedioxythiophene). *Macromolecules* [online]. 2003, 36(9), 3337-3344 [cit. 2019-01-09]. DOI: 10.1021/ma021715k. ISSN 0024-9297.

[59] XU, Yue, Ying TAO, Xiaoyu ZHENG, Hongyun MA, Jiayan LUO, Feiyu KANG a Quan-Hong YANG. A Metal-Free Supercapacitor Electrode Material with a Record High Volumetric Capacitance over 800 F cm −3. *Advanced Materials* [online]. 2015, 27(48), 8082-8087 [cit. 2019-01-09]. DOI: 10.1002/adma.201504151. ISSN 09359648.

[60] KAWAHARA, Jun, Peter Andersson ERSMAN, Kazuya KATOH a Magnus BERGGREN. Fast-Switching Printed Organic Electrochemical Transistors Including Electronic Vias Through Plastic and Paper Substrates. *IEEE Transactions on Electron Devices* [online]. 2013, 60(6), 2052-2056 [cit. 2019-01-09]. DOI: 10.1109/TED.2013.2258923. ISSN 0018-9383.

[61] DONAHUE, Mary J., Adam WILLIAMSON, Xenofon STRAKOSAS, Jacob T. FRIEDLEIN, Robert R. MCLEOD, Helena GLESKOVA a George G. MALLIARAS. High-Performance Vertical Organic Electrochemical Transistors. *Advanced Materials* [online]. 2018, 30(5) [cit. 2019-01-09]. DOI: 10.1002/adma.201705031. ISSN 09359648.

[62] DEMELAS, M., E. SCAVETTA, L. BASIRICÒ, R. ROGANI a A. BONFIGLIO. A deeper insight into the operation regime of all-polymeric electrochemical transistors. *Applied Physics Letters* [online]. 2013, 102(19): [cit. 2018-09-27]. DOI: 10.1063/1.4804423. ISSN 00036951.

[63] RIVNAY, Jonathan, Pierre LELEUX, Michele SESSOLO, Dion KHODAGHOLY, Thierry HERVÉ, Michel FIOCCHI a George G. MALLIARAS. Organic Electrochemical Transistors with Maximum Transconductance at Zero Gate Bias. *Advanced Materials* [online]. 2013, 25(48), 7010-7014 [cit. 2018-09-27]. DOI: 10.1002/adma.201303080. ISSN 09359648.

[64] OLIVIER, Yoann, Dorota NIEDZIALEK, Vincent LEMAUR, et al. 25th Anniversary Article: High-Mobility Hole and Electron Transport Conjugated Polymers. *Advanced Materials* [online]. 2014, 26(14), 2119-2136 [cit. 2019-01-09]. DOI: 10.1002/adma.201305809. ISSN 09359648.

[65] ELMAHMOUDY, Mohammed, Sahika INAL, Anne CHARRIER, Ilke UGUZ, George G. MALLIARAS a Sébastien SANAUR. Tailoring the Electrochemical and Mechanical Properties of PEDOT: PSS Films for Bioelectronics. *Macromolecular Materials and Engineering* [online]. 2017, 302(5) [cit. 2019-01-09]. DOI: 10.1002/mame.201600497. ISSN 14387492.

[66] INAL, Sahika, Jonathan RIVNAY, Anna I. HOFMANN, et al. Organic electrochemical transistors based on PEDOT with different anionic polyelectrolyte dopants. *Journal of Polymer Science Part B: Polymer Physics* [online]. 2016, 54(2), 147-151 [cit. 2019-01-09]. DOI: 10.1002/polb.23938. ISSN 08876266.

[67] INAL, Sahika, Jonathan RIVNAY, Pierre LELEUX, et al. A High Transconductance Accumulation Mode Electrochemical Transistor. *Advanced Materials* [online]. 2014, 26(44), 7450-7455 [cit. 2019-01-09]. DOI: 10.1002/adma.201403150. ISSN 09359648.

[68] ZEGLIO, Erica, Mikhail VAGIN, Chiara MUSUMECI, et al. Conjugated Polyelectrolyte Blends for Electrochromic and Electrochemical Transistor Devices. *Chemistry of Materials* [online]. 2015, 27(18), 6385-6393 [cit. 2019-01-09]. DOI: 10.1021/acs.chemmater.5b02501. ISSN 0897-4756.

[69] STRAKOSAS, Xenofon, Michele SESSOLO, Adel HAMA, Jonathan RIVNAY, Eleni STAVRINIDOU, George G. MALLIARAS a Roisin M. OWENS. A facile biofunctionalisation route for solution processable conducting polymer devices. *J. Mater. Chem. B* [online]. 2014, 2(17), 2537-2545 [cit. 2019-01-09]. DOI: 10.1039/C3TB21491E. ISSN 2050-750X.

[70] STAVRINIDOU, Eleni, Orawan WINTHER-JENSEN, Bijan S. SHEKIBI, et al. Engineering hydrophilic conducting composites with enhanced ion mobility. *Phys. Chem. Chem. Phys* [online]. 2014, 16(6), 2275-2279 [cit. 2019-01-09]. DOI: 10.1039/C3CP54061H. ISSN 1463-9076.

[71] ZEGLIO, Erica, Jens ERIKSSON, Roger GABRIELSSON, Niclas SOLIN a Olle INGANÄS. Highly Stable Conjugated Polyelectrolytes for Water-Based Hybrid Mode Electrochemical Transistors. *Advanced Materials* [online]. 2017, 29(19) [cit. 2019-01-09]. DOI: 10.1002/adma.201605787. ISSN 09359648.

[72] PACHECO-MORENO, Celia M., Murielle SCHRECK, Alberto D. SCACCABAROZZI, Philippe BOURGUN, Guillaume WANTZ, Molly M. STEVENS, Olivier J. DAUTEL a Natalie STINGELIN. The Importance of Materials Design to Make Ions Flow: Toward Novel Materials Platforms for Bioelectronics Applications. *Advanced Materials* [online]. 2017, 29(4) [cit. 2019-01-09]. DOI: 10.1002/adma.201604446. ISSN 09359648.

[73] INAL, Sahika, George G. MALLIARAS a Jonathan RIVNAY. Benchmarking organic mixed conductors for transistors. *Nature Communications* [online]. 2017, 8(1) [cit. 2019-01-09]. DOI: 10.1038/s41467-017-01812-w. ISSN 2041-1723.

[74] KHODAGHOLY, Dion, Vincenzo F. CURTO, Kevin J. FRASER, et al. Organic electrochemical transistor incorporating an ionogel as a solid state electrolyte for lactate sensing. *Journal of Materials Chemistry* [online]. 2012, 22(10) [cit. 2019-01-09]. DOI: 10.1039/c2jm15716k. ISSN 0959-9428.

[75] TARABELLA, Giuseppe, Clara SANTATO, Sang Yoon YANG, Salvatore IANNOTTA, George G. MALLIARAS a Fabio CICOIRA. Effect of the gate electrode on the response of organic electrochemical transistors. *Applied Physics Letters* [online]. 2010, 97(12) [cit. 2019-01-09]. DOI: 10.1063/1.3491216. ISSN 0003-6951.

[76] TANG, Hao, Prajwal KUMAR, Shiming ZHANG, Zhihui YI, Gregory De CRESCENZO, Clara SANTATO, Francesca SOAVI a Fabio CICOIRA. Conducting Polymer Transistors Making Use of Activated Carbon Gate Electrodes. *ACS Applied Materials & Interfaces* [online]. 2014, 7(1), 969-973 [cit. 2019-01-09]. DOI: 10.1021/am507708c. ISSN 1944-8244.

[77] WINTHER-JENSEN, Bjørn a Keld WEST. Vapor-Phase Polymerization of 3,4-Ethylenedioxythiophene: A Route to Highly Conducting Polymer Surface Layers. *Macromolecules* [online]. 2004, 37(12), 4538-4543 [cit. 2019-01-09]. DOI: 10.1021/ma049864l. ISSN 0024-9297.

[78] JIMISON, Leslie H., Adel HAMA, Xenofon STRAKOSAS, et al. PEDOT: TOS with PEG. *Journal of Materials Chemistry* [online]. 2012, 22(37) [cit. 2019-01-09]. DOI: 10.1039/c2jm32188b. ISSN 0959-9428.

[79] BONGO, Manuelle, Orawan WINTHER-JENSEN, Scott HIMMELBERGER, et al. PEDOT: gelatin composites mediate brain endothelial cell adhesion. *Journal of Materials Chemistry B* [online]. 2013, 1(31) [cit. 2019-01-09]. DOI: 10.1039/c3tb20374c. ISSN 2050-750X.

[80] KANETO, Keiichi, Tanemasa ASANO a Wataru TAKASHIMA. Memory Device Using a Conducting Polymer and Solid Polymer Electrolyte. *Japanese Journal of Applied Physics* [online]. 1991, 30(Part 2, No. 2A), L215-L217 [cit. 2019-01-09]. DOI: 10.1143/JJAP.30.L215. ISSN 0021-4922.

[81] MATSUE, Tomokazu, Matsuhiko NISHIZAWA, Takahiro SAWAGUCHI a Isamu UCHIDA. An enzyme switch sensitive to NADH. *Journal of the Chemical Society, Chemical Communications* [online]. 1991, (15) [cit. 2019-01-09]. DOI: 10.1039/c39910001029. ISSN 0022-4936.

[82] SAXENA, Vibha, Vinay SHIRODKAR a Rajiv PRAKASH. A comparative study of a polyindole-based microelectrochemical transistor in aqueous and non-aqueous electrolytes. *Journal of Solid State Electrochemistry* [online]. 2000, 4(4), 231-233 [cit. 2019-01-09]. DOI: 10.1007/s100080050200. ISSN 1432-8488.

[83] MABECK, Jeffrey T., John A. DEFRANCO, Daniel A. BERNARDS, George G. MALLIARAS, Sandrine HOCDÉ a Christopher J. CHASE. Microfluidic gating of an organic electrochemical transistor. *Applied Physics Letters* [online]. 2005, 87(1) [cit. 2019-01-09]. DOI: 10.1063/1.1991979. ISSN 0003-6951.

[84] BERNARDS, Daniel A., George G. MALLIARAS, Gilman E. S. TOOMBES a Sol M. GRUNER. Gating of an organic transistor through a bilayer lipid membrane with ion channels. *Applied Physics Letters* [online]. 2006, 89(5) [cit. 2019-01-10]. DOI: 10.1063/1.2266250. ISSN 0003-6951.

[85] ALAM, Maksudul M., Jun WANG, Yaoyao GUO, Stephanie P. LEE a Hsian-Rong TSENG. Electrolyte-Gated Transistors Based on Conducting Polymer Nanowire Junction Arrays. *The Journal of Physical Chemistry B* [online]. 2005, 109(26), 12777-12784 [cit. 2019-01-10]. DOI: 10.1021/jp050903k. ISSN 1520-6106.

[86] WAN, Alwin Ming-Doug, Sahika INAL, Tiffany WILLIAMS, et al. 3D conducting polymer platforms for electrical control of protein conformation and cellular functions. *Journal of Materials Chemistry B* [online]. 2015, 3(25), 5040-5048 [cit. 2019-01-10]. DOI: 10.1039/C5TB00390C. ISSN 2050-750X.

[87] TEHRANI, Payman, Nathaniel D ROBINSON, Thomas KUGLER, et al. Patterning polythiophene films using electrochemical over-oxidation. *Smart Materials and Structures* [online]. 2005, 14(4), N21-N25 [cit. 2019-01-10]. DOI: 10.1088/0964-1726/14/4/N03. ISSN 0964-1726.

[88] PERINKA, Nikola, Chang Hyun KIM, Marie KAPLANOVA a Yvan BONNASSIEUX. Preparation and Characterization of Thin Conductive Polymer Films on the base of PEDOT: PSS by Ink-Jet Printing. *Physics Procedia* [online]. 2013, 44, 120-129 [cit. 2019-01-10]. DOI: 10.1016/j.phpro.2013.04.016. ISSN 18753892.

[89] KOLODZIEJCZYK, Bartlomiej, Orawan WINTHER-JENSEN, Brooke A. PEREIRA, Santhosh S. NAIR a Bjorn WINTHER-JENSEN. Patterning of conducting layers on breathable substrates using laser engraving for gas sensors. *Journal of Applied Polymer Science* [online]. 2015, 132(35), n/a-n/a [cit. 2019-01-10]. DOI: 10.1002/app.42359. ISSN 00218995.

[90] GUALANDI, I., M. MARZOCCHI, A. ACHILLI, D. CAVEDALE, A. BONFIGLIO a B. FRABONI. Textile Organic Electrochemical Transistors as a Platform for Wearable Biosensors. *Scientific Reports* [online]. 2016, 6(1) [cit. 2019-01-10]. DOI: 10.1038/srep33637. ISSN 2045-2322.

[91] HAMEDI, Mahiar, Robert FORCHHEIMER a Olle INGANÄS. Towards woven logic from organic electronic fibres. *Nature Materials* [online]. 2007, 6(5), 357-362 [cit. 2019-01-10]. DOI: 10.1038/nmat1884. ISSN 1476-1122.

[92] WANG, Yuedan, Zhou ZHOU, Xing QING, et al. Ion sensors based on novel fiber organic electrochemical transistors for lead ion detection. *Analytical and Bioanalytical Chemistry* [online]. 2016, 408(21), 5779-5787 [cit. 2019-01-10]. DOI: 10.1007/s00216-016-9684-8. ISSN 1618-2642.

[93] TARABELLA, Giuseppe, Marco VILLANI, Davide CALESTANI, Roberto MOSCA, Salvatore IANNOTTA, Andrea ZAPPETTINI a Nicola COPPEDÈ. A single cotton fiber organic electrochemical transistor for liquid electrolyte saline sensing. *Journal of Materials Chemistry* [online]. 2012, 22(45) [cit. 2019-01-10]. DOI: 10.1039/c2jm34898e. ISSN 0959-9428.

[94] KAWAHARA, Jun, Peter ANDERSSON ERSMAN, Xin WANG, Göran GUSTAFSSON, Hjalmar GRANBERG a Magnus BERGGREN. Reconfigurable sticker label electronics manufactured from nanofibrillated cellulose-based self-adhesive organic electronic materials. *Organic Electronics* [online]. 2013, 14(11), 3061-3069 [cit. 2019-01-10]. DOI: 10.1016/j.orgel.2013.07.013. ISSN 15661199.

[95] RIVNAY, Jonathan, Róisín M. OWENS a George G. MALLIARAS. The Rise of Organic Bioelectronics. *Chemistry of Materials* [online]. 2013, 26(1), 679-685 [cit. 2019-01-10]. DOI: 10.1021/cm4022003. ISSN 0897-4756.

[96] WILLIAMSON, Adam, Marc FERRO, Pierre LELEUX, et al. Localized Neuron Stimulation with Organic Electrochemical Transistors on Delaminating Depth Probes. *Advanced Materials* [online]. 2015, 27(30), 4405-4410 [cit. 2019-01-10]. DOI: 10.1002/adma.201500218. ISSN 09359648.

[97] LEE, Wonryung, Dongmin KIM, Jonathan RIVNAY, et al. Integration of Organic Electrochemical and Field-Effect Transistors for Ultraflexible, High Temporal Resolution Electrophysiology Arrays. *Advanced Materials* [online]. 2016, 28(44), 9722-9728 [cit. 2019-01-10]. DOI: 10.1002/adma.201602237. ISSN 09359648.

[98] CAMPANA, Alessandra, Tobias CRAMER, Daniel T. SIMON, Magnus BERGGREN a Fabio BISCARINI. Electrocardiographic Recording with Conformable Organic Electrochemical Transistor Fabricated on Resorbable Bioscaffold. *Advanced Materials* [online]. 2014, 26(23), 3874-3878 [cit. 2019-01-10]. DOI: 10.1002/adma.201400263. ISSN 09359648.

[99] LELEUX, Pierre, Jonathan RIVNAY, Thomas LONJARET, Jean-Michel BADIER, Christian BÉNAR, Thierry HERVÉ, Patrick CHAUVEL a George G. MALLIARAS. Organic Electrochemical Transistors for Clinical Applications. *Advanced Healthcare Materials* [online]. 2015, 4(1), 142-147 [cit. 2019-01-10]. DOI: 10.1002/adhm.201400356. ISSN 21922640.

[100] UGUZ, Ilke, Mehran GANJI, Adel HAMA, et al. *Advanced Healthcare Materials* [online]. 2016, 5(24) [cit. 2019-01-10]. DOI: 10.1002/adhm.201600870. ISSN 21922640.

[101] YAO, Chunlei, Qianqian LI, Jing GUO, Feng YAN a I-Ming HSING. Rigid and Flexible Organic Electrochemical Transistor Arrays for Monitoring Action Potentials from Electrogenic Cells. *Advanced Healthcare Materials* [online]. 2015, 4(4), 528-533 [cit. 2019-01-10]. DOI: 10.1002/adhm.201400406. ISSN 21922640.

[102] GU, Xi, Chunlei YAO, Ying LIU a I-Ming HSING. 16-Channel Organic Electrochemical Transistor Array for In Vitro Conduction Mapping of Cardiac Action Potential. *Advanced Healthcare Materials* [online]. 2016, 5(18), 2345-2351 [cit. 2019-01-10]. DOI: 10.1002/adhm.201600189. ISSN 21922640.

[103] YAO, Chunlei, Changyan XIE, Peng LIN, Feng YAN, Pingbo HUANG a I-Ming HSING. Organic Electrochemical Transistor Array for Recording Transepithelial Ion Transport of Human Airway Epithelial Cells. *Advanced Materials* [online]. 2013, 25(45), 6575-6580 [cit. 2019-01-10]. DOI: 10.1002/adma.201302615. ISSN 09359648.

[104] FARIA, Gregório C., Duc T. DUONG, Alberto SALLEO, Christos A. POLYZOIDIS, Stergios LOGOTHETIDIS, Jonathan RIVNAY, Roisin OWENS a George G. MALLIARAS. Organic electrochemical transistors as impedance biosensors. *MRS Communications* [online]. 2014, 4(04), 189-194 [cit. 2019-01-10]. DOI: 10.1557/mrc.2014.35. ISSN 2159-6859.

[105] ZHANG, Yi, Sahika INAL, Chih-Yun HSIA, Magali FERRO, Marc FERRO, Susan DANIEL a Roisin M. OWENS. Supported Lipid Bilayer Assembly on PEDOT: PSS Films and Transistors. *Advanced Functional Materials* [online]. 2016, 26(40), 7304-7313 [cit. 2019-01-10]. DOI: 10.1002/adfm.201602123. ISSN 1616301X.

[106] RAMUZ, Marc, Adel HAMA, Miriam HUERTA, Jonathan RIVNAY, Pierre LELEUX a Róisín M. OWENS. Combined Optical and Electronic Sensing of Epithelial Cells Using Planar Organic Transistors. *Advanced Materials* [online]. 2014, 26(41), 7083-7090 [cit. 2019-01-10]. DOI: 10.1002/adma.201401706. ISSN 09359648.

[107] TRIA, Scherrine A., Marc RAMUZ, Miriam HUERTA, et al. Dynamic Monitoring of Salmonella typhimurium Infection of Polarized Epithelia Using Organic Transistors. *Advanced Healthcare Materials* [online]. 2014, 3(7), 1053-1060 [cit. 2019-01-10]. DOI: 10.1002/adhm.201300632. ISSN 21922640.

[108] BOLIN, Maria H., Karl SVENNERSTEN, David NILSSON, Anurak SAWATDEE, Edwin W. H. JAGER, Agneta RICHTER-DAHLFORS a Magnus BERGGREN. Active Control of Epithelial Cell-Density Gradients Grown Along the Channel of an Organic Electrochemical Transistor. *Advanced Materials* [online]. 2009, 21(43), 4379-4382 [cit. 2019-01-10]. DOI: 10.1002/adma.200901191. ISSN 09359648.

[109] WAN, Alwin Ming-Doug, Sahika INAL, Tiffany WILLIAMS, et al. 3D conducting polymer platforms for electrical control of protein conformation and cellular functions. *Journal of Materials Chemistry B* [online]. 2015, 3(25), 5040-5048 [cit. 2019-01-10]. DOI: 10.1039/C5TB00390C. ISSN 2050-750X.

[110] SESSOLO, Michele, Jonathan RIVNAY, Enrico BANDIELLO, George G. MALLIARAS a Henk J. BOLINK. Ion-Selective Organic Electrochemical Transistors. *Advanced Materials* [online]. 2014, 26(28), 4803-4807 [cit. 2019-01-10]. DOI: 10.1002/adma.201400731. ISSN 09359648.

[111] ZHU, Zheng-Tao, Jeffrey T. MABECK, Changcheng ZHU, Nathaniel C. CADY, Carl A. BATT a George G. MALLIARAS. A simple poly(3,4-ethylene dioxythiophene)/poly(styrene sulfonic acid) transistor for glucose sensing at neutral

pH. *Chemical Communications* [online]. 2004, (13) [cit. 2019-01-10]. DOI: 10.1039/b403327m. ISSN 1359-7345.

[112] TANG, Hao, Feng YAN, Peng LIN, Jianbin XU a Helen L. W. CHAN. Highly Sensitive Glucose Biosensors Based on Organic Electrochemical Transistors Using Platinum Gate Electrodes Modified with Enzyme and Nanomaterials. *Advanced Functional Materials* [online]. 2011, 21(12), 2264-2272 [cit. 2019-01-10]. DOI: 10.1002/adfm.201002117. ISSN 1616301X.

[113] PAPPA, Anna-Maria, Vincenzo F. CURTO, Marcel BRAENDLEIN, Xenofon STRAKOSAS, Mary J. DONAHUE, Michel FIOCCHI, George G. MALLIARAS a Roisin M. OWENS. Organic Transistor Arrays Integrated with Finger-Powered Microfluidics for Multianalyte Saliva Testing. *Advanced Healthcare Materials* [online]. 2016, 5(17), 2295-2302 [cit. 2019-01-10]. DOI: 10.1002/adhm.201600494. ISSN 21922640.

[114] BATTISTA, Edmondo, Vincenzo LETTERA, Marco VILLANI, et al. Enzymatic sensing with laccase-functionalized textile organic biosensors. *Organic Electronics* [online]. 2017, 40, 51-57 [cit. 2019-01-10]. DOI: 10.1016/j.orgel.2016.10.037. ISSN 15661199.

[115] BIHAR, Eloïse, Yingxin DENG, Takeo MIYAKE, Mohamed SAADAOUI, George G. MALLIARAS a Marco ROLANDI. A Disposable paper breathalyzer with an alcohol sensing organic electrochemical transistor. *Scientific Reports* [online]. 2016, 6(1) [cit. 2019-01-10]. DOI: 10.1038/srep27582. ISSN 2045-2322.

[116] BRAENDLEIN, Marcel, Anna-Maria PAPPA, Marc FERRO, Alexia LOPRESTI, Claire ACQUAVIVA, Emilie MAMESSIER, George G. MALLIARAS a Róisín M. OWENS. Lactate Detection in Tumor Cell Cultures Using Organic Transistor Circuits. *Advanced Materials* [online]. 2017, 29(13) [cit. 2019-01-10]. DOI: 10.1002/adma.201605744. ISSN 09359648.

[117] TYBRANDT, Klas, Suresh Babu KOLLIPARA a Magnus BERGGREN. Organic electrochemical transistors for signal amplification in fast scan cyclic voltammetry. *Sensors and Actuators B: Chemical* [online]. 2014, 195, 651-656 [cit. 2019-01-10]. DOI: 10.1016/j.snb.2014.01.097. ISSN 09254005.

[118] GUALANDI, Isacco, Domenica TONELLI, Federica MARIANI, Erika SCAVETTA, Marco MARZOCCHI a Beatrice FRABONI. Selective detection of dopamine with an all PEDOT: PSS Organic Electrochemical Transistor. *Scientific Reports* [online]. 2016, 6(1) [cit. 2019-01-10]. DOI: 10.1038/srep35419. ISSN 2045-2322.

[119] MAK, Chun Hin, Caizhi LIAO, Ying FU, Meng ZHANG, Chun Yin TANG, Yuen Hong TSANG, Helen L. W. CHAN a Feng YAN. Highly-sensitive epinephrine sensors based on organic electrochemical transistors with carbon nanomaterial modified gate electrodes. *Journal of Materials Chemistry C* [online]. 2015, 3(25), 6532-6538 [cit. 2019-01-10]. DOI: 10.1039/C5TC01100K. ISSN 2050-7526.

[120] LIN, Peng, Xiaoteng LUO, I-Ming HSING a Feng YAN. Organic Electrochemical Transistors Integrated in Flexible Microfluidic Systems and Used for Label-Free DNA Sensing. *Advanced Materials* [online]. 2011, 23(35), 4035-4040 [cit. 2019-01-10]. DOI: 10.1002/adma.201102017. ISSN 09359648.

[121] HE, Rong-Xiang, Meng ZHANG, Fei TAN, Polly H. M. LEUNG, Xing-Zhong ZHAO, Helen L. W. CHAN, Mo YANG a Feng YAN. Detection of bacteria with organic electrochemical transistors. *Journal of Materials Chemistry* [online]. 2012, 22(41) [cit. 2019-01-10]. DOI: 10.1039/c2jm33667g. ISSN 0959-9428.

[122] ZAOUK, Rabih, Benjamin Y. PARK a Marc J. MADOU. Introduction to Microfabrication Techniques. *Microfluidic Techniques* [online]. New Jersey: Humana Press, 2005, , 3-16 [cit. 2019-01-10]. DOI: 10.1385/1-59259-997-4:3. ISBN 1-59259-997-4.

[123] BASIRICO, Laura. *Inkjet Printing of Organic Transistor Devices*. Cagliari, 2012. Ph. D. Thesis. University of Cagliari

[124] MANNERBRO, Richard a Martin RANLÖF. *Inkjet and Screen Printed Electrochemical Organic Electronics*. Linköping, 2007. LITH-ISY-EX--07/3876--SE. Master Thesis. Linköping Institute of Technology.

[125] KAWASE, T., SIRRINGHAUS a T. SHIMODA. Inkjet Printed Via-Hole Interconnections and Resistors for All-Polymer Transistor Circuits. *Advanced Materials* [online]. 2001, 13(21) [cit. 2016-02-02]. DOI: 10.1002/1521-4095(200111)13:21<1601::AID-ADMA1601>3.0.CO;2-X.

[126] YOSHIOKA, Yuka, Paul D. CALVERT a Ghassan E. JABBOUR. Simple Modification of Sheet Resistivity of Conducting Polymeric Anodes via Combinatorial Ink-Jet Printing Techniques. *Macromolecular Rapid Communications* [online]. 2005, 26(4), 238-246 [cit. 2019-01-10]. DOI: 10.1002/marc.200400527. ISSN 1022-1336.

[127] LIU, Yi, Kody VARAHRAMYAN a Tianhong CUI. Low-Voltage All-Polymer Field-Effect Transistor Fabricated Using an Inkjet Printing Technique. *Macromolecular Rapid Communications* [online]. 2005, 26(24), 1955-1959 [cit. 2019-01-10]. DOI: 10.1002/marc.200500493. ISSN 1022-1336.

[128] KREBS, Frederik C. Fabrication and processing of polymer solar cells: A review of printing and coating techniques. *Solar Energy Materials and Solar Cells* [online]. 2009, 93(4), 394-412 [cit. 2019-01-10]. DOI: 10.1016/j.solmat.2008.10.004. ISSN 09270248.

[129] BAO, Zhenan, Yi FENG, Ananth DODABALAPUR, V. R. RAJU a Andrew J. LOVINGER. High-Performance Plastic Transistors Fabricated by Printing Techniques. *Chemistry of Materials* [online]. 1997, 9(6), 1299-1301 [cit. 2019-01-10]. DOI: 10.1021/cm9701163. ISSN 0897-4756.

[130] GARNIER, F., R. HAJLAOUI, A. YASSAR a P. SRIVASTAVA. All-Polymer Field-Effect Transistor Realized by Printing Techniques. *Science* [online]. 1994, 265(5179), 1684-1686 [cit. 2018-10-01]. DOI: 10.1126/science.265.5179.1684. ISSN 0036-8075.

[131] PARDO, D. A., G. E. JABBOUR a PEYGHAMBARIAN. Application of Screen Printing in the Fabrication of Organic Light-Emitting Devices. *Advanced Materials* [online]. 2000, 12(17), 1249-1252 [cit. 2018-10-01]. DOI: 10.1002/1521-4095(200009)12:17<1249::AID-ADMA1249>3.0.CO;2-Y.

[132] BECKER, E., R. PARASHKOV, G. GINEV, et al. All-organic thin-film transistors patterned by means of selective electropolymerization. *Applied Physics Letters* [online]. 2003, 83(19), 4044-4046 [cit. 2019-01-10]. DOI: 10.1063/1.1623951. ISSN 0003-6951.

[133] GELORME, Jeffrey, Robert COX a Sergio GUTIERREZ. *Photoresist composition and printed circuit boards and packages made therewith*. USA. US4882245A. Zapsáno 21.11.1989.

[134] ARSCOTT, Steve. SU-8 as a material for lab-on-a-chip-based mass spectrometry. *Lab on a Chip* [online]. 2014, 14(19) [cit. 2019-01-10]. DOI: 10.1039/C4LC00617H. ISSN 1473-0197.

[135] NEMANI, Krishnamurthy V., Karen L. MOODIE, Jeoffry B. BRENNICK, Alison SU a Barjor GIMI. In vitro and in vivo evaluation of SU-8 biocompatibility. *Materials Science and Engineering: C* [online]. 2013, 33(7), 4453-4459 [cit. 2019-01-10]. DOI: 10.1016/j.msec.2013.07.001. ISSN 09284931.

[136] LUURTSEMA, Gregory. *Spin coating for rectangular substrates* [online]. Berkeley, USA, 1997 [cit. 2018-10-01]. Master thesis. University of California, Berkeley.

[137] CARCANO, G., M. CERIANI a F. SOGLIO. Spin Coating with High Viscosity Photoresist on Square Substrates — Applications in the Thin Film Hybrid Microwave Integrated Circuit Field. *Microelectronics International* [online]. 1993, 10(3), 12-20 [cit. 2019-01-10]. DOI: 10.1108/eb044507. ISSN 1356-5362.

[138] KLAVINS, J., G. MOZOLEVSKIS, A. OZOLS A., E. NITISS a M. RUTKIS. Screen Printing of SU-8 Layers for Microstructure Fabrication / Ar Sietspiedi Uzklātu SU-8 Pārklājumi Mikro-Struktūru Izgatavošanai. *Latvian Journal of Physics and Technical Sciences* [online]. 2015, 52(5), 58-67 [cit. 2019-01-10]. DOI: 10.1515/lpts-2015-0029. ISSN 0868-8257.

[139] DULBECCO, R. PLAQUE FORMATION AND ISOLATION OF PURE LINES WITH POLIOMYELITIS VIRUSES. *Journal of Experimental Medicine* [online]. 1954, 99(2), 167-182 [cit. 2019-01-10]. DOI: 10.1084/jem.99.2.167. ISSN 0022-1007.

[140] *Dimatix Materials Printer DMP-2831: User Manual* [online]. Santa Clara CA, USA: FUJIFILM Dimatix, 2013 [cit. 2018-10-01]. Available at: http://www.fujifilmusa.com/shared/bin/DMP-2831_Datasheet_05-13.pdf

[141] *Rokuprint SD 05: User Manual* [online]. Dornstadt, Germany: Benzstrasse 10 D-89160 Dornstadt, 2012 [cit. 2018-10-01]. Available at: http://www.rokuprint.com/eng/debgcms/cmsdata/artikel/143/db_sd_05_e.pdf

[142] DektakXT Stylus Profiler: User Manual. *Https://www.bruker.com* [online]. USA: Bruker Corporation, 2011 [cit. 2018-10-01]. Available at: https://www.weizmann.ac.il/ChemicalResearchSupport/sites/ChemicalResearchSupport/files/uploads/DektakXT/2011-05-31-dektakxt-user.pdf

[143] SOTIRIOU, Niki. *Low temperature plasma enhanced chemical vapor deposition of graphene layers* [online]. Patras, Greece, 2017 [cit. 2018-10-01]. Available at: http://nemertes.lis.upatras.gr/jspui/bitstream/10889/11112/1/Master%20thesis.Niki%20Sotiriou.pdf. Master thesis. Department of Chemical Engineering, University of Patras.

[144] *Keithley 2400 series SourceMeter: Datasheet* [online]. United Kingdom: Tektronix UK, 2008 [cit. 2018-10-02]. Available at: https://www.tek.com/keithley-source-measure-units/keithley-smu-2400-series-sourcemeter

[145] *Oscilloscope Tektronix TDS 2024B: User Manual* [online]. United Kingdom: Tektronix UK, 2008 [cit. 2018-10-02]. Available at: https://www.tek.com/oscilloscope/tds2022b-manual/tds2022b-and-tds2024b

[146] EHLICH, Jiří. *Příprava organických elektrochemických tranzistorů pro biosenzoriku* [online]. Brno, 2015 [cit. 2018-10-02]. Dostupné z: https://www.vutbr.cz/studenti/zav-prace/detail/74159. Bakalářská práce. Fakulta Chemická, VUT v Brně. Vedoucí práce Doc. Ing. Ota Salyk, CSc.

[147] EHLICH, jiří. *Optimalizace tiskových metod přípravy organických polovodivých vrstev* [online]. Brno, 2017 [cit. 2018-10-02]. Dostupné z: https://www.vutbr.cz/studenti/zav-prace/detail/98442. Diplomová práce. Fakulta Chemická, VUT v Brně. Vedoucí práce Doc. Ing. Ota Salyk, CSc.

[148] ALEMU, Desalegn, Hung-Yu WEI, Kuo-Chuan HO a Chih-Wei CHU. *Highly conductive PEDOT: PSS electrode by simple film treatment with methanol for ITO-free polymer solar cells* [online]. 2012, 5(11) [cit. 2019-01-10]. DOI: 10.1039/c2ee22595f. ISSN 1754-5692.

[149] ŠAFAŘÍKOVÁ, Eva. *Testování biokompatibility materiálů pro experimentální práci v buněčné biologii* [online]. Brno, 2016 [cit. 2018-10-02]. Dostupné z: https://is.muni.cz/th/sfmls/?so=nx. Diplomová práce. Přírodovědecká fakulta, Masarykova univerzita. Vedoucí práce Mgr. Jan Víteček, Ph.D.

[150] SALYK, Ota, Jan VÍTEČEK, Lukáš OMASTA, Eva ŠAFAŘÍKOVÁ, Stanislav STŘÍTESKÝ, Martin VALA a Martin WEITER. Organic Electrochemical Transistor Microplate for Real-Time Cell Culture Monitoring. *Applied Sciences* [online]. 2017, 7(10) [cit. 2018-11-05]. DOI: 10.3390/app7100998. ISSN 2076-3417.

[151] VISTEJNOVA, Lucie, Jana DVORAKOVA, Martina HASOVA, Tomas MUTHNY, Vladimír VELEBNY, Karel SOUCEK, Lukas KUBALA. The comparison of impedance-based method of cell proliferation monitoring with commonly used metabolic-based techniques. *Neuroendocrinol. Lett*. 2009, 30, 121–127.

[152] STŘÍTESKÝ, Stanislav, Aneta MARKOVÁ, Jan VÍTEČEK, et al. Printing inks of electroactive polymer PEDOT: PSS. *Journal of Biomedical Materials Research Part A* [online]. 2018, 106(4), 1121-1128 [cit. 2019-01-10]. DOI: 10.1002/jbm.a.36314. ISSN 15493296.